ISTANBUL TECHNICAL UNIVERSITY ★ GRADUATE SCHOOL OF SCIENCE ENGINEERING AND TECHNOLOGY

EXPERIMENTAL PHYSICAL MODELING OF HYDRODYNAMICS OF A FIXED OWC WITH DEVELOPMENT OF ANALYTICAL AND NUMERICAL MODELS

Ph.D. THESIS

Anıl ÇELİK

Department of Coastal Sciences and Engineering

Coastal Sciences and Engineering Programme

NOVEMBER 2019

ISTANBUL TECHNICAL UNIVERSITY ★ GRADUATE SCHOOL OF SCIENCE ENGINEERING AND TECHNOLOGY

EXPERIMENTAL PHYSICAL MODELING OF HYDRODYNAMICS OF A FIXED OWC WITH DEVELOPMENT OF ANALYTICAL AND NUMERICAL MODELS

Ph.D. THESIS

Anıl ÇELİK
(517142001)

Department of Coastal Sciences and Engineering

Coastal Sciences and Engineering Programme

Thesis Advisor: Prof. Abdüsselam ALTUNKAYNAK

NOVEMBER 2019

<u>ISTANBUL TEKNİK ÜNİVERSİTESİ ★ FEN BİLİMLERİ ENSTİTÜSÜ</u>

SABİT SALINIMLI SU SÜTUNU DALGA ENERJİ DÖNÜŞTÜRÜCÜ HİDRODİNAMİĞİNİN DENEYSEL ANALİTİK VE NÜMERİK OLARAK MODELLENMESİ

DOKTORA TEZİ

Anıl ÇELİK
(517142001)

Kıyı Bilimleri ve Mühendisliği Anabilim Dalı

Kıyı Bilimleri ve Mühendisliği Programı

Tez Danışmanı: Prof. Dr. Abdüsselam ALTUNKAYNAK

KASIM 2019

Anıl Çelik, a Ph.D. student of İTU Graduate School of Science Engineering and Technology student ID 517142001, successfully defended the thesis/dissertation entitled "EXPERIMENTAL PHYSICAL MODELING OF HYDRODYNAMICS OF A FIXED OWC WITH DEVELOPMENT OF ANALYTICAL AND NUMERICAL MODELS", which he prepared after fulfilling the requirements specified in the associated legislations, before the jury whose signatures are below.

Thesis Advisor : **Prof. Dr. Abdüsselam ALTUNKAYNAK** ....
İstanbul Technical University

Jury Members : **Prof. Dr. Mehmet ÖZGER** ....
Istanbul Technical University

Assoc. Prof. Tarkan ERDİK ....
Istanbul Technical University

Prof. Dr. Necati AĞIRALİOĞLU ....
Istanbul Bilim. University

Assoc. Prof. Berna Ayat AYDOĞAN ....
Yıldız Technical University

Date of Submission : 2 October 2019
Date of Defense : 4 November 2019

To my lifelong advisor,

FOREWORD

Water waves are fascinating and energy transported within the waves is enourmess. If an efficient way can be devised to extract water wave energy, dwindling energy problem of the world and replacement of fosil-based energy resources with renewables ones may effectively be solved.

I am overwhelmingly grateful to my mentor Professor Abdüsselam ALTUNKAYNAK for not only he gave me the opportunity to study this excellent subject but also for showing me a path to follow for the rest of my life, which, hopefully, will be full of serving to my country. I am also very indebted to him for the unlimited support, inspiration and motivation he supplied and ignoring my misbehaviors during my studies.

I also thank to Prof. Dr. Mehmet ÖZGER, and Assoc. Prof. Dr.Tarkan ERDİK and my brothers Alaaddin, Hamza and Kerem for their assistance during all parts of my study. I highly appreciate the financial support provided by ITU BAP Unit (Project No:39828).

Of course, performing a Phd. requires great dedication and concentration for all times which, obviously necessitates disregarding the family to a great extent. I especially thanks to my wife Seda ÇELİK for her understanding, endurance and encouragement during the long thesis period and helping me write the articles and thesis. I am also very grateful to my parents for their endless support and prayers not only for the thesis studies but for whole my life.

October 2019 Anıl ÇELİK

TABLE OF CONTENTS

Page

ABBREVIATIONS

BEM	: Boundary Element Method
CE	: Coefficient of Efficiency
CFD	: Computational Fluid Dynamics
FAVOR	: Fractional Area/Volume Obstacle Representation
IVP	: Initial Value Problem
LDM	: Logarithmic Decrement Method
LIMPET	: Land Installed Marine Powered Energy Transformer
N-S	: Navier-Stokes
NSE	: Nash-Sutcliffe Coefficient
NWT	: Numerical Wave Tank
OWC	: Oscillating Water Column
PT	: Pressure Transducer
PTO	: Power Take-off
RANSVOF	: Reynolds Averaged Navier-Stokes Volume of Fluid
Re	: Reynolds Number
RE	: Relative Error
RMSE	: Root Mean Square Error
SDOF	: Single Degree of Freedom
SWL	: Still Water Level
VOF	: Volume of Fluid
WEC	: Wave Energy Converter
WG	: Wave Gauge
WNO	: Wave Number
2D	: Two Dimensional
3D	: Three Dimensional

SYMBOLS

A	: Mass of an arbitrary system
$\mathbf{A_0}$	: Cross-sectional orifice area
$\mathbf{A_w}$	: Horizontal water column surface area
$\mathbf{A_x}$	: Area fraction in x direction
$\mathbf{A_y}$	: Area fraction in y direction
$\mathbf{A_z}$	: Area fraction in z direction
a	: Elevation amount of water column with respect to still water depth
B	: Damping coefficient of an arbitrary system
b	: Plexiglas width of the OWC
$\mathbf{c_g}$	: Group velocity
$\mathbf{c_1}$	: Arbitrary constant
$\mathbf{C1_\varepsilon}$	: constant
$\mathbf{C2_\varepsilon}$	: constant
$\mathbf{C3_\varepsilon}$	: constant
$\mathbf{c_2}$	: Arbitrary constant
C	: Restoring coefficient of an arbitrary system
$\mathbf{d'}$	: Empirically obtained effective length
d	: Height of the water column oscillation
d	: Damping coefficient of the OWC system
$\mathbf{d^*}$	: Dimensionless damping coefficient
Diff	: Diffusion term
$\mathbf{Diff_\varepsilon}$	: Diffusion term
$\mathbf{E_0}$	: Average of the experimental data
$\mathbf{E_i}$	: Direct measurement of damping ratio
$\mathbf{E_h}$	: Capture width
E	: Average incident wave energy per unit length and per unit width
$\mathbf{f_x}$	: Viscous acceleration in the x direction
$\mathbf{f_y}$	: Viscous acceleration in the y direction
$\mathbf{f_z}$	: Viscous acceleration in the z direction

F_{air}	: Air pressure force
F_{exc}	: Incident wave force
F_0	: Amplitude of the incident wave force
g	: Gravitational acceleration
G_x	: Body acceleration in the x direction
G_y	: Body acceleration in the y direction
G_z	: Body acceleration in the z direction
G_k	: Buoyancy production term
H	: Wave height
H	: Still water depth
l	: OWC length
k	: Incident wave number
Kh	: Dimensionless wave frequency
L_m	: Corresponding length of model
L	: Wavelength.
L_r	: Length scale
L_c	: Characteristic length
L_p	: Corresponding length of prototype
m	: Mass of the water column
m_a	: Added mass
N_i	: Direct measurement of natural period
P_k	: Turbulent kinetic energy term
P	: Dynamic pressure under the incident wave
P_{av}	: Pressure under the water column averaged in the x direction
p_{air}	: Differential air pressure in the chamber
P_{air}	: Pneumatic power of the OWC
P_i	: i^{th} incident wave power for unit width and length
R	: Orifice diameter
r_1	: A function of m, d and ω_n
r_2	: A function of m, d and ω_n
R	: Orthogonal transformation tensor
t	: Time
t_f	: Time needed for elevated chamber surface level to diminish to the value of 0.1% of a
T_d	: Damped period

T	: Incident wave period
U	: Characteristic velocity
(u,v,w)	: Velocity components corresponding to Cartesian coordinate system
$\mathbf{V_f}$	: Fractional value
x	: Wave propagation direction (perpendicular to the front wall of the OWC chamber)
(x,y,z)	: Cartesian coordinate system
w	: OWC width
$\boldsymbol{\omega_n}$	: Natural frequency
$\boldsymbol{\omega_r}$	: Resonant frequency
v(t)	: Average velocity of the water column displacement
$\mathbf{V^3}$	: Third order approximation of the average vertical velocity of the free surface
$\bar{\mathbf{x}}$	: Opening height of the chamber
$\bar{y}$	: Immersion depth of the chamber front wall
y(t)	: Vertical displacement of the water column with respect to still water
$\mathbf{Y_0}$	: Amplitude of the water column oscillations
ξ	: Geometry coefficient
ε	: Rate of dissipation of kinetic energy
ρ	: Density
$\boldsymbol{\mu_d}$	: Dynamic viscosity
μ	: Transmitted wave height
ω	: Angular frequency (incident wave)
α	: Relative opening height
β	: Relative immersion depth
δ	: Captured wave length ratio
η	: Relative average water column surface amplitude
τ	: Orifice ratio
ν	: Kinematic viscosity
$\forall_p$	: Volume of the prototype
$\forall_m$	: Volume of the model
$\dot{y}(t)$	: First time derivative of the water column displacement
$\ddot{y}(t)$	: Second time derivative of the water column displacement,
θ	: Phase angle
δ	: Logarithmic Decrement

$\mathbf{y_i}$	**:** i^{th} positive or negative peak of the free decay times series data
$\boldsymbol{\zeta}$	**:** Damping ratio
$\boldsymbol{\eta}$	**:** Free surface of the incident wave
$\boldsymbol{\lambda}$	**:** Corresponding physical experimental value to the analytical model result

LIST OF TABLES

Page

LIST OF FIGURES

Page

EXPERIMENTAL PHYSICAL MODELING OF HYDRODYNAMICS OF A FIXED OWC WITH DEVELOPMENT OF ANALYTICAL AND NUMERICAL MODELS

SUMMARY

Transition from detrimental fossil based fuels to renewable energy sources is vitally important for the world's future since energy consumption increases with industrial and population growth and mankind is not likely to abandon his ongoing lifestyle. For this purpose, targets have been determined for renewable energy usage throughout the world but the goals seem to fail because renewable energy percentage in the world's total energy consumption does not grow fast enough. Ocean waves, one form of the renewable energy sources, is a concentrated form of solar energy with 50 times larger power intensity, therefore, energy harvesting from ocean waves have attracted great attention. Efforts have already been ended up more than 1000 wave energy extraction devices and techniques patented in the world. However, in spite of its high potential and energy density, wave energy is almost a zero contributor to the renewable energy market. So far, an approved commercialized wave energy converter has not been able to come into existence because the complicated physics (i.e. hydrodynamics, aerodynamics and thermodynamics) of an OWC device has not been comprehended by all means. Ultimately, wave energy technology is not cost-effective yet compared with those of solar and wind energy. This study has attempted to contribute to the understanding of complicated wave-structure and two phase fluid interactions by physical experimental, analytical and numerical numerical modeling methods.

Up to date, various type of wave energy converters (WECs) has been devised, however, OWC type WECs appear to be the most promising ones thanks to their simplicity, stability, accessibility and environmental friendly features. OWC technology takes advantage of the oscillating dynamic pressure under an incident wave that acts on a water column inside a partially submerged hollow chamber through a seaward opening. The oscillatory motion of the water column forces the trapped air above it to exit the chamber from a narrow duct at the back or top of the system. In this study, a generic type bottom-standing OWC was chosen for investigation.

Oscillations of the water column under the excitation of incident wave pressure is the first conversion process of the wave energy in the form of kinetic energy. Kinetic energy of the water column is further transformed into pneumatic energy as thewaer column rises up and retreats back. Hence, water column motion is as an intermediate conveying process for wave energy conversion. Since the water column is excited by the dynamic wave pressure under the front wall of the chamber, influence of the wave characteristics in an efficient wave energy conversion process is obvious. To reveal the effects of wave parameters on the complex OWC dynamics and performance four distinct regular waves are generated. Literature review also manifests the significance of optimizing the power take-off (PTO) damping and front wall immersion depth of the chamber according to incident wave properties for feasible energy extraction. PTO mechanism (e.g. a turbine) generates differential air pressure, which enables energy

extraction, by confining the air above the water column. Orifice is used, in this study, to simulate the PTO mechanism of the OWC device. On the other hand, front wall draught determines the amount of incident wave energy transmitted into the chamber and effects the dynamics of the water column. Therefore, in this present study, physical experimental, numerical and analytical approaches are utilized for various PTO dampings (orifice sizes) and underwater chamber openings. Depending on the total damping on the water column, OWC device may be characterized as an overdamped or underdamped system. It is understood that, chamber opening size is irrelevant in this context. For the smallest orifice size used in this study the system is found to be overdamped whereas the system was underdamped for the remaining orifice sizes.

Oscillation amplitudes and motion behavior of the water column are very influential for wave energy extraction. Therefore, predicting the amplitudes and identifying the motion behaviors with respect to varying wave characteristics and geometric design parameters are of great importance. For the overdamped case, physical experiments are conducted with nine different sizes of opening heights under various regular wave series. Average oscillation amplitudes inside the chamber are measured. It is found that there is a critical relative opening height ratio (α) that makes the amplitudes maximum regardless of incident wave parameters generated. Exponential and linear relationships are found between average fluctuations and defined dimensionless parameters 'dimensionless wave frequency' and 'captured wavelength', respectively. A pertinent mathematical model is developed to predict the oscillation amplitudes under varying relative opening heights and wave parameters. The results of the mathematical model indicated good agreement with experimental data. Also chamber water surface profiles are observed and related to defined dimensionless wave parameters. Another factor (named as excessive harmful energy) is detected which also induces sloshing motion inside the chamber after the determined critical ratio value is exceeded. It is found that under all incident waves, the highest oscillation amplitudes occur at relative opening height equal to 0.67 which is a unique value. It can be concluded that mathematical model can be used to estimate water column amplitudes from relative opening height and wave parameters.

A more general mathematical modeling of the water column is further developed via as a one degree of freedom (SDOF) simple mechanical modelling, which is a basic method yet able to capture the essential physics of the motion of the water column. In addition, oscillations of the water column are coupled with thermodynamics and aerodynamics of the air column. Thus, all of the aspects of the conversion process have to be solved simultaneously. For the overdamped case, water surface average oscillations in the chamber and related phase angles are estimated by the developed mechanical model. Overall resistive force against the motion of the water column is represented by introduced damping coefficient in the equations and determined experimentally by a novel approach that does not exist in the previous literature. The optimum damping is experimentally obtained for a particular relative opening height of the chamber that corresponds to the highest average chamber water surface oscillations regardless of the wave parameters used. Water surface oscillation amplitudes are estimated (calculated) by the developed mathematical model under different wave conditions and chamber opening heights. The mathematical model results were validated by the data obtained via performed physical experiments for this thesis. It is observed that a good agreement exists between the physical experimental data and the simple mechanical (mathematical) model results.

For the underdamped case, for the first time, hydrodynamic parameters namely, equivalent linear damping ratio, added mass, natural and resonant frequencies of a fixed OWC for various underwater chamber openings and orifice sizes are determined by performing physical experimental and 3D numerical free decay tests via utilizing 0logarithmic decrement method. Numerical model results are verified with experimental model values.

Damping ratio of the system is found to be exponentially and linearly decaying as the orifice size and underwater opening increases. To the best of author's knowledge, for the first time, determined damping ratio also includes the viscous losses under the front wall opening of the OWC system. This is very crucial in its own right because accurate prediction of viscous losses is almost impossible via analytical treatment, thus, potential and linear theories that assume ideal fluid which simply neglects viscous losses, are used. Water column within the chamber is again modeled as a one degree of freedom (SDOF) mechanical system and, obtained damping and added mass values are substituted into the model. Surface water column oscillation amplitudes are determined by both solving the model and performing physical experiments under the generated monochromatic incident waves. Remarkable agreement is found between the analytical model results and physical experimental data when the water column surface acted approximately as a rigid-body. However, when a significant amount of sloshing occurs in the chamber model results diverged from the experimental values. It is observed that relatively higher PTO damping and smaller underwater chamber openings substantially restrain the sloshing motion otherwise inherently generated in the chamber. Also, for all openings and orifice sizes used in this study, determined resonant frequencies of the OWC well matches with those that obtained from the experimental data. Most importantly, for the first time, an empirical formula is developed by the experimental data obtained in this very thesis for approximation of natural frequency of an OWC.

As mentioned previously, OWC front wall opening and power take-off (PTO) damping optimization are very significant for feasible energy extraction. Therefore, a comprehensive experimental investigation was performed to determine the influence of underwater opening height of the chamber, power take-off damping and wave steepness on the energy converter efficiency. Also OWC device performance is distincly calculated for all parameters used in this thesis. A broad range of opening heights and power take-off dampings were utilized in physical experiments under various wave steepness values. Water column oscillations, velocities and motion behaviors were also examined. Optimal orifice ratios were determined to obtain maximum efficiency under different wave steepness values. Based on the results, the key finding of this study is, for a certain range of wave steepness, optimal damping that should be applied on the system does not only depend on the wave characteristics, but also opening height of the chamber. The motion of water column surface behavior also affects the performance of the converter considerably.

SABİT SALINIMLI SU SÜTUNU DALGA ENERJİ DÖNÜŞTÜRÜCÜ HİDRODİNAMİĞİNİN DENEYSEL ANALİTİK VE NÜMERİK OLARAK MODELLENMESİ

ÖZET

Dünyanın ve insanlığın geleceği açısından yenilenebilir enerjinin konvansiyonel enerji kaynaklarının yerini alması elzemdir. Bu konunun değerlendirildiği uluslararası toplantılarda hedefler konmuş olmasına rağmen henüz kayda değer bir başarı elde edilememiştir. Yenilenebilir enerji kaynaklarının kullanım oranının artması için tüm yenilenebilir enerji türlerinden istifade edilmelidir. Bir tür yenilenebilir enerji kaynağı olan dalga enerjisi insanlığın ilgisini çekmiş ve 1000'den fazla dalga enerji dönüştürücü patentleme işlemi yapılmıştır. Buna rağmen güneş ve rüzgâr enerji kaynaklarından çok daha fazla enerji yoğunluğuna sahip dalga enerjisinden hemen hemen hiç faydalanılamamaktadır. Dünya yüzeyinin yaklaşık üçte ikisinin sularla kaplı olduğu düşünüldüğünde bu şaşılacak bir durumdur. Henüz ticari üretime geçmiş bir dalga enerji dönüştürücünün bulunamaması üretilen elektrik enerjisinin maliyetlerinin hala çok yüksek olmasından ötürüdür. Bunun sebebi ise detaylı ve karmaşık dalga-yapı ve yapı içindeki iki farklı akışkanın etkileşimlerinin tam olarak anlaşılamamasından ötürüdür. Bu motivasyonla, dalga enerji dönüşüm süreçlerinin daha iyi anlaşılmasına katkı sağlamak için bu çalışmaya başlanmıştır. Bugüne kadar icat edilen dalga dönüştürücülerinden salınımlı su sütunu (SSS) tipi dalga enerjisi dönüştürücü işleyiş basitliği, stabil oluşu, kolay ulaşılabilirliği ve çevre dostu olması dolayısıyla bir adım öne çıkmıştır. Bu çalışma kapsamında da dikdörtgen kesitli sabit genel bir SSS seçilmiştir. Bu yapıların çalışma prensibi şu şekildedir: İçi boş, dört tarafı kapalı kısmi olarak suya batırılmış ve suyun altında kalan kısmında deniz suyuyla irtibatı sağlayan bir açıklık bulunan herhangi bir geometrideki yapı deniz tabanına veya herhangi bir yapıya sabitlenir. Bu yapının arka kısmında ise dar bir hava çıkış borusu bulunur. Yapıya gelen dalgaların dalga tepelerinin enerji dönüştürücü içerisindeki su seviyesini yükseltmesiyle yapı içindeki su seviyesinin üstünde hapsolmuş bulunan hava sıkışır ve basınç artar. Bu basınç farkı havayı çıkış borusundan hızla dışarı çıkmaya zorlar. Dalga çukurunun yapıyla teması noktasında bu sistemin tersi oluşur ve hava oluşacak vakum etkisiyle yapı içine çekilir (Bu işlemler dalgafrenksı ile belli bir faz açısında gerçekleşir). Çıkış borusu önüne konacak, çift taraflı hava akış durumunda dahi aynı yöne dönecek bir tribün ve onunda bağlı olduğu bir jeneratör yardımı ile dalga enerjisi hava enerjisine oda tribündeki dönme enerjisine oda nihayet elektrik enerjisine çevrilir. SSS yapısı içinde dalga etkisi altında salınımı yapan su sütünü, dalga enerjisinin kinetik enerjiye dönüşmüş halidir. Salınım yapan su sütunu daha sonra kendi enerjisini üzerinde hapsolmuş bulunan havaya aktarır ve böylece dalga enerjisi pnömatik enerjiye dönüştürülmüş olur. Bu bağlamda yapı içinde hareket eden su sütunu, dalga ile hava arasında enerji iletim görevini görür. Bu nedenle su sütunu salınım miktarları ve karakteristikleri önem arz etmektedir. Yapının maruz kaldığı dalgaların karakteristiklerinin salınımlar üzerindeki etkisi açıktır. Bu etkileri ve bu etkilerin yapının performansı üzerinde oluşturduğu değişimleri gözlemleyebilmek için dört ayrı düzenli dalga üretilmiştir. Ayrıca, detaylı

literatür taraması sonucunda, aynı zamanda (türbin) su sütunu üzerinde yaptığı sönumleme düzeyinin ve yapının sualtı açıklık yüksekliğinin de çok önemli olduğu anlaşılmıştır. Bu çalışmada, enerji alma yapısı değişik çaplarda ki (değişik sönümleme düzeylerine karşı gelen) orifisler kullanılarak simüle edilmiştir. Yapı açıklık miktarı salınımlı su sütununa iletilen dalga enerji miktarını belirlemektedir. Sonuç olarak bu çalışmada yapı verimini etkileyen en önemli parametrelerin incelenmesi noktasında, kullanılan deneysel, nümerik ve analitik yöntemler, farklı orifis çapları ve su altı açıktıkları için farklı dalga parametreleri altında denenmiştir. Beş farklı ofis çapı ve dokuz farklı yapı açıklık yüksekliği ve dört farklı düzenli dalga kullanılmıştır. Su sütunun salınım düzeyi elektriğe dönüştürülebilen dalga enerjisi miktarını direk etkilediği için, salınım miktarlarının bu çalışmada kullanılan parametrelerin değişimlerine vereceği tepkilerin tahmini önemlidir. Seçilen enerji alma yapısının su sütunu salınımı üzerine uyguladığı sönümleme miktarına göre SSS yapısı aşırı sönümlenmiş veya az sönümlenmiş sistem olmak üzere ikiye ayrılır ve farklı dinamikler içerirler. En küçük orifis çapında (en yüksek sönümleme düzeyi), sistemin aşırı karakteristiğe sahip olduğu serbest düşüm testlerinde belirlenmiştir. Aşırı sönümlenmiş sistem için yapılan deneysel çalışmalarda, su sütunu salınım genliği ölçülmüş ve gelen dalga özelliklerinden bağımsız olarak salınım genliğinin maksimum olduğu bir kritik yapı su altı açıklık miktarı tespit edilmiştir. Açıklık yüksekliğinin daha da artmasının yapı içinde çalkantılara sebebiyet verdiği görülmüştür. Çalkantının ise yapı verimini olumsuz etkilediği bilinmektedir. Bu yüzden yapı su altı açıklığının kritik açıklık yüksekliğinden fazla olduğu durumlarda yapı içine transfer edilen fazla enerji miktarı zararlı enerji olarak adlandırılmıştır. Su salınımı genliğinin boyutsuz dalga frekansıyla üstel, boyutsuz dalga boyuyla ise lineer ilişki içinde olduğu görülmüştür. Salınım genliği ile açıklık ve dalga parametreleri arasında matematiksel bağlantı kurulmuş ve bu bağıntının deneysel verilerle uyum içinde olduğu görülmüştür. Bu matematik ilişki kullanılarak salınım genlikleri yapı sualtı açıklık ve dalga parametrelerine göre bulunabilmektedir. Su sütunu yüzeyi profil davranışları, dalga parametreleri ve yapı sualtı açıklık yüksekliğine göre belirlenmiştir. Tek serbestili basit mekanik modelleme yaklaşımı kullanılarak daha genel bir matematik model geliştirilmiştir. Bu yaklaşım basit olmasına rağmen, su sütunu harektlerinin dinamik özelliklerini bünyesinde barındırabilmektedir. Bu yaklaşımşla modellenen su sütunu hareket denklemleri aynı zamanda SSS yapısının termodinamik denklemlerine bağlı olduklarından ötürü ancak beraber eşzamanlı olarak çözülmeleri gerekmektedir. Bu yüzden su sütunu hareketlerinin doğru modellenmesi önemlidir. Geliştirilen matematik modelin çözümlenebilmesi için tespiti gerekli olan toplam lineer eş sönümleme katsayısı lineer bir yaklaşımla, daha önce literatürde kullanılmamış olan serbest salınım deneysel testleriyle bulunmuştur. Dalga parametrelerinden bağımsız olarak belirli bir yapı sualtı açıklığının minimum sonümle katsayısına karşılık geldiği görülmüştür. Böylece su sütunu salınım genlikleri ve gelen dalgaya göre faz açıları hesaplanmış, sonuçlar deneysel verilerle doğrulanmıştır.

Az sönümlenmiş sistemler için ise, ilk defa, serbest salınım metodu kullanılmak suretiyle SSS hidrodinamik parametreleri; toplam lineer eş sönümleme katsayısı, eklenmiş kütle, doğal ve rezonans frekans değerleri lineer bir yaklaşımla tahmin edilmeştir. Bu metot ayrıca üç boyutlu nümerik modelleme tekniği ile de simüle edilmiş ve deneysel çalışmalarla karşılaştırılarak doğruluğu tasdik edilmiştir. Böylece çok daha ucuza ve az bir zamanda, serbest salınım metodu, numerik çalışmalarla farklı geometrik ve hidrodinamik parametrelere sahip yapılar için, farklı zemin ve gelen dalga şartlarında uygulanabilecektir. Az sönümlü SSS yapılarında, sönümleme katsayısının orifis çapı arttıkça ve sualtı açıklığı miktarı düştükçe, azaldığı görülmüştür. Bulunan sönümleme katsayısı, ilk defa, suya daldırılmış olan yapı ön duvar altındaki sürtünme ve oluşabilecek çevrinti etkilerinide içinde barındırmaktadır. Bulunan hidrodinamik parametreler, geliştirilen tek serbestili basit mekanik modelde kullanılmış ve salınım zaman serileri hesaplanmıştır. Salınım zaman serileri deneysel olarak da ölçülmüş ve yapı yüzeyinde aşırı çalkantıların olduğu durumlar hariç mekanik model sonuçları ile çok uyumlu bulunmuştur. Su sütunu yüzey çalkantılarının yapının dalga geliş yönündeki genişliğinin dalga boyuna oranının bir fonksiyonu olduğu tespit edilmiştir. Bu oran küçüldükçe çalkantı miktarının arttığı tesbit edilmiştir. Su sütunu içinde oluşan ve yapının hidrodinamik verimliliği açısından istenmeyen bir hareket çeşidi olan çalkalanmanın, sönümleme miktarı arttıkça (orifis çapı arttıkça) ve su altı yapı açıklığı düştükçe, azaldığı görülmüştür. Daha önce literatürde, SSS yapılarının doğal frekansının hesaplanmasında farklı sistemler için geliştirilen anpirik formüller kullanılınırken, bu çalışmada elde edilen deneysel verilerle, ilk defa sadece salınımlı su sütunu doğal frekansı için yeni bir ampirik formül geliştirlmiştir. Eklenmiş kütlenin ise her koşulda belli bir aralıkta olduğu tesbit edilmiş ve literatürde bulunan daha önceki çalışmalarla uyumlu olduğu görülmüştür.

Son olarak SSS yapısının enerji dönüşüm verimliliği nicel ve nitel olarak, bu çalışmada kullanılan farklı dalga parametreleri, yapının sualtı açıklığı ve değişik türbinlerin oluşturduğu sönümleme miktarları için deneysel ölçümlerle hesap edilmiştir. Farklı parametrelerin verim üzerindeki etkisi araştırılmış, optimum türbin sönümleme ve sualtı açıklık yüksekliği gelen dalga özelliklerine göre belirlenmiştir. Sonuçlar göstermektedir ki, belli bir dalga eğimi aralığında, optimum tribün sönümleme düzeyi sadece dalga parametrelerine göre değil aynı zamanda yapının sualtı açıklığı yüksekliğine göre değişmektedir. Ayrıca, tahmin edildiği üzere çalkalanmanın enerji verimliliği üzerinde çok ciddi olumsuz etkileri olduğu nicel olarak da görülmüştür.

1. INTRODUCTION

1.1 Background

It is a well-known fact that, replacing our current energy sources with renewable ones is very crucial for our future (Url-1). While energy demand is increasing by growing population and industry, with the realization that conventional energy sources are still excessive and more accessible than others, it is not an easy task (Url-2). But unlimited and almost untapped ocean wave energy which has relatively greater power intensity compared to solar and wind energy, can be one of the auxiliaries in helping humanity achieve their responsibility for future generations. Ocean waves provide approximately 26.000TWh energy per year in a global scale (Mark et al., 2010). Efforts have already been ended up more than 1000 wave energy extraction devices and techniques patented in the world (McCormick, 1981).

Currently, four main types of wave energy conversion technology are present namely point absorbers, overtopping terminators, oscillating water columns (OWCs) and attenuators (Mahnamfar and Altunkaynak, 2017; Falcao and Henriques, 2016). However, OWC type WECs are the most promising and studied one with its simplicity, accessibility, reliability, stability, adoptability and, environmental friendly and easy to construct features. Moreover, bottom standing OWC has no moving parts under water providing much easier maintenance. OWC device can also be integrated into breakwaters to absorb part of the incident wave energy as well as to generate electricity in a cost sharing fashion. Therefore, OWCs are well accepted by the wave energy community. It consists of a partially submerged hollow chamber with a seaward opening beneath the water level that has air trapped above it and a narrow duct at the top or rear of the device open to the atmosphere. Oscillating dynamic pressure under the incident waves acting on the inlet cause the water column inside the chamber move in a reciprocating manner which, in turn, generates the pressure variations above it. Pressure air differential formed in the chamber forces air to flow in and out with high velocities through the duct. Then the generated pneumatic power can be further converted into electric power by a bidirectional turbine attached to the device which turns in the same way independent of airflow direction. A navy officer of Japan Yoshio Masuda, who is one of the first pioneers in the field, used wave energy to power navigation buoys oscillating under random waves with a turbine attached. This system is named as oscillating water column afterwards (Falcao and Henriques, 2016).

OWCs are the most studied type of WECs due its vast advantages. This accumulation of knowledge paved the way to the stage of deploying full-scale prototypes such as bottom-standing 400kW Pico Plant on the Island of Pico, Azores, Portugal, 500kW LIMPET OWC plant on the Island of Islay, Scotland, UK, Oceanlinx OWC, Port Kembla, Australia, a breakwater integrated OWC at the port of Mutriku in Northern Spain. It is reported that in the Limpet OWC system, more than sixty thousand kilowatts of energy have been generated and transmitted to the national energy grid (Heath, 2012). However, unfortunately, some of the OWCs were destroyed during or after the installation due to the harsh sea conditions (Falcao and Henriques, 2016) and what is worse is actualized hydrodynamic efficiencies have found to be well below the predicted values (Carbon Trust, 2005).

Despite the progress been made, it is not a straightforward task to figure out a unique design and commercialize it globally because the wave climate is not the same everywhere and wave-body and two-phase fluid interactions are very complex to be solved mathematically and by numerical methods; even full Navier-Stokes solver CFDs cannot cope with the related complexity of the wave energy conversion processes. Hence, hydrodynamics of an OWC structure has not been comprehended by all means and much still remains to be accomplished (Drew et al., 2009; Heath, 2012; Hsieh et al., 2012; Lopez et al., 2015; Ning, et al., 2016; Panelba et al., 2017). This is the reason that wave energy converter (WEC) technology has not been reached to a cost-effective level to compete with more developed renewable energy sources (i.e. wind and solar energy) (Simonetti et al., 2017).

With this motivation, in this thesis, comprehensive experimental, analytical and numerical investigations have been conducted to contribute to the existing core body of knowledge and improve the state of art technology. As stated previously, flowing data from the active prototypes indicates that performance of the OWC type wave energy converters are lower than that of expected. To increase the overall efficiency of an OWC, identifying the most relevant and significant factors is of great importance.

A comprehensive literature survey, in that respect, indicates that underwater opening size of the OWC chamber (Evans and Porter, 1995; Zhang et al., 2012; Luo et al., 2014; Mahnamfar and Altunkaynak, 2015; Çelik and Altunkaynak, 2018), applied PTO damping (He and Huang, 2014; Lopez et al., 2014 and 2015; Rezanejad et al., 2017; Brusca et al. 2017; Simonetti at al. 2017) and incident wave characteristics (Kamath et al 2015; Mahnamfar and Altunkaynak, 2015; Ning et al. 2016; Elhanafi et al., 2017; Mahnamfar and Altunkaynak, 2015 and 2017; Kuo et al., 2017; Çelik and Altunkaynak, 2018) are the most influential parameters on device performance. Some studies also refer to the sloshing of the water column surface which is reported as a reduction factor on the performance of the device yet a wide experimental investigation of this phenomenon does not exist in the literature.

Therefore, all utilized methods within this thesis to better understand the dynamics of the wave energy conversion processes will include the effects of these parameters.

Methods that will be utilized for the objectives of this thesis, will include experimental and analytical approaches and, numerical methods to a certain degree. Although advanced CFD softwares have progressed in modelling complex geometries and revealed the nature of different wave energy conversion aspects in a more realistic fashion, they are still expensive, time-consuming and need high computational power. Besides, numerical methods have their inherent limitations; i.e. errors associated with numerical methods inevitably penetrate into the results. Thereby, application of numerical methods in the scope of this study will be limited. Additionally, experimental validation is always required due to the challenging nature of highly non-linear wave-converter interactions and air-water coupling dynamics (Ning et al., 2016). In this respect, experimental analysis plays a significant role in the design and optimization process of OWC development by ensuring better understanding of complex phenomena arising from non-linear and two-phase fluid structure interactions.

Oscillation of the water column under harmonic dynamic pressure of the incident wave is the starting point of the wave energy conversion. That is, incident wave energy is conveyed to the air column by the motions of the water column. Furthermore, by the nature of the OWC type wave energy conversion technology, water column motions are coupled with the thermodynamic and aerodynamic processes and therefore have to be solved simultaneously. Because of this, accurate mathematical modeling of the water column motions is not only essential but an initial requirement to solve the air dynamics as well as to estimate the hydrodynamic efficiency of the wave energy converter. In addition, developed mathematical model has to be applicable for different kind of design and environmental parameters and, power take off dampings under different operation conditions before constructing a full-scale prototype. Because, any failure at this stage would waste considerable amount of money and labor force and more importantly, reduce motivation.

To model the water column surface motion, a simple mechanical model has been utilized for this thesis. Simple mechanical modelling is a rather simple yet beneficial analytical approach to describe the motion of the water column free surface without compromising any essential features of the phenomenon. (Karami et al., 2012; Fairhurst and Van Niekerk, 2016; Lino et al., 2016; Rezanejad and Soares, 2018). As already discussed, equations of simple mechanical model are coupled with the thermodynamic and aerodynamic equations of the air column. Hence, rather simple equations obtained from mechanical modelling can be solved simultaneously with the related thermodynamic equations of the air column dynamics (Freeman et al. 2013). However, for simple mechanical modeling to yield correct results, accurate estimation of the hydrodynamic coefficients, i.e. added mass and system damping, is essential. At this point, by free decay tests, some of the hydrodynamic parameters (i.e. damping, added mass, resonant and natural frequency) of an OWC device may be predicted.

For the first time, in this thesis, experimental free decay tests are carried out for WECs. LDM method is utilized to approximate the overall damping (representing all damping forces that the OWC experiences) and added mass of the OWC system. In effect, experimental free decay test is a commonly used technique in Naval and Offshore engineering (Asmuth et al., 2015; Handschel et al., 2015; Liu et al., 2016). However, implementation of free decay test for OWCs are very limited. Recently, in their 2D CFD model, Simonetti et al. (2015), Elhanafi et al. (2017) and Vyzikas et al. (2017) utilized free decay tests and estimated the resonant frequency of an OWC via logarithmic decrement method (LDM). The studies did not mainly focus on the free decay tests but rather performed in a supplementary fashion. To the best of author's knowledge, free decay tests have not been carried out for any WEC experimentally. One of the advantages of the LDM method is that, additionally, it enables the calculation of natural and resonant frequencies of the OWC device by using free decay test data. This is particularly important because, to extract the most of the incident wave energy, resonant frequency of the WEC device has to be tuned to the prevailing incident wave frequency of the installation region. Near the resonant condition, restoring and inertial forces acting on the water column cancel each other and the dynamics of the water column is driven by the excitation force and the damping of the system (Chakrabarti and Cotter, 1991; Rao, 2011). Therefore, determination of system's damping has a particular importance in understanding the related dynamics of the water column near resonant frequencies. Accurate estimation of the resonant frequency of the OWC device for various underwater chamber opening sizes and PTO dampings will enable the abovementioned tuning process. On the other hand, natural frequency of a dynamic system reveals important information about the underlying physics. Accordingly, accurate prediction of natural and resonant frequencies is of great importance. Admittedly, experimental model-scale studies are not easy. Performing model-scale tests for various geometrically different wave energy converters would be very expensive and time consuming with a quite amount of labor force. On the other hand, numerical computational methods would be very advantageous over experimental studies if accurate results would be obtained (drawbacks of numerical methods were mentioned previously). The desired change in the virtual experimental setup can be carried out relatively easier and quicker so that many possible configurations and alterations relating OWC geometry and surrounding environment would be easily performed. Free decay test is rather simple method to implement yet reveals significant information about wave energy conversion process. For instance, complicated wave-structure interactions do not exist due to the absence of incident waves. Consequently, it is considered that advanced CFD softwares should accurately replicate the experimentally obtained free decay data due to the reduced complexity. Therefore, commercial CFD software Flow 3D will be utilized to virtually model the experimental setup and simulate the free decay tests.

Scientifically, any kind of developed model has to be validated according to the experimental data (Ibn al-Haytham, 1021). Therefore, obtained analytical model results are compared with experimentally measured water column surface oscillation data under same incident waves to validate the developed mathematical model which also implies the validation of the hydrodynamic parameters.

To estimate the maximum hydrodynamic efficiency of a wave energy converter with respect to various significant related factors, physical experimental model scale tests have to be performed. As discussed previously, underwater opening size of the chamber, PTO damping and incident wave properties are the most influential factors on the performance of an OWC device. However, comprehensive literature review designates that there is not an experimental model scale study that extensively investigates the effects of these factors on the device performance in a consolidated manner. To approximate the PTO damping for a particular opening size and vice versa that yields the maximum efficiency under a specific wave climate, to understand the interrelations between PTO damping and opening height of the chamber for various wave conditions and how the hydrodynamic characteristics of an OWC are influenced by these factors are crucial in terms of wave energy conversion efficiency. Therefore, in this thesis, a comprehensive experimental campaign has been carried out to investigate the coupling between the underwater opening, PTO mechanism and incident wave parameters, possible sloshing effects in the chamber and quantify the hydrodynamic efficiency of a bottom-fixed OWC with different combinations of chamber opening heights and PTO dampings (simulated by various orifice diameters) under the excitation of different regular wave conditions for optimization of the OWC efficiency.

1.2 Purpose Of The Thesis

The objectives of the studies conducted in this thesis can be stated as, to develop a simple yet accurate mathematical model to predict the water column average oscillating amplitudes and phase angles under the excitation of regular incident waves; to obtain, for the first time, damping, added mass, natural and resonant frequencies of a widely used generic, rectangular cross-sectioned OWC type WEC for different underwater chamber openings and PTO dampings via performing physical experimental free-decay tests and utilizing LDM method; to perform physical experimental model scale tests and measure the average water column surface oscillating amplitudes under the excitation of same regular waves used in the analytical model; to compare the experimentally and analytically obtained average oscillating amplitudes and validate the determined hydrodynamic parameters and representability of the water column surface dynamics by a simple mechanical model; to investigate the effects of different chamber underwater opening and PTO damping values that an OWC possess on its chamber water column surface average oscillating data and motion behaviors and performance of the device under various regular wave conditions by analytical and physical experimental model-scale methods; to investigate the coupling between the underwater opening and PTO mechanism and quantify the hydrodynamic efficiency of a bottom-fixed OWC with different combinations of chamber opening heights and PTO dampings (simulated by various orifice diameters) under the excitation of different monochromatic wave conditions for efficiency optimization purposes and to gain physical insights and better understand the complicated wave-structure and two phase fluid interactions of the wave energy conversion processes and if possible, develop empirical relationships that ease the complexity of mathematical representations.

1.3 Literature Review

First attempts of theoretical analysis for an OWC device were conducted by McCormick (1974, 1976) on wave energy conversion buoys and accelerated during the 1973 oil crisis. Evans (1978) used a rigid body model and studied the hydrodynamics of a fixed OWC system theoretically ignoring the spatial variation of the free surface in the chamber. He assumed the free surface of the chamber as a rigid weightless piston with a small width relative to the incident wave length. Under these assumptions oscillating body theory was able to be used. Rigid-body approach was improved by allowing simulation of non-uniform pressure distributions on the free surface of the water column (Falcao and Sarmento, 1980; Falnes and McIver, 1985). Evans and Porter (1995) considered a two-dimensional simple theoretical model of a fixed OWC and attempted to calculate the hydrodynamic characteristics of the system. They developed an approach using Galerking Method. They claimed that immersion depth of the front wall and chamber length are the main parameters affecting the hydrodynamic efficiency. While early theoretical and numerical studies implemented potential flow theory, by the increase of computational power, computational fluid dynamics (CFD) softwares based on fully non-linear Navier-Stokes equations have been utilized as analysis tools. Zhang et al. (2012) numerically investigated the hydrodynamic performance of an OWC under different wave conditions and front wall geometries. After validation of their results with previous experimental investigations, they found that immersion depth of the front wall is a main parameter for device performance, however, orifice dimensions should also be chosen adequately so that the necessary pressure differential could form in the air chamber for sufficient energy extraction. Lopez et al. (2014, 2016) implemented a validated Reynolds averaged Navier-Stokes volume of fluid (RANS-VOF) model and tested different incident waves with a wide range of damping levels by taking site-specific wave climate variability into consideration. They outlined the relevance of the PTO damping on the efficiency of the OWC device, so that, it is the most important parameter that must be optimized for the wave climate of the desired region. Kamath et al. (2015) also used a two-dimensional (2D) CFD simulation to explore the effects of PTO induced damping on the hydrodynamics of the chamber but, differently, PTO damping on the chamber is modeled by Darcy's law for flow through porous media. They showed that OWC device with a PTO damping can be modeled by numerical methods successfully thus, useful insight can be obtained. Ning et al. (2016) simulated the dynamic wave forces on the front wall of a fixed OWC converter. They found that the incident wave force is strongly related to the ratio of water column surface area to orifice area and total wave force decreases with the increase of the wavelength and increases with the raising wave height. Mahnamfar and Altunkaynak (2017) compared two different OWC designs with both fully non-linear CFD software and physical experimental modelling. They found that the numerical model results tend to follow the experimental values very closely and concluded that CFD softwares are promising tools for modelling wave energy conversion and obtaining physical insights about wave-converter interactions. Elhanafi et al. (2017) used a fully non-linear CFD model to analyze the device performance with respect to different wave parameters and turbine damping. They concluded that all tested parameters namely the wavelength, wave height and turbine damping are important for efficiency with a special emphasize on the front wall geometry of the chamber due to energy dissipating vortex generation. Kuo et al. (2017) used the commercial software FLOW 3D to investigate the so called "capture width" (a performance indicator) of a full-size OWC caisson breakwater under different wave parameters. The result was that the relationship between the maximum average power produced by alternating air and dimensionless wavelength ratio can be implemented to optimize the design features of OWC caisson breakwaters.

On the other hand, experimental investigation is a vitally important tool for wave energy converter (WEC) analysis. Wang et al. (2002) performed physical model scale experiments in a wave flume to investigate the effects of different bottom slopes on the hydrodynamics of OWC converters. They concluded that near bottom depths influence the hydrodynamic efficiency of the OWC type wave energy converters. Morris-Thomas et al. (2007) experimentally investigated the effects of the front wall geometry on the hydrodynamic efficiency of a fixed OWC tool under monochromatic waves. They observed that magnitude and shape of the efficiency curves are affected from the geometry of the front wall. Hsieh et al. (2012) experimentally studied two chamber OWC type wave energy converters and reported that this kind of design can improve the overall hydrodynamic efficiency. He and Huang (2014) conducted physical experiments to research the hydrodynamic performance of a pile-supported OWC structure as a breakwater. They revealed that, in addition to their high hydrodynamic performance as a breakwater, pile-supported OWC structures can also be used to extract wave energy. Lopez et al. (2015) used particle imaging velocimetry (PIV) technique to investigate the flow characteristics of wave structure interactions. They found that turbine-induced damping and the front wall lip of the OWC structure are very important parameters for wave energy utilization. Chang et al. (2016) conducted experiments to investigate the geometric design parameters of an OWC converter. They found that back plate angle optimization is crucial for enhancing the wave amplification factor inside an OWC tool. Mahnamfar and Altunkaynak (2015) made an investigation for the optimization of an OWC system by using both physical and numerical models. They changed the geometric parameters of an OWC structure with an angular front plate and tested at several circumstances. Experimental model results were compared with the numerical model results. Nash-Sutcliffe coefficient of Efficiency (NSE) parameter was used as performance evaluation criteria and the NSE values found to be 0.97. Çelik and Altunkaynak (2018) performed physical experiments to optimize the chamber geometry of an OWC for various wave conditions. They developed mathematical model to predict water column fluctuations under varying relative opening heights with respect to different wave characteristics using the experimental data.

1.4 Hypothesis

Simple mechanical modeling methods and free decay tests are mostly used for oscillating rigid bodies, where, oscillating fluids in U-tubes or connected reservoirs, water masses in the moonpools that are located in the ship-hulls are a few exceptions. Therefore, water column trapped in a hollow chamber is considered to be modelled by a simple mechanical model and accordingly free decay tests are suitable for obtaining hydrodynamic parameters. Due to exponentially increasing energy density under an incident wave, transmitted wave energy into the chamber should increase with underwater opening height of the chamber yielding greater hydrodynamic efficiency. However, as the opening height increase, stronger wave structure interactions that may distort the stability of the water column and air leakage occurrence under the front wall of the chamber which would depressurize the air column, are expected. While applied PTO damping enables the wave energy extraction, relatively higher damping values (relatively large orifice sizes) are thought to suppress the water column oscillations. On the other hand, relatively lower PTO damping values (relatively smaller orifice sizes) should not be enough to form a noteworthy differential air pressure for feasible incident wave energy extraction. Hydrodynamic efficiency is considered to be maximum for an optimum PTO damping value. Incident wave properties, obviously, have to be important in terms of conveying wave energy in to the chamber in the form of oscillating water column kinetic energy, in a relative smother and extractable form.

2. MATERIALS AND METHODS

2.1 Physical Experimental Model-Scale Tests

In this thesis, three distinct experimental studies are performed namely, free decay, incident wave force determination and water column oscillation and pressure tests. Experiments are conducted in 21m long 1m wide and 1m depth wave flume present in the Hydraulic Laboratory of Istanbul Technical University as shown Figure 2.1. All measurements are sampled at an average rate of 125Hz by a 64-bit data acquisition system and stored in the computer for future analysis. All physical and numerical experiments are conducted in still water with a depth of 0.60 m.

Figure 2.1 : Laboratory wave flume

For this research, a fixed generic bottom-standing type, 1:30 scale of the full-size prototype OWC with a rectangular cross-section is chosen for experiments. OWC is constructed from 0.15m thick transparent plexiglas material for its strength and observational purposes. Front wall opening of the chamber was adjustable for different heights. Figure 2.2a is a physical picture of the OWC device and Figure 2.2b illustrates the OWC along with its dimensions. Power–take off mechanism (PTO) is simulated by an orifice. To generate various PTO damping values different orifice sizes are used. OWC is installed longitudinally in the wave flume in such a way that the sidewalls of the OWC are parallel to the glass walls of the wave flume. Totally, 243 sets of experiments are conducted in this study.

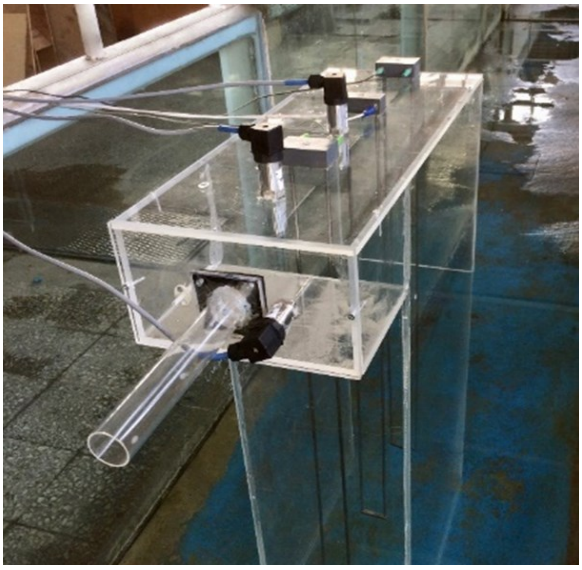

Figure 2.2 : Physical picture of the OWC used in experiments.

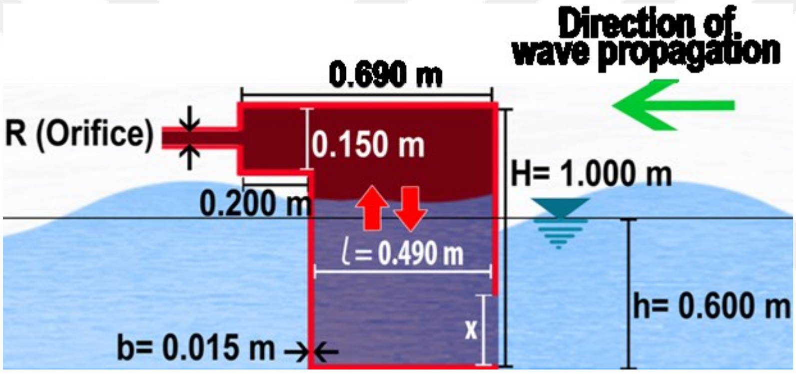

Figure 2.3 : Dimensions of the OWC system.

2.1.1 Free decay tests

For the free decay tests initial water level in the chamber is elevated to a predetermined value by generating negative gauge pressure in the air column via a vacuum pump and afterwards, outlet of the orifice is closed by a cap. To ensure that the OWC is air-tight, all joining parts and the cap is carefully controlled and no change in the elevation of the raised water column is observed (indication of no air leakage). When the cap is removed initially excited water column experiences freely decaying oscillations with respect to still water level. Data is recorded as time series for future analysis. Two different initial displacement values are considered, 0.10m and 0.15m, however, calculated hydrodynamic parameters by using both initial values were very close to each other. This implies that the results of this study is found to be independent of the chosen initial displacement value where, Simonetti et al. (2015) also reported the same result in their study. A typical time history of free decay of the normalized water column surface oscillation (with respect to still water depth) is depicted in Figure 2.3.

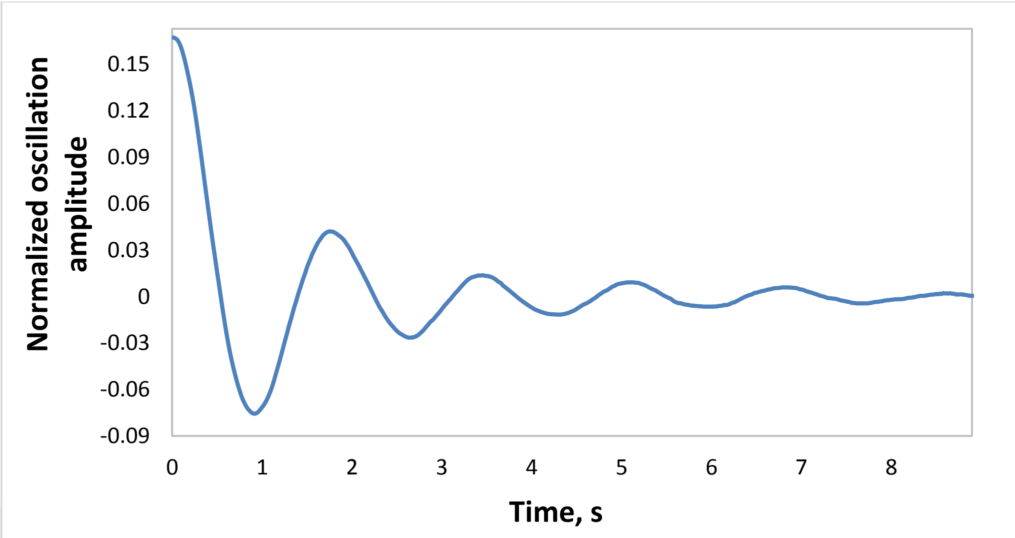

Figure 2.4 : A typical recorded experimental free decay time-series.

Resistance type twin-wave gauges are used for measuring water column surface displacements. To capture any possible distortion of the surface, three wave gauges are installed on the right, middle and left center of the chamber roof as shown in Figure 2.4 and Figure 2.5. Measurements from the wave gauges are averaged to obtain a representative value. As the water column oscillates waves are radiated out of the chamber through the underwater opening. To prevent the reflection of the radiated waves from the wave generating plate, it is disassembled and a wave absorbing beach with a 1:4 slope is constructed at the far end of the wave flume. Overall experimental set up is indicated in Figure 2.6.

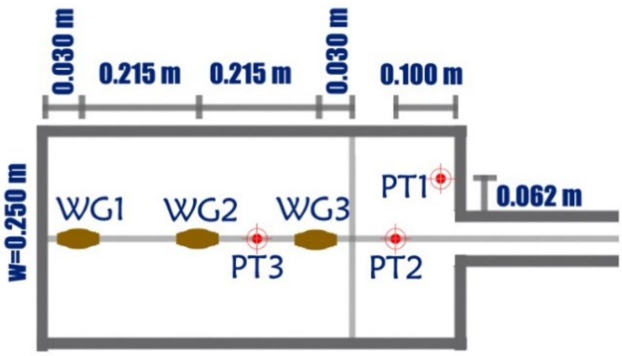

Figure 2.5 : Top view of the OWC.

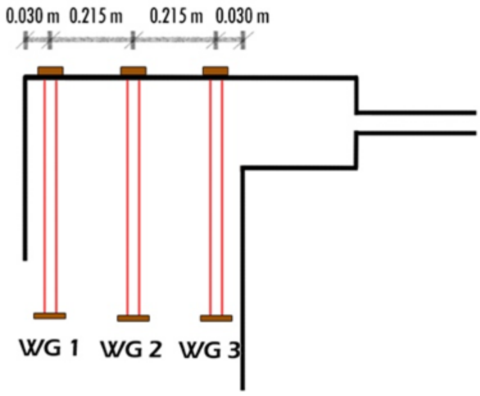

Figure 2.6 : Wave gauges inside the chamber.

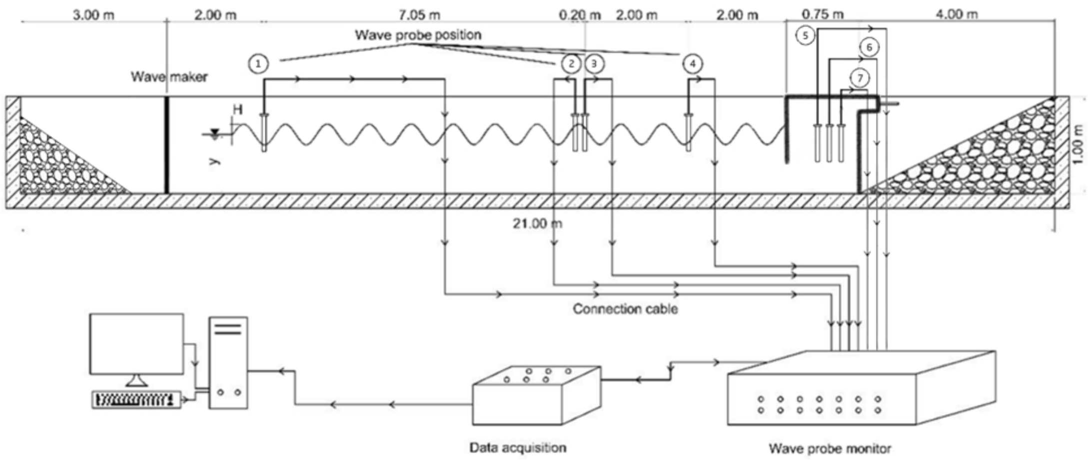

Figure 2.7 : Overall schematic of the experimental set-up.

Opening heights, immersion depths and orifice sizes are expressed in dimensionless forms:

$$\alpha = \frac{x}{h} \tag{2.1}$$

$$\beta = \frac{y}{h} \tag{2.2}$$

$$\tau = \frac{A_o}{A_w} \tag{2.3}$$

where, α is the relative opening, β is the relative immersion, $\underline{x}$ is the underwater opening height of the chamber (m), $\underline{y}$ is the immersion depth of the frontwall (m), h is the still water depth (m), τ is the orifice ratio, A_o and A_w represent the cross-sectional orifice area and the water column surface area (m^2), respectively. Table 2.1 and Table 2.2 shows the values of the used relative openings and orifice ratios in this study, respectively. Smallest orifice size is given by the suffix 6 rather than 1 to indicate a significant distinction in the system dynamics where it is the only case that OWC is overdamped.

Table 2.1 : Various relative opening heights and immersion depths.

Case No	$\underline{x}$	$\underline{y}$	α	β
Case 1	0.20	0.40	0.33	0.67
Case 2	0.25	0.35	0.42	0.58
Case 3	0.30	0.30	0.50	0.50
Case 4	0.35	0.25	0.58	0.42
Case 5	0.40	0.20	0.67	0.33
Case 6	0.45	0.15	0.75	0.25
Case 7	0.50	0.10	0.83	0.17
Case 8	0.55	0.05	0.92	0.08
Case 9	0.60	0.00	1.00	0.00

Table 2.2 : Orifice ratios used in this study.

τ	τ_1	τ_2	τ_3	τ_4	τ_5	τ_6
Orifice ratio	0.40%	0.58%	0.79%	1.03%	1.30%	0.30%

Free decay tests are performed for nine different opening heights and four different orifice sizes. However, two largest opening heights did not yield any valuable data because of the air leakage under the front wall of the chamber when the trough of the incident wave reaches the front wall.

2.1.2 Incident wave force determination tests

To solve the simple mechanical model of the oscillating water column (will be described later in the section), incident wave forces acting on the water column have to be obtained. For the purposes of this study, regular waves with different characteristics are generated. Parameters of the generated incident waves are tabulated in Table 2.3, where, the first column refers to the generated incident wave number, H is the wave height (m) and T is the wave period (s). Figure 2.7 illustrates a 3D representation of the OWC in the wave tank with direction of wave propagation along with the transverse dimensions.

Table 2.3 : Parameters of generated waves.

Parameter	W1	W2	W3	W4
H (m)	0.07	0.11	0.13	0.12
T (s)	1.8	1.26	1.06	0.88

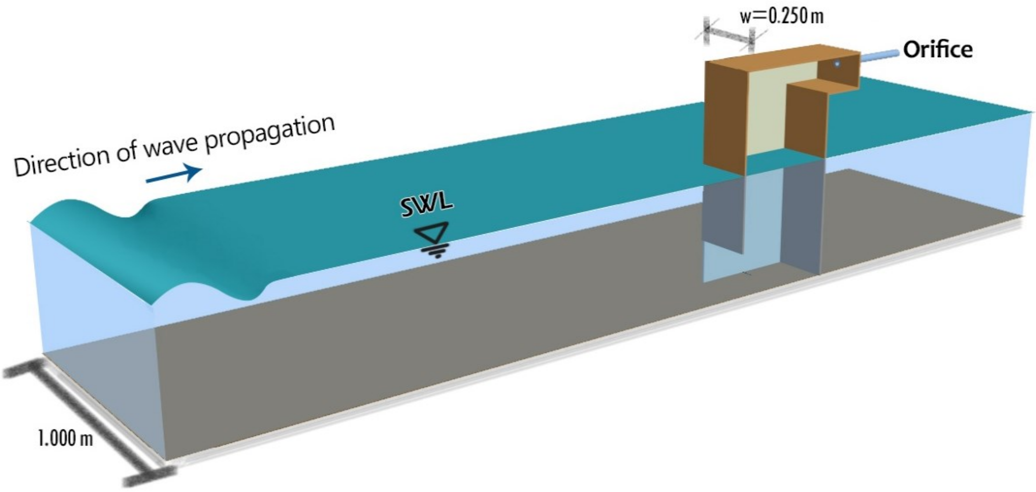

Figure 2.8 : 3D representation of the OWC in the wave.

To determine the incident wave forces orifice of the system is sealed carefully to avoid any air leakage during the tests and air pressure in the chamber is measured by three pressure transducers and averaged (Kelly et al. 2017; Stewart 1993). Locations of the pressure transducers are shown in Figure 2.4. However, in order to determine the wave forces incident on the water column accurately, air column has to be incompressible. During the closed orifice tests, measurements and observations indicated that the water column remained almost stationary under the bombardment of all generated incident waves justifying the incompressibility assumption. Besides, several studies (Sheng et al. 2013; Sheng and Lewis, 2016; Kelly et al. 2017; Çelik and Altunkaynak, 2018) reported that for small-scale model tests air inside the chamber can safely be considered incompressible. OWC structure is immobilized to the wave flume carriages with F-type iron claps to prevent any possible movement. Water column displacement and pressure measurements are limited to 25 seconds to avoid any corruption of data by reaching the re-reflected waves from the wave generator plate to the OWC structure. A period of four minutes (more if necessary) is placed between the two successive generation of incident waves to damp out any possible residual energy present in the wave flume. In addition, a beach with a 1:4 slope is constructed at the near end of the wave flume to absorb the ongoing waves past the OWC structure. Wave force (N) is calculated by the equation:

$$F = P_{air}(t)A_w \tag{2.4}$$

where, $P_{air}(t)$ is the averaged gage pressure (Pa) of the air column. Figure 2.8 illustrates a typical example of wave force time history with respect to dimensionless time (time (t) divided by period of the generated wave (T)). Sinusoidal approximation of the force time series data, which very well represents the measured wave forces are also inserted into the figure. Amplitudes of the sinusoidal approximation is calculated by averaging the experimentally obtained amplitudes after the steady state motion is attained.

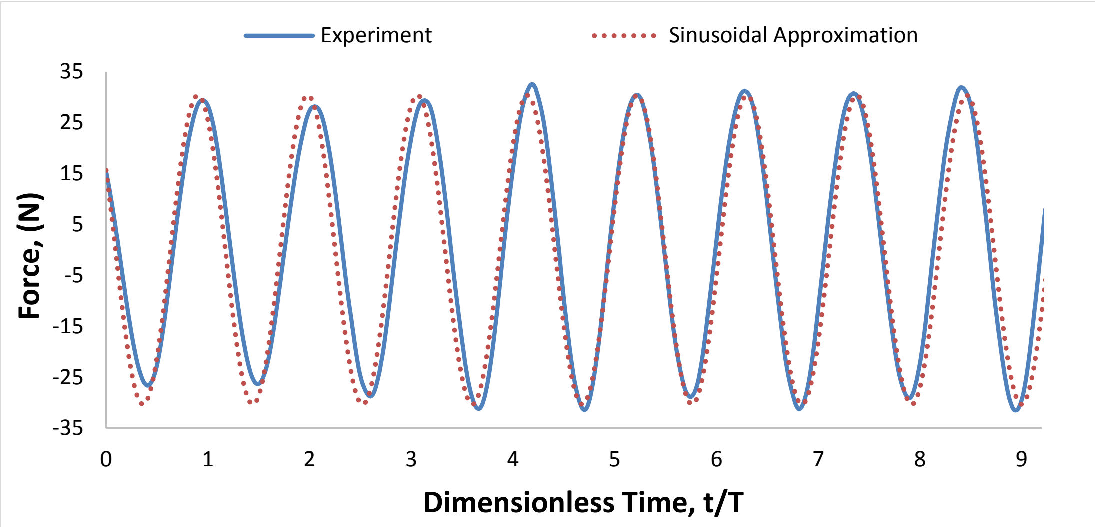

Figure 2.9 : An comparison of a wave force time series (W1 and $\alpha = 0.50$).

2.1.3 Water column oscillation and pressure tests

The same setup as in the previous case is used for the experiments, however, in this particular experiment orifice is opened to the atmosphere so that the water column was able to move freely. The objective of the water column oscillation and pressure model tests was to measure the average water column displacements under the forcing of the incident waves for all the relative openings and orifice ratios utilized, in order to compare the experimental model results with the analytical model values and calculate the hydrodynamic efficiency of the OWC device.

2.1.4 Scale-model effects

Experimental model scale tests, which are performed in a controllable and accessible environment with repeatable conditions are crucial for improvement of wave energy conversion technology. Optimization and assessment of the device performance may be obtained easily in a cost and time-effective manner. However, extrapolation of obtained results to full-scale prototype requires careful consideration to avoid undesirable scale effects. Accordingly, length scale is defined as (Hughes, 2014):

$$L_r = \frac{L_m}{L_p} \tag{2.5}$$

Herein, L_m and L_p are the corresponding lengths of model and prototype, respectively where subscripts m and p stand for model and prototype, respectively (Falcao and Henriques, 2014).

To attain full-similarity, numeric values of both Froude number (Fr) and Reynolds number (Re) have to match for both prototype and model scales (Payne, 2008), which is the case for many free surface flow problems. Froude number and Reynolds number are defined as:

$$Fr = \frac{U}{\sqrt{gL}} \tag{2.6}$$

$$Re = \frac{\rho U L}{\mu} \tag{2.7}$$

where U is the characteristic velocity (m/s), g is the acceleration of gravity (m/s^2), ρ is the density (kg/m^3), μ is the dynamic viscosity (kg/ms) and L is the characteristic length of the system (m). However, in practice, to retain Froude number and Reynolds number same for both model scale and full-scale is almost impossible to achieve (if L_r is not close to unity) since it requires to increase g and/or decrease ν, where ν is the kinematic viscosity (m^2/s) (Payne, 2008; Falcao and Henriques, 2014).

$$\nu = \frac{\mu}{\rho} \tag{2.8}$$

Fortunately, in general, viscous effects are negligible during the wave-structure interactions and thus similarity can be attained if Froude numbers of both prototype and model scale match. This fact is a general modelling rule (Payne, 2008; Hsieh et al., 2012; Falcao and Henriques, 2014; Sheng et al., 2014; Vyzikas et al. 2017). Therefore, Reynolds similarity is neglected in this study and constancy of Froude number for model and prototype scale has been considered.

As mentioned previously, incompressible air assumption is reasonable in small-scale model experiments. However, compressibility effects can be significant in full-scale size prototypes. If geometric similarity is achieved by a scale factor of L_r, obviously, volume scale factor of the chamber becomes:

$$L_\forall = \frac{\forall_p}{\forall_m} = (L_r)^3 \tag{2.9}$$

where, $\forall_p$ and $\forall_m$ represents the volume of the model and the prototype respectively.

However, to accurately scale the air compressibility using Froude similarity, chamber volume scale ratio has to be ${L_r}^2$, rather than ${L_r}^3$ (Falcao and Henriques, 2014; Sheng et al., 2014). Therefore, care has to be taken when interpreting the results since Froude similarity used in this study does not take compressibility effects correctly into account. Weber (2007) investigated the effects of neglecting air compressibility in the model-scale experiments and reported that, on average, approximately 10% reduction on the efficiency of the OWC type wave energy converter should be considered if the scaling requirement of air compressibility is omitted. Therefore, obtained efficiency values in this study, has to be considered as an upper-bound when the results are extrapolated to full scale size prototype.

2.2 Analytical Methods

2.2.1 Simple mechanical modeling

Simple mechanical modeling, which assumes rigid-body motion of the water column, is a rather simple yet beneficial analytical approach to describe the motion of the water column free surface without compromising any essential features of the phenomenon if large sloshing in the chamber does not take place (Karami et al., 2012; Fairhurst and Van Niekerk, 2016; Lino et al., 2016; Rezanejad and Soares, 2018). Fortunately, in practice, most of the wave energy applications involve planar surface fluctuations (Wang et al, 2002) and this fact coincides with the rigid-body assumption of the developed mathematical model. On the other hand, equations of mechanical modelling are coupled with the thermodynamic and aerodynamic equations of the air column. Hence, rather simple equations obtained from simple mechanical modelling can be solved simultaneously with the related equations of the air column dynamics (Freeman et al., 2013).

Therefore, in this thesis, a simple mechanical model, which is the equation of motion of a rigid-body merely derived from Newton's second law, is implemented to simulate the water column surface motions in the chamber. With the assumption of linear PTO damping; radiation, viscous and PTO dampings can be represented in the mechanical model in a single damping term. Accordingly, equation of motion of the water column can be expressed as:

$$(m + m_a)\ddot{y}(t) + d\dot{y}(t) + \rho g A_w y(t) = F_{exc} \quad (2.10)$$

where, $y(t)$ is the vertical displacement (m) of the water column with respect to still water level, $\dot{y}(t)$ (m/s) and $\ddot{y}(t)$ (m/s^2) are the first and second time derivatives of the water column displacement, respectively, F_{exc} is the wave excitation force (N) acting on the water column, m is the mass (kg) of the water column, m_a is the added mass (kg) and d is the damping coefficient (kg/s) of the system (sum of the radiation and PTO damping coefficients) (McCormick, 2009). Added mass is the accelerated mass of the fluid with the motion of the water column.

On the left hand side of the equation, first, second and third terms represent the inertial, damping and hydrostatic restoring forces, respectively. Under a regular incident wave excitation, driving force is sinusoidal and can be expressed as:

$$F_{exc} = F_0 \cos(\omega t) \quad (2.11)$$

where F_0 is the amplitude of the sinusoidal wave force.

In that case, solution of 2.10 is presented by Rao, (2011):

$$y(t) = Y_0 cos(\omega t - \theta) \quad (2.12)$$

where Y_0 is the amplitude of the water column motion (m) and θ is the phase angle which are defined as:

$$Y_0 = \frac{{F_0}/{(m+m_a)}}{\sqrt{(\omega_n^2 - \omega^2)^2 + (\frac{d}{(m+m_a)}\omega)^2}} \quad (2.13)$$

$$\theta = \tan^{-1} \frac{d\omega}{m(\omega_n^2 - \omega^2)} \quad (2.14)$$

A quick examination of the solution reveals that, obvious difficulty in obtaining the solutions is the accurate estimation of added mass and damping coefficient.

2.2.2 Determination of damping via free decay tests for overdamped systems

A heavily damped system that can never cross the static equilibrium position with an only imposed initial displacement is termed as an overdamped system. A quite general method to determine the damping of an overdamped system will be utilized as prescribed below.

In the absence of the external forces, the differential equation governing the dynamics of the water column will be:

$$(m + m_a)\ddot{y}(t) + d\dot{y}(t) + \rho g A_w y(t) = 0 \tag{2.15}$$

Later in the section, solution of the preceding equation under the harmonic excitation of an incident wave will be discussed.

For the calculation of dynamic wave pressure under the incident wave, Froude–Krylov hypothesis, which involves the assumption that the pressure field under the incident wave is completely undisturbed by the presence of the structure, will be utilized (McCormick, 2009, Fang and Luo, 2005, Url-3). Froude–Krylov hypothesis is often used in the literature to calculate the wave forces on OWCs and submerged piercing bodies i.e. Sundar V. (2016), Oh and Jang (2015), McCormick (2009), Szumko (1989), Dean and Dalrymple (1984). Therefore, due to the assumption of Froude–Krylov hypothesis, added mass term will be omitted.

After some algebraic manipulations, 2.15 becomes:

$$\ddot{y}(t) + \frac{d}{m}\dot{y}(t) + \omega_{\mathrm{n}}^2 y(t) = 0 \tag{2.16}$$

where ω_{n} is the natural (angular) frequency of the system (1/s) which is defined as:

$$\omega_{\mathrm{n}} = \sqrt{\frac{\rho g A}{m}} \tag{2.17}$$

Well known solution to this homogenous ordinary differential equation is in the form:

$$y(t) = c_1 e^{r_1 t} + c_2 e^{r_2 t} \tag{2.18}$$

where $c_1$and c_2 are arbitrary constants (m) and $r_1$and r_2 are functions of m, d and ω_{n} (s^{-1}) which are expressed by the quadratic formula:

$$r_{1,2} = -\frac{d}{2m} \pm \sqrt{(\frac{d}{2m})^2 - \omega_{\mathrm{n}}^2} \tag{2.19}$$

To determine r_1 and r_2, next step should be the calculation of the damping coefficient d, which is unknown priori. Additional condition is needed that satisfies 2.18 to compute the damping coefficient d. This additional condition is determined by transforming the question into an initial value problem (IVP) as follows:

In the physical experiments, if we raise up the water column level by an amount a via generating a negative gauge pressure above it and release the system, sometime later the energy associated with the system will be depleted due to the dissipative forces in a non-oscillatory behavior due to the relatively high PTO damping applied on the

OWC system. These kind of highly damped systems are called “overdamped systems”. Mathematically, $y(t)$ which is given by 2.18 will be zero only at the limit as time approaches infinity. Therefore, t_f is defined as the time needed for initial chamber surface level to diminish to 0.1% of a.

So, additional condition is defined as:

$$y(t_f) = 0.001a \tag{2.20}$$

This kind of experimental setup will yield two initial values as follows:

$$y(0) = a \tag{2.21}$$

$$\dot{y}(0) = 0 \tag{2.22}$$

Additional condition is determined by finding t_f via measuring the time it takes the water column height to decrease to level $0.001a$.

Substitution of 2.21 and 2.22 into 2.18 yields c_1 and c_2:

$$c_1 = \frac{-a.r_2}{r_1 - r_2} \tag{2.23}$$

$$c_2 = \frac{r_1 a}{r_1 - r_2} \tag{2.24}$$

By substitution of 2.23 and 2.24 into 2.18, and evaluating the condition that is given in 2.20, following expression is obtained:

$$r_1 e^{r_2 t_f} - r_2 e^{r_2 t_f} = 0.001(r_1 - r_2) \tag{2.25}$$

Because damping coefficient cannot be obtained explicitly from 2.19 and 2.25, it is computed iteratively.

This type of experimental determination of damping coefficient will involve all type of resistive forces on the water column. In real situations, generally the power take-off and radiation damping forces will exhibit some degree of non-linearity. In this study, determined damping coefficient d will practically represent overall linear equivalent damping coefficient which will allow us to solve a linear differential equation. If we take account the insolvability of the non-linear differential equations analytically (except some simplest special cases), this method may give at least a reasonable approach for solving the system response.

2.2.2.1 Validation of simple mechanical model results

To obtain a quantitative measure of the discrepancy between the analytical model results and experimental model values, relative error (RE) is defined as:

$$RE = \frac{\lambda_0 - \lambda}{\lambda} \tag{2.26}$$

where λ_0 is the analytical model result and λ is the physical experimental value.

2.2.3 Determination of damping via free decay tests (underdamped systems)

“Underdamped” term is used for the initially excited systems that experience freely decaying oscillations afterwards. For the underdamped systems, assuming a rigid motion with a linear overall damping, free decay data can be used to measure the rate of decay of oscillations via LDM method (Rao, 2011). Such models are single degree of freedom systems (SDOF) and in the absence of an external force, they can mathematically be in general form (as represented in 2.16):

$$\mathrm{A}\ddot{y}(t) + \mathrm{B}\dot{y}(t) + \mathrm{C}y(t) = 0 \tag{2.27}$$

During the free decay experiments surface of the water column remained almost horizontal, no distortion was observed and water column mass moved in unison. Hence, such a model that assumes the water column as a rigid body, can satisfactorily be used to model the free decaying of water column motions.

2.2.4 Logarithmic decrement method

To meet the purposes of this present investigation, a linear equivalent overall damping is considered. In other words, calculated overall damping ratio includes all types of dampings that oppose the motion of the water column in an equivalent linearized form (e.g. viscous, radiation and PTO dampings, McCormick, 2009). Logarithmic decrement method (LDM) can be used to determine the damping ratio of underdamped rigid-body systems (Rao, 2011). Therefore, in order to utilize the LDM for an OWC, water column has to sufficiently act in a rigid-body manner, that is, all the water column should oscillate in unison since the relative motion between the fluid particles are not allowed. During the experiments rigid-body motion of the water column is observed and no sloshing motions were generated, the free surface of the water column almost stayed planar so that water column oscillation can be considered as a single degree of freedom (SDOF) type in the piston (heave) mode. A generic decaying response of an initially displaced system is shown in Figure 2.10.

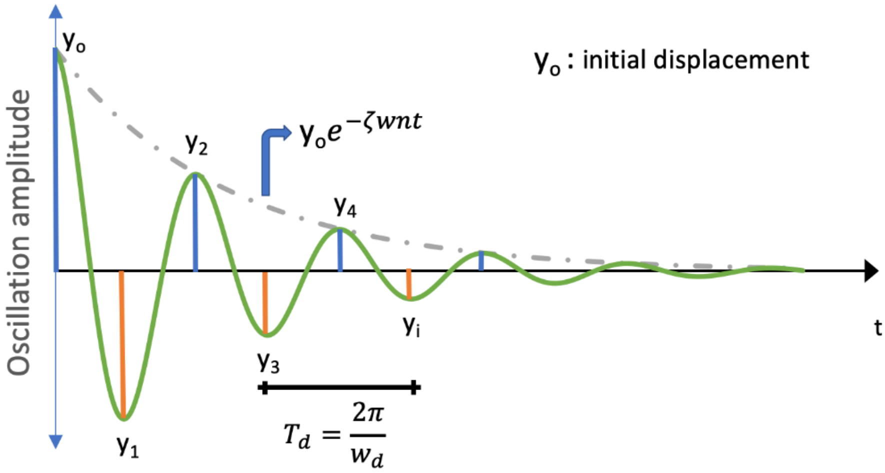

Figure 2.10 : Time-response of a freely decaying system.

Logarithmic decrement is defined as:

$$\delta = \ln \frac{y_i}{y_{i+2}} \tag{2.28}$$

where y_i and y_{i+2} are the two successive positive or negative peaks of the free decay times series data. For SDOF systems, the damping value that provides the fastest return to system's undisturbed steady-state position is called critical damping. The ratio of the damping coefficient to the critical damping is defined as the damping ratio which can be calculated by the expression:

$$\zeta = \frac{\delta}{\sqrt{(2\pi)^2 + \delta^2}} \tag{2.29}$$

Damping of the system determined by this method will approximate the overall equivalent linear damping of the system; that is, according to McCormick, 2009, all types of damping mechanisms (e.g. viscous, radiation and PTO dampings) that oppose the motion of the water column are involved in the damping coefficient present in 2.16. Damped period of the system, T_d (s) is a direct measure from the decaying oscillation time series via determining the time period between zero-crossings of the time series data. By knowing T_d, damped and undamped natural frequency of the system may easily be calculated, respectively, as follows:

$$w_d = \frac{2\pi}{T_d} \tag{2.30}$$

$$w_n = \frac{w_d}{\sqrt{1-\zeta^2}} \tag{2.31}$$

For an oscillating water column, total mass of the system consists of two components i.e. mass of the water column and excited water mass by the motion of the water column. With the computation of the above parameters, following expression yields the added mass value (McCormick, 2009).

$$m_a = \frac{\rho g A_w}{w_n^2} - m \tag{2.32}$$

where, ρ is the density (kg/m^3) of the water, g is the gravitaitonal constant (m/s^2) and m is the mass (kg) of the water column.

2.2.5 Analytical determination of wave force

One way of determining the incident wave force acting on the water column is to calculate the dynamic pressure under the lip of the frontwall. As mentioned previously the method that only considers the dynamic incident wave pressure and neglects the presence of the structure is called Froude-Krylov hypothesis. In determination of the excitation force for the overdamped case, this hypothesis will be utilized.

Under the frame of linear wave theory, water column in the chamber is harmonically excited via the oscillating dynamic pressure generated under the incident waves.

Based on linear wave theory, it is described as follows (Dean and Dalrymple, 1984):

$$p(x, z, t) = \rho g \eta \frac{\cosh k(h+z)}{\cosh kh} \tag{2.33}$$

$$\eta(x, t) = \frac{H}{2}\cos(kx - \omega t) \tag{2.34}$$

$$k = \frac{2\pi}{L} \tag{2.35}$$

$$\omega = \frac{2\pi}{T} \tag{2.36}$$

where p is the dynamic pressure under the incident wave (Pa), x is the wave propogation direction (perpendicular to the front wall of the OWC chamber), z is the vertical axis with repect to still water level and negative in the downwards direction, η is the water surface displacement of the incident wave (m).

The wave pressure is spatially averaged with respect to x-axis over the length of the structure, l to find the average wave excitation force on the water column. This is accomplished by averaging $\cos(kx - \omega t)$ term as follows:

$$\overline{\cos(kx - \omega t)} = \frac{1}{l}\int_{-\frac{l}{2}}^{\frac{l}{2}} \cos(kx - \omega t)\, dx = \frac{2}{kl}\sin\left(\frac{kl}{2}\right)\cos(\omega t) \qquad (2.37)$$

Then, average pressure p_{av}, at a specified depth z, is described as:

$$p_{av}(z,t) = \frac{\rho g H}{kl}\frac{\cosh k(h+z)}{\cosh kh}\sin\left(\frac{kl}{2}\right)\cos(\omega t) \qquad (2.38)$$

Then, the force acting on the water column is obtained by multiplying the space averaged pressure under the water column by the chamber area:

$$F_{exc} = p_{av}A_w \qquad (2.39)$$

2.39 can also be expressed in terms of sinusoidal form:

$$F_{exc} = F_0\cos(\omega t) \qquad (2.40)$$

where F_0 is the maximum amplitude of the wave force (N) which is given by the equation:

$$F_0 = \frac{\rho g H A_w}{kl}\frac{\cosh k(h+z)}{\cosh(kh)}\sin\left(\frac{kl}{2}\right) \qquad (2.41)$$

Finally,

2.10 can be written explicitly:

$$m\ddot{y}(t) + d\dot{y}(t) + \rho g A_w y(t) = \frac{\rho g H A}{kl}\frac{\cosh k(h+z)}{\cosh(kh)}\sin\left(\frac{kl}{2}\right)cos(\omega t) \qquad (2.42)$$

To solve 2.42, damping coefficient should be determined.

2.2.6 Efficiency calculation

According to linear wave theory, average incident wave energy per unit length and width (J/m^2) is calculated by the following expression:

$$E = \frac{1}{8}\rho g H^2 \qquad (2.43)$$

Transmission rate of an incident wave energy is defined as incident wave power and given by the expression for unit width as follows (Dean and Dalrymple, 1984):

$$P = E.c_g \qquad (2.44)$$

Herein, c_g is the group velocity (m/s) at which the energy is transmitted and described as:

$$c_g = \frac{\omega}{k}\left[\frac{1}{2}(1 + \frac{2kh}{\sinh(2kh)})\right] \tag{2.45}$$

According to Sheng and Lewis (2016), for small scale model experiments, air compressibility can confidently be ignored. To further validate the preceding statement quantitatively, closed chamber (closed orifice) experiments were carried out for all different cases and free surface oscillations of the water column were measured. It is found that, regardless of the geometric configuration of the converter, applied PTO damping and incident wave parameters, calculated compression of air column was less than 1% implying the incompressibility of the OWC model used for the present study. Therefore, pneumatic power generated in the orifice can be calculated as follows (Morris-Thomas et al., 2007):

$$P_{air} = \frac{1}{T}\int_0^T p(t)_{air}\, \mathrm{A_w} v(t).\,dt \tag{2.46}$$

where, $p(t)_{air}$ is the instantaneous differential air pressure in the chamber (Pa) and $v(t)$ is the average vertical velocity of the free surface of the water column (ms^{-1}) which is estimated by a third order time derivative formula as follows (Rezanejad et al., 2017)

$$V^3(d_i) = \frac{-11d_i + 18d_{i+1} - 9d_{i+2} + 2d_{i+3}}{6\delta t} \tag{2.47}$$

where $\mathrm{V^3(d_i)}$ is the third order approximation of the velocity, $\mathrm{d_i}$ is the average (averaged of the measurements obtained from WG1, WG2 and WG3) chamber surface displacement and δt is the time-step which is 0.01s.

A commonly used performance indicator of an OWC is the hydrodynamic efficiency of the converter (so called 'capture width') which is expressed as:

$$E_h = \frac{P_{air}}{P.w} \tag{2.48}$$

where, w is the width of the OWC device (m).

E_h is a key parameter for evaluation of the OWC performance. Calculated hydrodynamic efficiency values under different cases are fundamental for OWC type wave energy converter optimization.

2.3 Numerical Model

Present study utilizes commercial CFD software, Flow-3D to simulate the free decay tests for the specific OWC device used for the experiments. A 3D numerical wave tank (NWT) was generated for this purpose. Volume of fluid (VOF) method, which was initially invented by Hirt and Nichols (1981), was implemented for free surface modelling. The software uses Eularian approach with rectangular grids to generate a non-uniform mesh for computing. VOF method facilitates pre-defined fluid fraction function F, which has the following time dependent governing equation.

$$\frac{\partial F}{\partial t} + u\frac{\partial F}{\partial x} + v\frac{\partial F}{\partial y} + w\frac{\partial F}{\partial z} = 0 \tag{2.49}$$

Here, t is the time, (x, y, z) represent the Cartesian coordinate system and (u, v, w) are the corresponding velocity components.

By definition, F takes values between 0 and 1, where values of 1 and 2 describes the water (Fluid No. 1) and air (Fluid No. 2), respectively. Values between 0 and 1 correspond to combination of both air and water phases. In the present study, two-phase fluid model that is capable of simulating air and water phases simultaneously was selected for air-water coupling.

Continuity and momentum equations that govern the fluid flow are given by the following expressions.

$$\frac{\partial}{\partial x}\left(u.A_x\right) + \frac{\partial}{\partial y}\left(v.A_y\right) + \frac{\partial}{\partial z}\left(w.A_z\right) = 0 \tag{2.50}$$

$$\frac{\partial u}{\partial t} + \frac{1}{V_F}\left[u.A_x.\frac{\partial u}{\partial x} + v.A_y.\frac{\partial u}{\partial y} + w.A_z.\frac{\partial u}{\partial z}\right] = -\frac{1}{\rho}\frac{\partial P}{\partial x} + G_x + f_x \tag{2.51}$$

$$\frac{\partial v}{\partial t} + \frac{1}{V_F}\left[u.A_x.\frac{\partial v}{\partial x} + v.A_y.\frac{\partial v}{\partial y} + w.A_z.\frac{\partial v}{\partial z}\right] = -\frac{1}{\rho}\frac{\partial P}{\partial y} + G_y + f_y \tag{2.52}$$

$$\frac{\partial w}{\partial t} + \frac{1}{V_F}\left[u.A_x.\frac{\partial w}{\partial x} + v.A_y.\frac{\partial w}{\partial y} + w.A_z.\frac{\partial w}{\partial z}\right] = -\frac{1}{\rho}\frac{\partial P}{\partial z} + G_z + f_z \tag{2.53}$$

where u, v, w and A_x, A_y, A_z are velocities and similar area fractions in x, y and z directions, respectively. Vf is the fractional value, ρ is the fluid density, P is the pressure, G_x, G_y, G_z and f_x, f_y, f_z are body and viscous accelerations in the x, y and z directions, respectively. Density and dynamic viscosity of the air was assumed to be constant as ρ = 1.225 kg/m^3 and μ= 1.789×10^{-5} kg/(ms) (Flow science Inc., 2012).

Expressions for the viscous acceleration with a variable dynamic viscosity μ are given as follows:

$$\rho V_F f_x = wsx - \left[\frac{\partial}{\partial x}\left(A_x \tau_{xx}\right) + R\frac{\partial}{\partial y}\left(A_y \tau_{xy}\right) + \frac{\partial}{\partial z}\left(A_z \tau_{xz}\right) + \frac{\xi}{x}\left(A_x \tau_{xx} - A_y \tau_{yy}\right)\right] \quad (2.54)$$

$$\rho V_F f_y = wsy - \left[\frac{\partial}{\partial x}\left(A_x \tau_{xy}\right) + R\frac{\partial}{\partial y}\left(A_y \tau_{yy}\right) + \frac{\partial}{\partial z}\left(A_z \tau_{yz}\right) + \frac{\xi}{x}\left(A_x + A_y \tau_{xy}\right)\right] \quad (2.55)$$

$$\rho V_F f_z = wsz - \left[\frac{\partial}{\partial x}\left(A_x \tau_{xz}\right) + R\frac{\partial}{\partial y}\left(A_y \tau_{yz}\right) + \frac{\partial}{\partial z}\left(A_z \tau_{zz}\right) + \frac{\xi}{x}\left(A_x \tau_{xz}\right)\right] \quad (2.56)$$

Here, the first terms on the right-hand side of the equations represent wall shear stresses and ξ is a geometry coefficient and equals 1 for Cartesian geometry and 0 for cylindrical geometry where,

$$\tau_{xx} = -2\mu\left[\frac{\partial u}{\partial x} - \frac{1}{3}\left(\frac{\partial u}{\partial x} + R\frac{\partial v}{\partial y} + \frac{\partial w}{\partial z} + \frac{\xi u}{x}\right)\right] \quad (2.57)$$

$$\tau_{yy} = -2\mu\left[R\frac{\partial v}{\partial y} + \xi\frac{u}{x} - \frac{1}{3}\left(\frac{\partial u}{\partial x} + R\frac{\partial v}{\partial y} + \frac{\partial w}{\partial z} + \frac{\xi u}{x}\right)\right] \quad (2.58)$$

$$\tau_{zz} = -2\mu\left[\frac{\partial w}{\partial z} - \frac{1}{3}\left(\frac{\partial u}{\partial x} + R\frac{\partial v}{\partial y} + \frac{\partial w}{\partial z} + \frac{\xi u}{x}\right)\right] \quad (2.59)$$

$$\tau_{xy} = -\mu\left[\frac{\partial v}{\partial x} + R\frac{\partial u}{\partial y} - \frac{\xi v}{x}\right] \quad (2.60)$$

$$\tau_{xz} = -\mu\left[\frac{\partial u}{\partial z} + \frac{\partial w}{\partial x}\right] \quad (2.61)$$

$$\tau_{yz} = -\mu\left[\frac{\partial v}{\partial z} + R\frac{\partial w}{\partial y}\right] \quad (2.62)$$

Here, R represents an orthogonal transformation tensor. Reynolds stresses in the viscous acceleration were calculated with k-ε model (Rodi, 1980).

2.3.1 k- ε turbulent model

In the present study, k - ε turbulence model was applied. Kinetic energy (k) and its rate of dissipation (ε), which are represented individually for the transport equations, are expressed as:

$$\frac{\partial k}{\partial t}+\frac{1}{V_F}\left[uA_x\frac{\partial k}{\partial x}+vA_y\frac{\partial k}{\partial y}+wA_z\frac{\partial k}{\partial z}\right]=P_k+G_k+Diff-\varepsilon \tag{2.63}$$

$$\frac{\partial \varepsilon}{\partial t}+\frac{1}{V_F}\left[uA_x\frac{\partial \varepsilon}{\partial x}+vA_y\frac{\partial \varepsilon}{\partial y}+wA_z\frac{\partial \varepsilon}{\partial z}\right]=\frac{C_{1\varepsilon}.\varepsilon}{k}\left(P_k+C_{3\varepsilon}.G_k\right)+Diff_\varepsilon-C_{2\varepsilon}.\frac{\varepsilon^2}{k} \tag{2.64}$$

where, P_k and G_k are the turbulent kinetic energy and buoyancy production terms, respectively, Diff and $Diff_\varepsilon$ represent diffusion term, $C1_\varepsilon$, $C2_\varepsilon$ and $C3_\varepsilon$ are constants. For this numerical model, $C1_\varepsilon$ and $C2_\varepsilon$ were selected as 1.44 and 1.92, respectively. Values are designated to k and ε for every mesh cell having one or more of its faces partially or totally blocked by a rigid wall.

For the numerical model, three-dimensional, single precision, implicit and segregated solver was chosen in the software. A second order implicit time discretization, with a time-step of 0.015 and a maximum of 100 iterations per time step was used.

2.3.2 Boundary conditions

A NWT identical to the physical wave flume was generated. Walls of the NWT were the natural boundaries for upper and lower boundary conditions in the x (x_{min}, x_{max}) and y (y_{min}, y_{max}) directions where flume bottom was the boundary, zmin and atmospheric boundary condition was selected for zmax. No slip condition was applied for the walls of the structure and the flume. Penetration of the fluid into the solid walls was prevented by setting the normal component of the velocity zero. ε = 0.01 was selected for surface roughness. Gravitational field was set to 9.81 m/s^2 in the negative z direction. Limited compressibility model was applied. For appropriate mesh network design, a crude computational grid is utilized and solutions are obtained relatively faster. Solutions were further obtained as sequential refinements are made. This process was carried on until the results sufficiently converged and accordingly, appropriate computational grid was determined with a uniform mesh size 0.02m as illustrated in Figure 5. From 24 to 36 hours of computation time was needed for each configuration of the OWC to perform the numerical simulation. However, Vyzikas et al. (2017) reported few seconds of simulation time for the free decay tests. This should be due to the 2D numerical model that was developed rather than a 3D model.

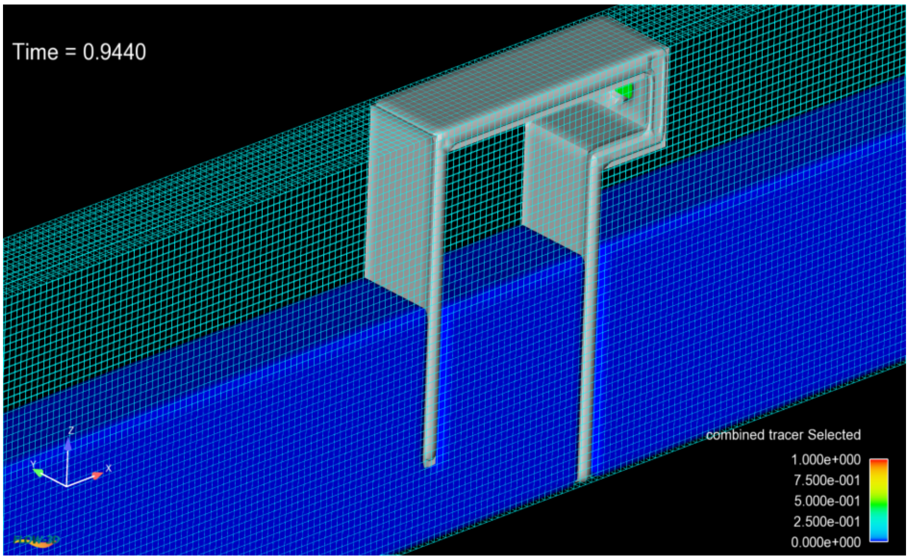

Figure 2.11 : Mesh of the OWC used in the numerical model.

2.3.3 Validation method for numerical model

To quantitatively compare the experimental and numerical model results root mean square error ($RMSE$) and coefficient of efficiency (CE) are utilized as performance-evaluation criteria. The RMSE is defined as:

$$RMSE = \sqrt{\frac{1}{n}\sum_{i=1}^{n}(E_i - N_i)^2} \tag{2.65}$$

and the CE can be expressed as:

$$CE = \left[1 - \frac{\sum_{i=1}^{n}(E_i - N_i)^2}{\sum_{i=1}^{n}(E_i - E_o)^2}\right], \tag{2.66}$$

where n is the total number of observation data; E_i and N_i represent the direct measurements (e.g. damping ratio, ζ and damped natural period, T_d) obtained from experimental and simulated time series, respectively and E_o is the average of the experimental data. The RMSE and CE are utilized as performance-evaluation criteria of numerical model results.

3. RESULTS AND DISCUSSION

3.1 Overdamped Case

During the free decay experiments it was observed that, the system was only overdamped when the orifice ratio was the smallest (very high PTO damping), 0.30%. Because of the heavily dissipative nature of the applied PTO damping, initially transmitted energy into the system (water column) is totally depleted before crossing down the equilibrium point (still water level). Thereby, orifice ratio of the chamber was constant (0.30%) during the experiments to investigate an overdamped OWC device.

3.1.1 Water column surface oscillations and motion behaviors

In this section, effects of various relative openings and regular wave parameters on the chamber water column surface oscillations and motion behaviors are investigated. Mathematical models are also developed to predict water column oscillation amplitudes inside the chamber from opening height and wave parameter values. The predicted values are validated by physical experimental model results.

3.1.1.1 Effect of wave parameters

It is well known that water column surface profile in the chamber is strongly related to the frequency of the incident progressive waves impinging on the converter through the underwater chamber opening (Morris-Thomas et al., 2007). If the water column surface profile remains nearly horizontal under the excitation of the incident waves during oscillation, the water column surface can be considered as a weightless rigid-piston moving periodically. But sometimes depending on the frequency of the incident waves the surface profile acts like an excited liquid in a closed container in a symmetric about the origin manner which can be defined as a sloshing motion profile. For some cases water column action inside the chamber behaves as a combination of these two described profiles, piston-type and sloshing motion. Observations through the experiments indicated that when incoming wave frequency is less than a particular value, piston type motion is generated in the chamber. When a certain larger frequency value is exceeded, sloshing motion is observed. Between these frequencies an interval exists with a narrow bandwidth which water column surface profile behavior comprises of both distinct motions. These water column surface profiles generated in the chamber were the same for all opening heights. These profiles are shown in Figure 3.1.

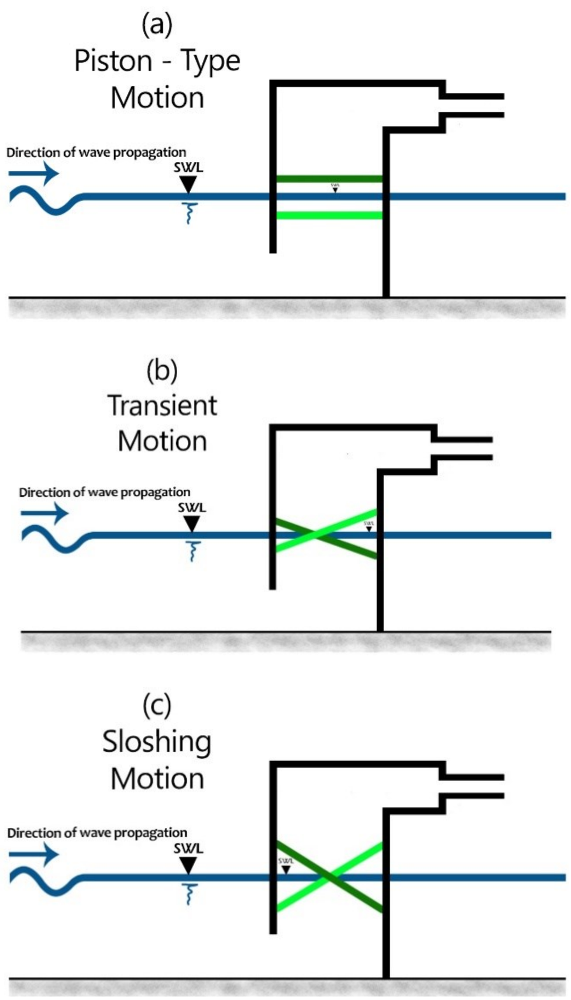

Figure 3.1 : a) piston type b) transition type c) sloshing type motions.

Transmitted wave height, μ is defined as:

$$\mu = \frac{d}{H} \tag{3.1}$$

where, d is average water column surface oscillation amplitude for one wave period (m) and H is the incident wave height (m).

Dimensionless wave frequency, Kh is described as:

$$Kh = \frac{\omega^2}{g}h = \ kh\tanh(kh) \qquad (3.2)$$

The transmitted wave height μ versus Kh graph is shown in Figure 3.2 for different relative opening heights, α. Corresponding Kh values for different wave series are shown over the data points on the graph. Some of the exponential decay function fittings (for a clear vision) are included onto the graph for better interpretation of the data. Coefficient of correlation, R2 values of all fittings are found to be in range between 0.991 and 0.997.

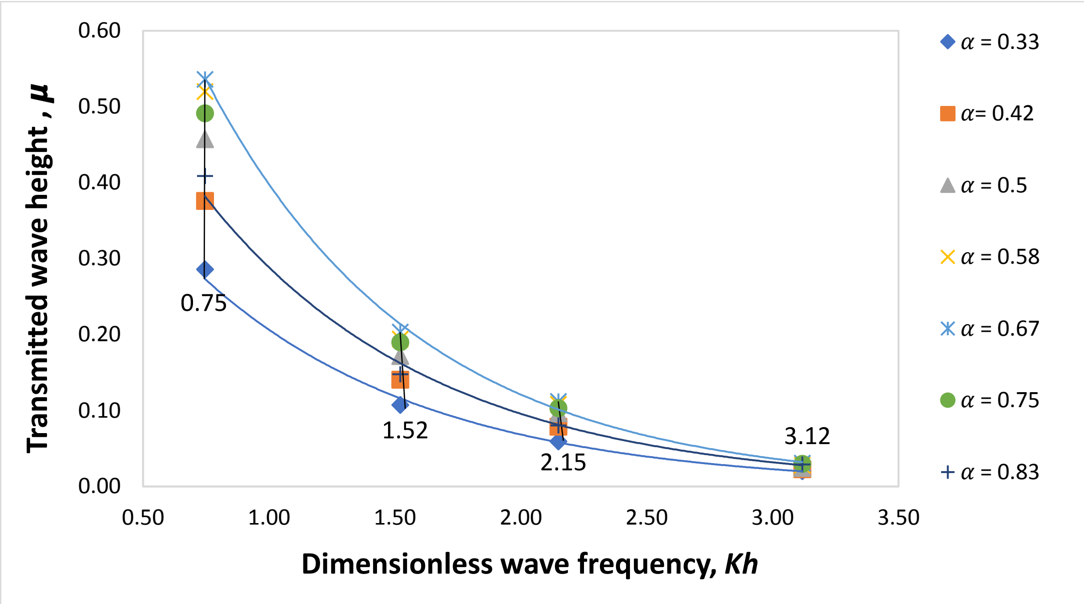

Figure 3.2 : The μ versus Kh.

It is realized at first glance that as the Kh increases μ becomes smaller due to increasing contribution of sloshing behavior to the surface profile in the chamber. It is observed that for the Kh values 0.75 and 1.52, the behavior of the water column surface is approximately piston-type motion. When Kh is 2.15, the profile behavior comprises of both type of motions where sloshing motion is dominant and for Kh value 3.12 sloshing type of motion prevails. Therefore, somewhere between $1.52 < Kh < 2.15$ but closer to the Kh value 2.15, there should be a transition zone that the profile dominancy is transformed from one to another. It is noteworthy that as Kh gets smaller from transition zone towards the piston-type generating values, μ increases much more rapidly than other intervals. Since most of the contribution to the μ values comes from piston–type motion, in this interval, a small increase in the Kh causes a greater decrease for average μ values via increasing sloshing type of motion. But as the piston type motion almost vanishes in the sloshing dominant and fully sloshing intervals and as the average μ values are already quite diminished in a fully and sloshing dominant surface profiles, increasing Kh values do not effect μ as much as in the opposite case. These behaviors hold on for all relative opening heights, except the effect of varying Kh declines as α becomes smaller. Figure 3.2 shows that non-linearity decreases as the immersion depth advances to bottom due to exponentially decay in energy. As the gap between the bottom and the chamber closes down, it leads to a relatively smaller change of transmission of wave energy as the Kh varies. Consequently, transmitted wave height is less sensitive to the effects of varying Kh. The most non-linearity (exponential growth) is measured for α value 0.67 among others. This value is important because bigger rate of change with respect to decreasing Kh values is obtained. This phenomenon and exponential decay in the energy will be further discussed later in the paper. By using Figure 3.2, for the particular design used in this experimental study for a given wave height, H and period, T or wave length, L, average chamber water column oscillation amplitude in the chamber, $\underline{d}$ can approximately be measured for any relative opening height using the exponential fittings.

In case of a fully sloshing motion inside the chamber, feasible amount of energy exploitation is almost impossible. Because the volume of the air in the chamber nearly stays constant thus trapped air above the water column cannot be pressurized. To further explain this phenomenon, Figure 3.3 shows the dimensionless time series, t/T (time (t) divided by period of generated wave (T)) for the transmitted wave heights at the front wall, center and the rear wall of the chamber for Case 4 which α and β values are 0.58 and 0.42, respectively under the incident W4. This wave series has the highest frequency among the other ones which generates the smallest average oscillation amplitude due to almost fully sloshing mode formed in the chamber. At this point, it is also noteworthy that, for any other case the figure will look the same with a different sloshing amplitude.

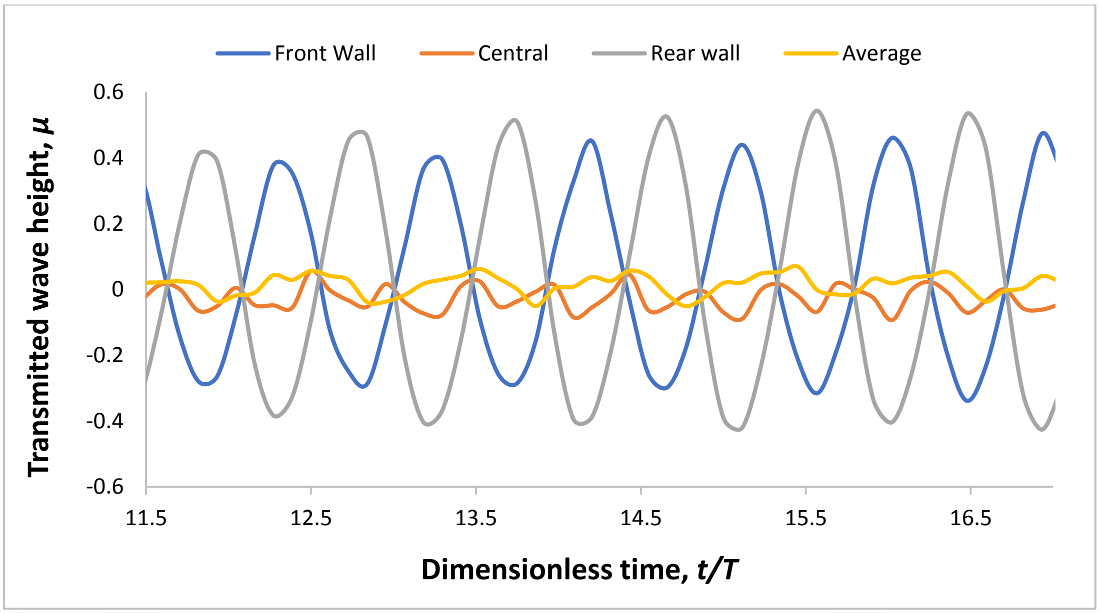

Figure 3.3 : μ versus $\frac{t}{T}$ for W4 Case 4.

Transmitted wave heights measured with the (WG3) which is located at the right-hand side of the chamber has approximately 180° phase difference with the fluctuation value at the left-hand side (WG1) of the chamber and a very small fluctuation at the middle (WG2). Also, it is seen from Figure 3.3 that average water column surface fluctuation values are very small, hence energy extraction could not be efficiently possible. The opening height of the chamber did not effect this behavior of the surface profile but the difference is the increment for sloshing angle of the profile with increasing of the opening height. This result is predictable because higher transmission of energy into the chamber takes place as the opening height increases.

Under incident wave W1, opposite case was observed. The column water surface profile almost behaves without sloshing. W1 has the smallest frequency among others. Figure 3.4 shows the transmitted wave height versus dimensionless time series for this situation.

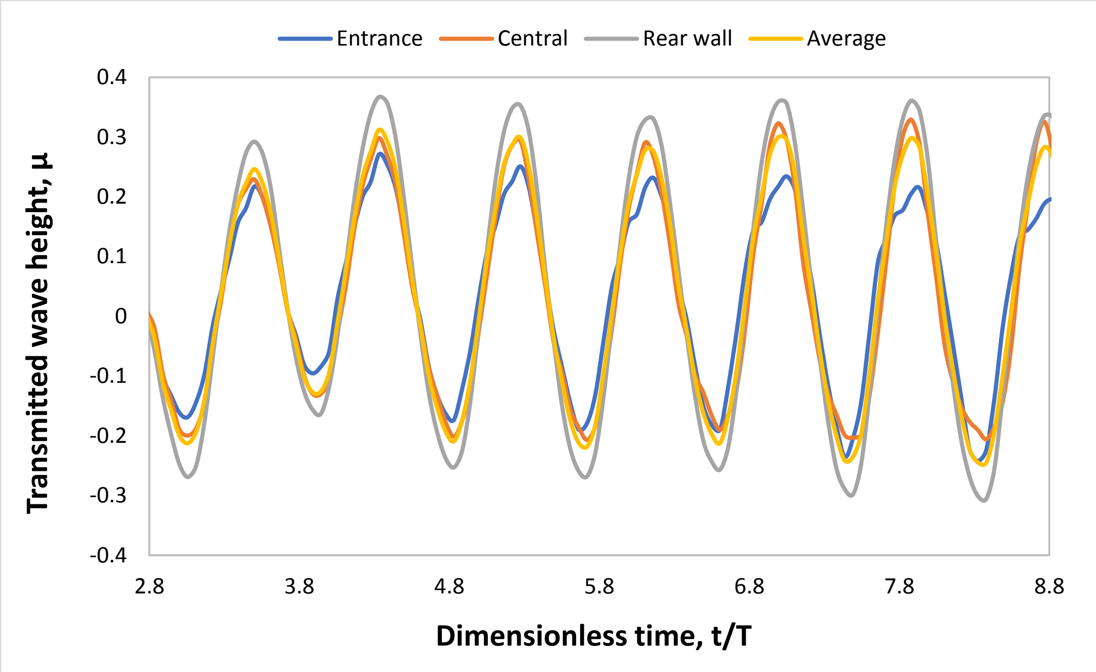

Figure 3.4 : μ versus $\frac{t}{T}$ for W1 Case 4.

As it is seen from Figure 3.4, unlike the W4, measured values of transmitted wave heights for three positions are in phase. They altogether contribute to the average transmitted wave height value in a building manner. If we compare the averaged μ value with the central point it can be realized that they almost overlap each other. So, for this situation transmitted wave heights can be represented by the fluctuation value at the center of the surface as Brendmo et al. (1996) stated in their study.

It is reported that if the chamber width is very small compared to the exposed incident wave length, water column surface profile behavior can be considered as piston type (Falnes and McIver, 1985).

Captured wave length ratio, δ is defined as:

$$\delta = \frac{L}{l} \tag{3.3}$$

where L is the incident wave length (m) and the l is the chamber length (m).

Measured transmitted wave height values versus captured wave length ratios for different relative opening heights with the regression lines are depicted in Figure 3.5.

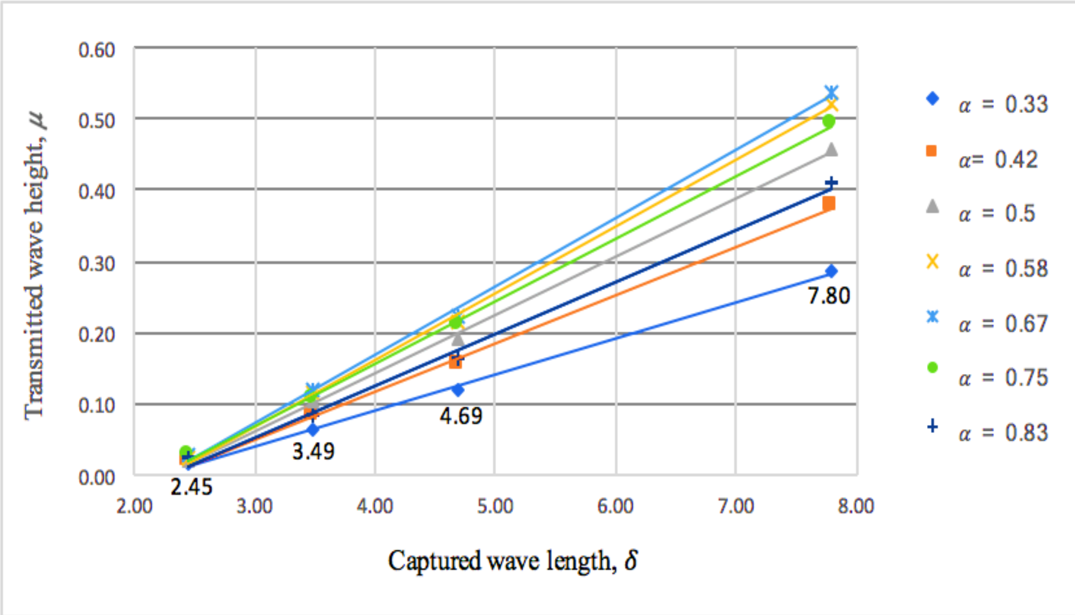

Figure 3.5 : μ versus δ.

Interestingly an impressive linear relationship exists between the two variables as it is seen from the fitted regression lines. R^2 values of all regression lines are approximately 1. μ values are higly dependent on captured wave length ratios. These results are very essential for harnessing large amounts of energy. The extreme cases, fully sloshing and piston type motions occur for the interval $\delta \lesssim 3$ and $\delta \gtrsim 4.25$, respectively. Somewhere between these captured wave length ratios, there is a transition interval where water column surface behavior transforms from sloshing dominant to piston type dominant motion. It is evident from the graph that when the water column is excited in a piston type manner, the transmitted wave heights get bigger which is desired for higher efficiency. Therefore, corresponding captured wave length intervals are of great importance. As transmitted wave heights increase with bigger captured wave lengths, when δ value moves from lower to higher values the piston behavior starts to dominate approximately around the δ value is 4.25. When δ value is around 3.75, surface profile transforms into sloshing dominant region and fully sloshing motion occurs at the approximate value of 3. To form a piston type motion behaviour in the chamber for higher efficiencies, captured wave length ratios less than 4 should be strictly avoided. Furthermore, Figure 3.5 shows that, this encountered phenomenon is valid for any relative opening height but the change is the increase in the variation of μ as the relative opening height gets bigger. Again, the biggest slope was obtained when the α value was 0.67 which indicates the importance of this specific ratio.

3.1.1.2 Effect of varying opening height

To understand the effects of varying opening heights on the water column surface fluctuations, the wave parameters were kept constant. The relative opening heights were altered under regular wave series given in Table 2.3 at a constant water depth 0.60 m. The results for the wave series that has the highest frequency are excluded since they are not of interest in terms of efficient energy extraction.

Relative average water column surface oscillation amplitude is defined as:

$$\eta = \frac{d}{h} \tag{3.4}$$

where, d is average water column surface oscillation amplitude and h is the water depth. Relative average water column oscillation amplitude versus relative opening height is indicated in Figure 3.6 with quadrating fittings for wave series W1, W2 and W3.

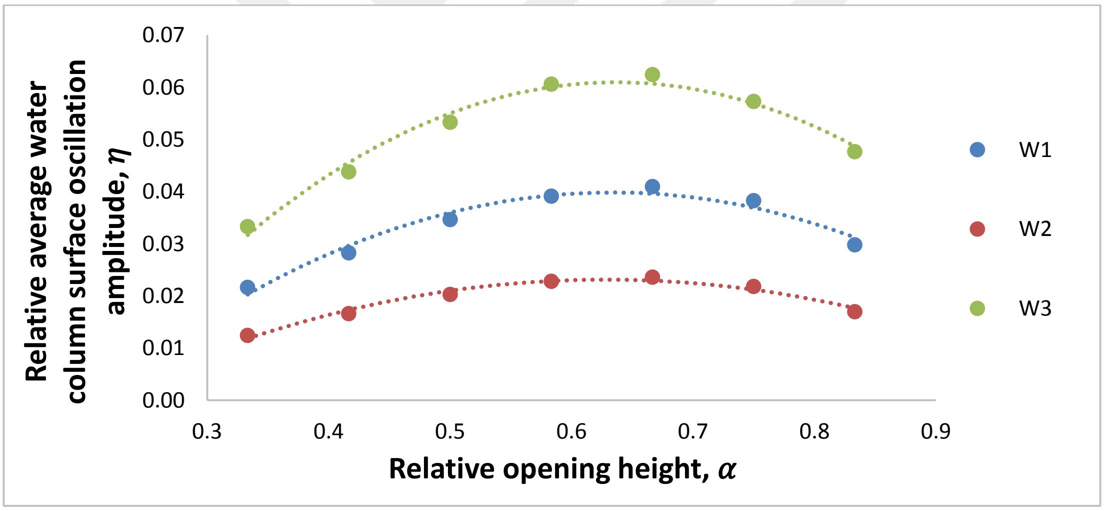

Figure 3.6 : The α versus η.

As it is obviously seen from Figure 3.6, largest η values were generated in the chamber when the ratio of the relative opening height is around 0.67 independent of wave parameters. The relative average fluctuations increase from α values 0.33 to 0.67 while opposite trend is measured from 0.67 to 0.83 for all wave series. After the peak ratio 0.67, relative average fluctuations decline more rapidly than they increased up to this value. With the aid of observations what it is thought happening is, for relative opening heights from 0.33 to 0.67 the profile behavior of the water column surface remains quite same whatever the profile was generated by the incident wave. But after this ratio an additional sloshing motion is added to the behavior of the profile. This sloshing motion decreases the fluctuations because of the averaging process of measurements at the locations of right, center and left hand side of the chamber. So there is a critical value around the ratio 0.67 that when exceeded the additional energy transmitted into the system is superimposed as a sloshing motion on to the already generated surface profile. The energy flux generated by incident waves are not distributed evenly below the surface. It decreases exponentially towards the seabed. So, the higher contribution to the energy flux comes from the parts near the surface thus the additional transmitted part of the flux after the α value 0.67 is relatively higher. This excessive flux forms greater reflection from the rear wall of the chamber. As α value advances further beyond the critical value reflection grows. In this manner, when the higher transmitted rate of energy after the value 0.67 encounters the back wall of the OWC strucure, a standing wave forms due to almost perfect reflection. Therefore, the rate of energy transmition into the chamber is so high that additional conveyed energy into the chamber is transformed to kinetic energy in the form of vertical motion of the water particles near the rear wall due to reflection, in turn stimulating the sloshing motion inside the chamber. The vertical motion velocities of the water particles are very high at the right half, especially at the back wall of the chamber. Since the remaining part of the water column cannot keep pace with right half in the vertical direction, this excessive flux forms sloshing motion in the chamber that approximately generates $180°$ degrees of phase difference for the water column fluctuations and velocities between the front and rear wall. Then this symmetric about the origin type of motion is joined to the surface profile of the water column whatever it was, after the α value 0.67. Because we average them, surface fluctuations start to decrease after the critical ratio is exceeded. As it goes further beyond the value 0.67, the consequences are the same regardless of wave parameters. In the previous section it wass concluded that, when captured wave length δ is less than an approximate value, sloshing motion is generated in the chamber. Besides a relatively small captured wave length δ, energy flux after the critical α value 0.67 also generates an additional sloshing motion inside the chamber. So, beyond this ratio, additional energy transmitted into the chamber can be considered as an "excessive harmful energy" since it is not just turned into an unextractable form but it absorbs the already available energy up to this value. This significant event should be taken into consideration seriously in designing OWC systems. Furthermore, this event is independent of wave parameters. It becomes even more crucial if there are some tidal fluctuations in the water level. If such a phenomenon exists, the relative opening height values should be chosen according to an appropriate range to harness the most energy in the OWC plant service time.

3.1.1.3 Description of mathematical model for constant wave parameters

In this experimental study, to determine the effects of relative opening heights and immersion depths on the average water column fluctuations, wave parameters were kept constant as the opening height and immersion depth were altered. Independent of the wave series used, parameters of Case 1 developed the smallest relative average water column surface fluctuation values that can be seen in Figure 3.6. After inspection of the measured data, a proportionality is found between relative average water column oscillation amplitude η and a combination of power functions of α and β as follows:

$$\eta \propto \beta^{1.1}\alpha^{2} \tag{3.5}$$

This equation implies that η is proportional to the square of relative opening height α and relative immersion depth β raised to power 1.1.

η versus $\beta^{1.1}\alpha^{2}$ plot with regression lines with an average R^2= 0.96 value is shown in Figure 3.7.

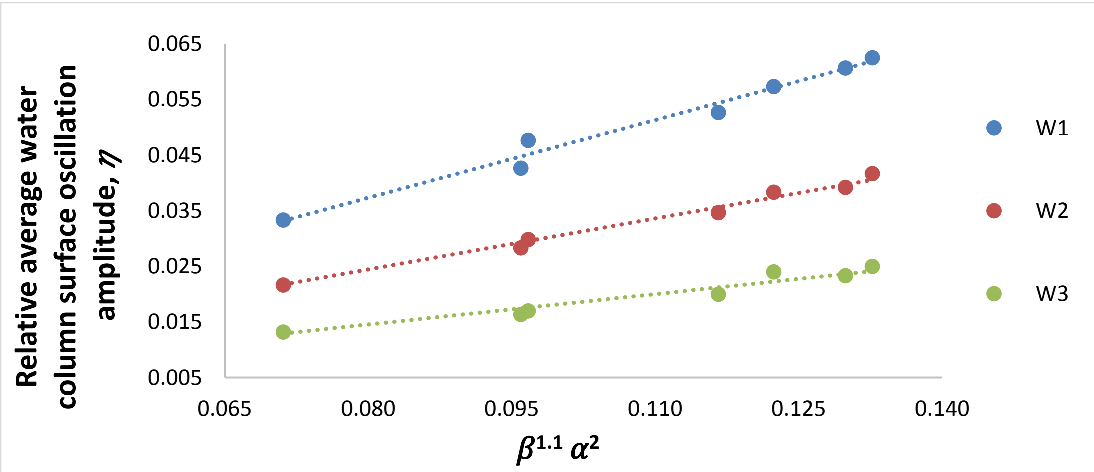

Figure 3.7 : η versus $\beta^{1.1}\alpha^{2}$.

For different wave series, the only difference is the slope of the regression lines. Among the wave series, W1 generates not only the highest average fluctuations in the chamber but also the biggest slope as $\beta^{1.1}\alpha^{2}$ value increases.

To further illustrate this proportionality, the terms η_i, α_i and β_i will be introduced for i values $1,2,3,4,5,6\ and\ 7$ where subscript i indicates the case number. Therefore η_i will represent the average water column surface oscillation amplitude for corresponding values of α_i and β_i. Then these values will be normalized with respect to η_1, α_1 and β_1 as, respectively:

$$\frac{\eta_i}{\eta_1},\ \frac{\alpha_i}{\alpha_1} \text{ and } \frac{\beta_i}{\beta_1} \tag{3.6}$$

It should be reminded that the η_1 is the smallest value generated in the chamber which represents the amplitude value for Case 1. As a result, these ratios describe the variations of the corresponding values with respect to Case 1. In order to equation 3.2 hold true also following expression should be correct for all i values and for all wave series:

$$\frac{\eta_i}{\eta_1} \approx \frac{\alpha_i^2}{\alpha_1^2} \cdot \frac{\beta_i^{1.1}}{\beta_1^{1.1}} \approx f(\alpha_i, \beta_i) \tag{3.7}$$

The values of $\frac{\eta_i}{\eta_1}$ and $f(\alpha_i, \beta_i)$ are depicted in Figure 3.8 with varying dimensionless opening heights.

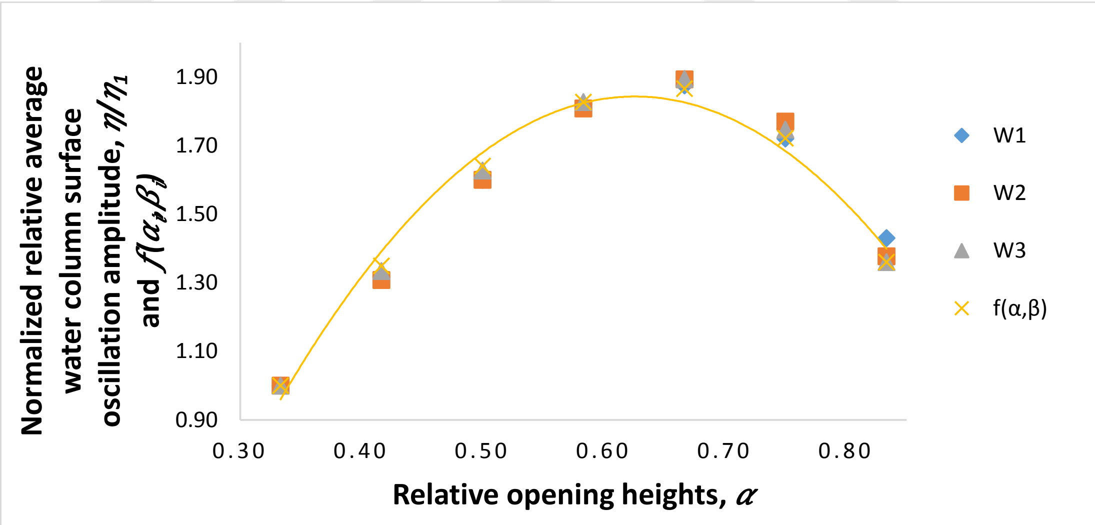

Figure 3.8 : Variations of η/η_1 versus α with $f(\alpha, \beta)$.

For all i values, there exists a good fit between η_i/η_1 and $f(\alpha_i, \beta_i)$ values which shows that suggested proportionality in 3.2 is approximately accurate.

The reasoning for this proportionality could be explained in the following manner:

Since the lowest point of the front wall was always under the still water surface during the experiments, a partial reflection occurred depending on the immersion depth which, in turn, will form a partial standing wave having higher amplitude relative to the incident progressive wave (as observed during our studies). The amount of this amplification increases by the immersion depth increment while the reflection phenomenon from the front wall approaches to perfect reflection. This leap in the wave height just in front of the chamber leads to an enhanced pressure distribution on the surface of inlet area because the pressure beneath the wave is proportional with wave height. This pressure increment corresponds to a greater excitation force on to the water column through the inlet section of the chamber resulting higher fluctuations. It is also reasonable to expect a greater average fluctuation increasing exponentially inside the chamber as the relative opening height increases. Because as mentioned earlier, the energy flux in a wave exponentially increases as it is ascended near the surface. After the peak value of η_i/η_1, corresponding values of α and β assembles together in a manner such that η_i/η_1values start to decrease.

From the plot it can also be realized that the peak point in Figure 3.8 which corresponds to approximately α value 0.67 is very significant as we mentioned earlier. Because it is the value which generates the greatest fluctuation values and also when exceeded the relative average fluctuations start to decrease for further applicable cases. In designing OWC plants this critical value should be taken into consideration. To the best of our knowledge, since there is no reference to this critical phenomenon in the literature, for different geometric design parameters this critical value notion and its approximate value has to be investigated.

It was stated that, there existed a proportionality between η and $\beta^{1,1}\alpha^2$ with different proportionality ratios for each incident wave as can be seen from Figure 3.8. But when the normalized values of η and $\beta^{1.1}\alpha^2$ for all cases were plotted under different wave series in Figure 3.8, interestingly it has been understood that variation of η values with respect to relative opening heights, α, do not depend on wave parameters. Normalized relative average amplitude as a function of dimensionless opening height α can be represented by a quadratic regression curve quite accurately using the discrete data as plotted in Figure 3.8. R2 of this regression curve is found to be 0.984. So this equation can be used to model the variations of relative water column surface fluctuations for any opening and immersion depth confidently. One can predetermine the fluctuation variations regardless of wave parameters.

Proportionality relationship, can be converted to an equation by introducing a proportionality constant c as follows :

$$\eta = c\beta^{1.1}\alpha^{2} \tag{3.8}$$

The value of the constant c can be calculated if any oscillation amplitude d corresponding to a particular β and α values is known for a particular incident wave series. Equation 3.5 is valuable in terms of time, money and labor consuming nature of the experimental studies. Before conducting further experiments, amplitude values can be computed for at least as a first approximation.

α and β values are related to each other with the equation :

$$\alpha + \beta = 1 \tag{3.9}$$

Hence, 3.5 can be expressed as follows:

$$\eta = c(1-\alpha)^{1.1}\alpha^{2} \tag{3.10}$$

When η is differentiated with respect to α it leads to,

$$\frac{d\eta}{d\alpha} = c(2\alpha(1-\alpha)^{1.1} - 1.1\alpha^{2}(1-\alpha)^{0.1}) \tag{3.11}$$

To find the maximum value of η, 3.8 has to equalize to zero.

$$\frac{d\eta}{d\alpha} = c(2\alpha(1-\alpha)^{1.1} - 1.1\alpha^{2}(1-\alpha)^{0.1}) = 0 \tag{3.12}$$

The solution to the equation 3.9 is possible if the expression in the parenthesis is equal to zero which becomes:

$$(2\alpha(1-\alpha)^{1.1} - 1.1\alpha^{2}(1-\alpha)^{0.1}) = 0 \tag{3.13}$$

α value obtained from the equation above is 0.65 which is very close to 0.67.

The second derivative of η with respect to α yields the following equation :

$$\frac{d^{2}\eta}{d\alpha^{2}} = c\left(2(1-\alpha)^{1.1} - 4.4\alpha(1-\alpha)^{0.1} + \frac{0.11\alpha^{2}}{(1-\alpha)^{0.9}}\right) \tag{3.14}$$

When α is equal to 0.65, the value of the $\frac{d^{2}\eta}{d\alpha^{2}}$ is a negative number times c. Since c is always positive, the conclusion is, 3.5 reaches its maximum value when α = 0.65.

3.1.1.4 Description of mathematical model for constant opening height

How relative average water column surface fluctuations depend on the wave parameters is also important for us. Because once the wave energy converter system is installed, water column in the converter system will be excited by waves possessing different characteristics which can lead undesired efficiency problems. Therefore, to predict the response of the system to diverse wave parameters is crucial. Because of this reason, relative average oscillation amplitude values were measured as incident wave series were altered, while dimensionless opening heights held constant for all cases. The experimental data indicate a proportional relationship as follows:

$$\eta \propto HL^2 \tag{3.15}$$

This relationship for all relative opening heights with regression lines is plotted in Figure 3.9. R^2 values vary in range between 0.97 and 0.99.

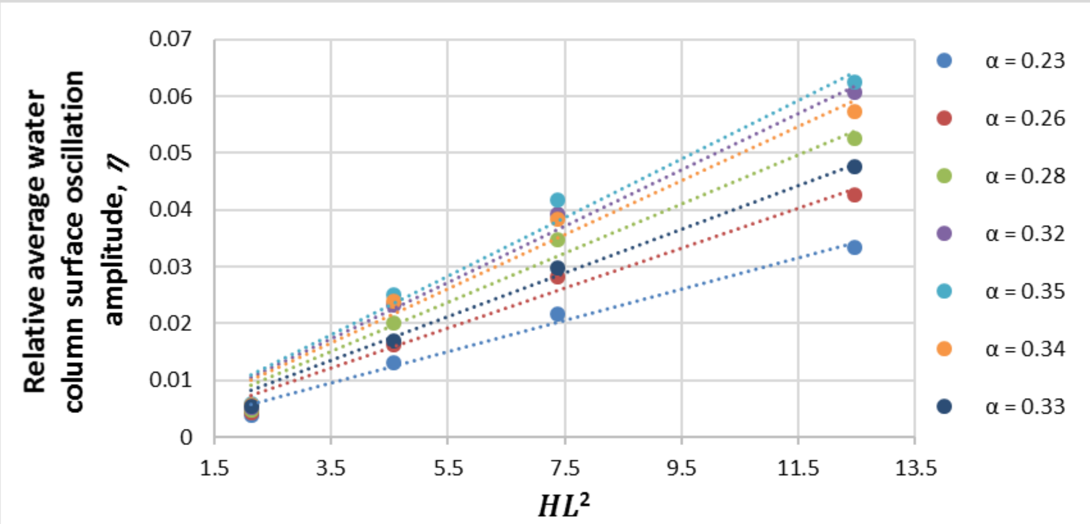

Figure 3.9 : η versus H. L^2.

From the figure, this linear relationship between η and HL^2 is obviously seen. Average water column surface fluctuation values have quadratic relationship with L and linear with H values. That is predictable because it was observed previously that waves with higher wave lengths generate piston type motion that has higher transmission rates yield greater average fluctuations in the chamber. Wave height is of second priority since its effect is linear because the pressure distribution beneath the wave is proportional to wave height. Being proportional with HL^2 is valid for all opening heights with slightly different slopes. As in the previous investigations, the biggest slope is for α value 0.67. It is also evident that, there is an admirable fit between the experimental data and mathematical model.

Finally, two mathematical models, Eqs. 3.2 and 3.12 can be combined to obtain a more general description of relative average water column oscillation amplitude as follows:

$$\eta \propto \beta^{1.1}\alpha^2 H L^2 \tag{3.16}$$

Because there exists a good agreement between mathematical model results and experimental data, proposed equations can be used in practical applications. If any of the surface fluctuation value is known corresponding to any wave parameter, proportionality constant can be determined. Then, any variable can be changed to obtain corresponding relative average oscillation amplitude. Of course, this is valid for fixed rectangular OWC system with the design parameters used in this study. But since fixed OWC system are common and widely installed for testing purposes at different places with various wave climates (Falcao and Henriques, 2016), the results of this study will come in useful for further optimization studies.

3.1.2 Damping coefficient and simple mathematical modelling

3.1.2.1 Damping coefficient evaluation

Figure 3.10 shows the calculated damping coefficients as described in section 2.2.2 for different relative opening heights. Quadrating fittings are also included for easier interpretation.

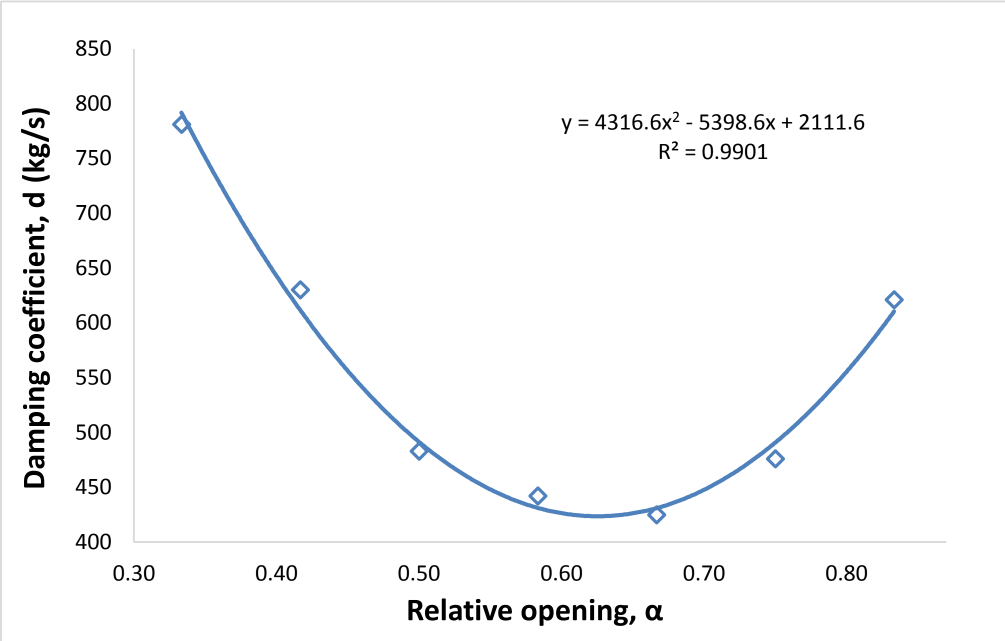

Figure 3.10 : Relative opening versus damping coefficients.

Damping is generated due to the resistive forces on the motion of the water column. Raised water column in the structure will be discharged through its opening to reach the equilibrium level after the removal of the cap on the exit of the orifice. Evidently, the discharge process will not be easy for relatively smaller opening heights and the motion of the water column will be somewhat restrained. Therefore, it is expected that maximum damping occurs when the relative opening ratio, α, is minimum because the opening height of the structure towards the exterior water mass becomes smallest for this α value. As it is seen from Figure 3.10, the biggest damping occurred when the α value is 0.33. As α gets bigger opening height increases and damping value decreases due to the preceding reasoning. But, surprisingly, for the α value of 0.67 damping coefficient becomes minimum and after this value starts to increase. Thus, a convex quadratic relationship forms between B and α as depicted in Figure 3.10. Reason for this kind of relationship should be explained as: the water column raises due to the generated pressure differential by the vacuum pump between the air pressure inside the chamber and outside pressure. When the cap is on, weight of the water column mass (with the raised part) plus the air pressure force on the water column surface balance with the exterior forces, hence, the system stays stationary. When the cap is removed, air is going to enter into the chamber and increase the interior air pressure. Net force on the water column will no longer be zero and raised water column will move to the outer side of the chamber. As soon as the pressure inside the chamber equals the outside (atmospheric) pressure and the water column reaches its equilibrium position, the motion ends. Since the water exits through the opening of the chamber, its height should also play an important role on the discharge process. Relatively small opening heights will slow down the transition of the water column out of the structure and generate high damping. As we increase the relative opening height value from 0.33 to 0.67, damping diminishes. For greater α values, most of the water column is free to move side to side easier than it was before, thus, water in the chamber will attempt to pass to the outer side very quickly. But, the air volume that can flow into the chamber through the orifice cannot be as much as the water volume leaving out of the chamber because, the raised water column leaves the chamber faster than air entering inside (for relatively bigger opening heights). In other words, when the water discharge towards the wave flume is bigger than the volume flow rate of air into the chamber, interior pressure will not reach atmospheric pressure instantly but will be delayed by some amount of time. So, during this inhalation process, air stays mostly rarefied under the atmospheric pressure. Consequently, damping increases because negative interior pressure forms above the water column which opposes its motion. As a result, value of α around 0.67 is the optimum opening height configuration that generates the minimum damping. The largest average free surface fluctuations in the chamber are also obtained for this particular opening height value because in this case the resistive forces on the water column was minimum.

Significance of this result further increases because for all wave conditions used in this study (including very short and long waves) maximum average free surface fluctuations (minimum damping) were generated when relative opening height was 0.67. Furthermore, by using the quadratic fitting formula that has a R^2 value of 0.99, damping coefficient values for any other opening height can be calculated with great accuracy.

In terms of generality, dimensionless damping coefficient, d^*, is also defined as:

$$d^* = \frac{dt_f}{a} \tag{3.17}$$

Figure 3.11 shows the dimensionless damping coefficient versus relative opening height relationship.

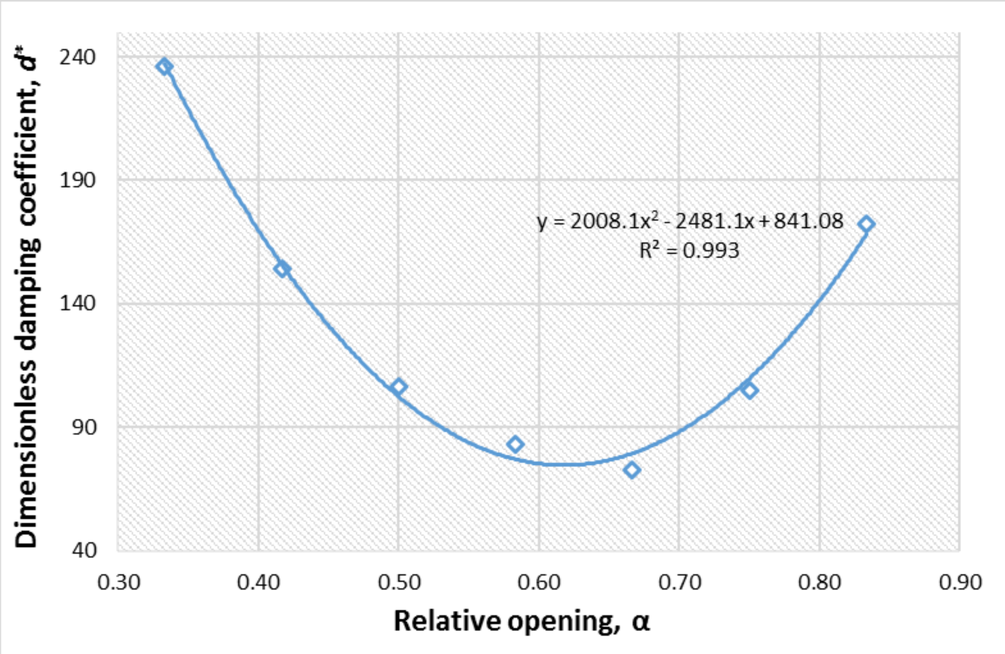

Figure 3.11 : Relative opening versus dimensionless damping coefficient.

3.1.2.2 Simple mechanical model results

Average surface oscillation amplitude values

Simple mechanical model results and experimental values are plotted for different α values under wave series W1, W2 and W3 in Figs. 3.12, 3.13 and 3.14, respectively. The results of the last wave series (W4) have been excluded from the analysis since an almost fully sloshing motion was generated in the chamber which is of no interest in terms of feasible energy extraction.

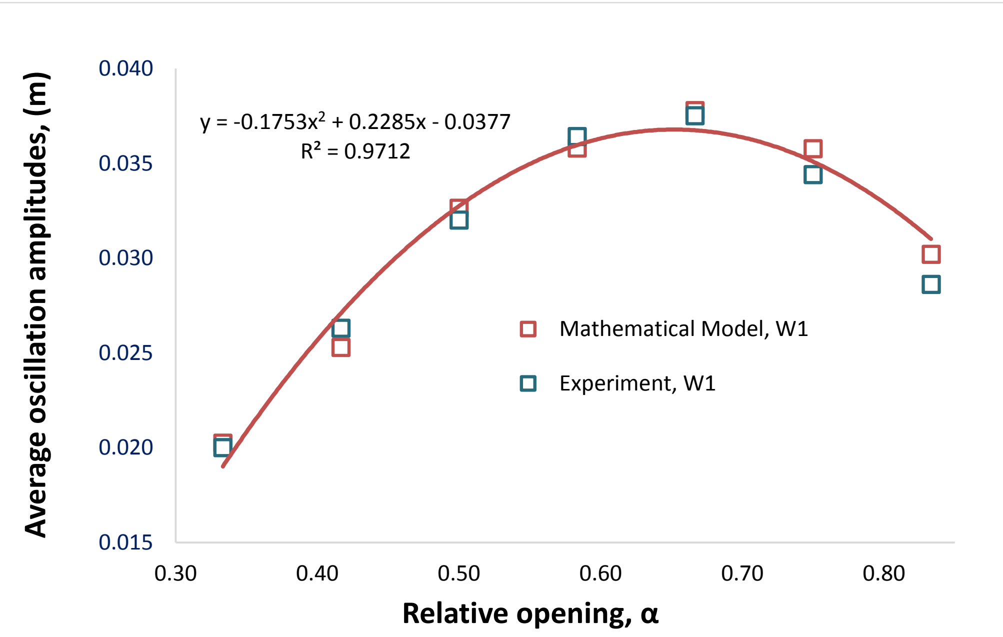

Figure 3.12 : Mathematical model versus experiment (W1).

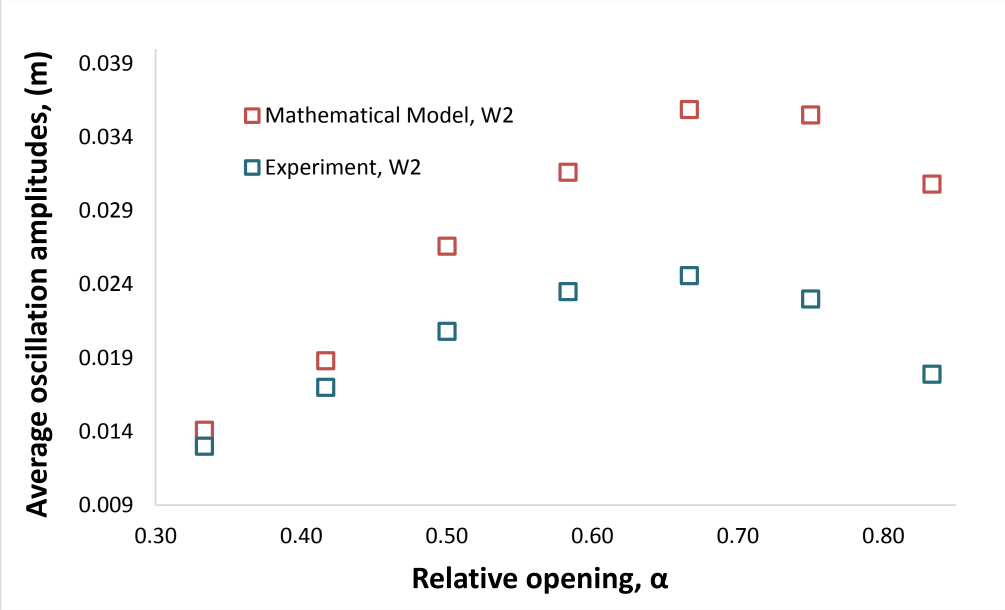

Figure 3.13 : Mathematical model versus experiment (W2..

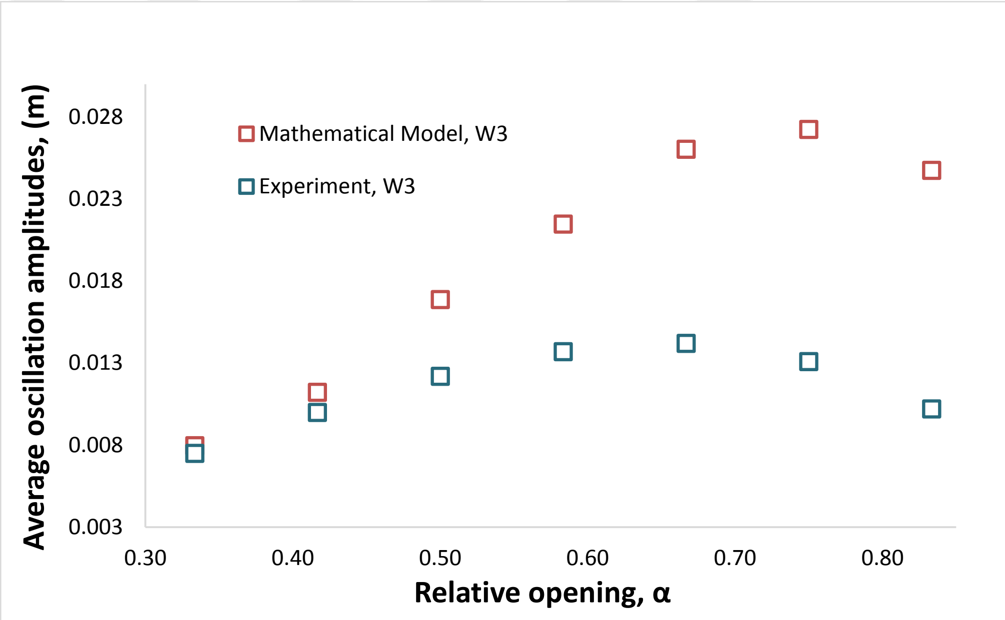

Figure 3.14 : Mathematical model versus experiment (W3).

It is obvious that the mathematical model results are matched very well with the experimental data for all different α values under wave series W1 as shown in Figure 3.12. This was expected after the examination of the water column surface motion behavior through the transparent side of the system. It was observed that the water column surface acts almost as a rigid piston with a planar surface under the harmonic excitation of W1. Flat surface rigid body motion of the water column is one of the primary assumptions made in the development of the simple mathematical model. For α value of 0.50, fluctuation time series of the water column at the center right, middle, and left of the chamber with respect to dimensionless time series, t/T (time (t) divided by the period of generated wave (T)) is shown in Figure 3.15. As can be observed from the figure, fluctuations at center right, middle and left of the chamber are in phase and close to each other in magnitude.

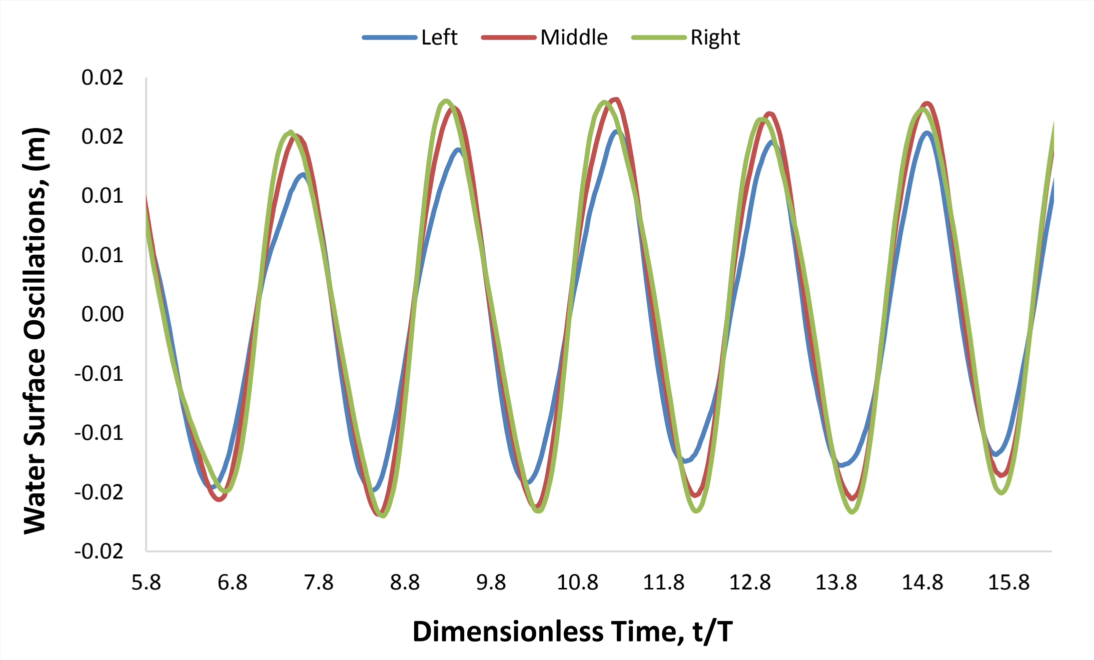

Figure 3.15 : Center right, middle and left displacements (W1 and α, 0.50).

Frequency content is also well captured by the model as Figure 3.16 shows experimental data and model fluctuation results with respect to dimensionless time series, for α value of 0.67.

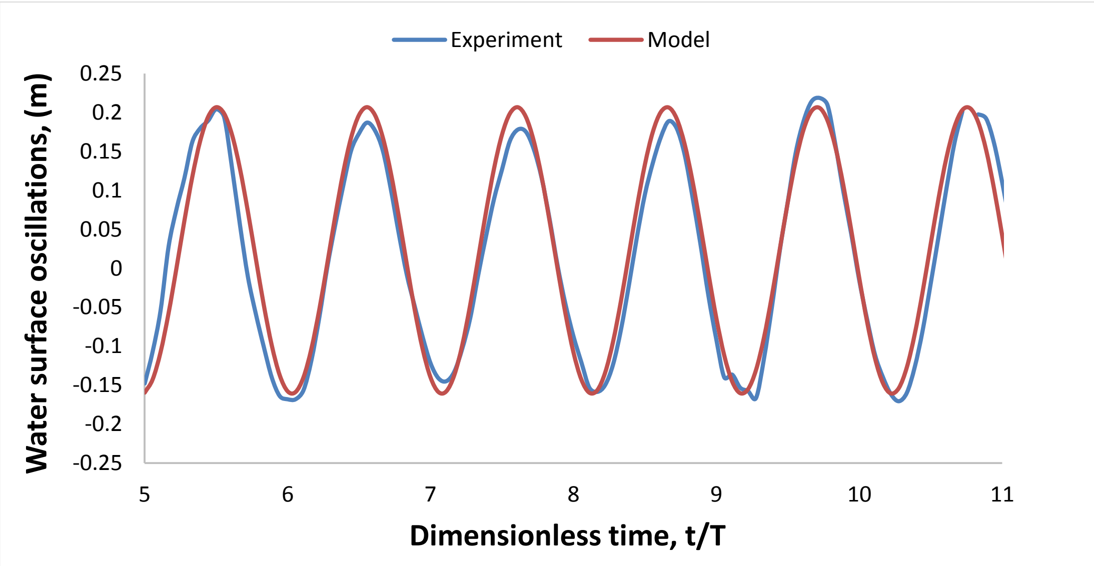

Figure 3.16 : Mathematical model versus experiment (W1 and α, 0.67).

For α values 0.75 and 0.83, the mathematical model slightly overestimated the experimental average fluctuation values in the chamber. This is due to the introduced concept 'Excessive harmful energy' by Çelik and Altunkaynak, (2018). Energy under the incident waves decays exponentially towards the seabed, thus, near surface depths contain more energy. Relatively higher energy transmitted into the system generates sloshing motion in the chamber independent of the incident wave characteristics. So, for α values bigger than 0.67, an additional sloshing motion inevitably joins on the motion type that would already be generated in the chamber due to the incident wave characteristics (even for a piston rigid body motion type). But the magnitude of this phenomenon decreases with the wave frequency so, the effect is little for wave series W1 which has the smallest frequency among others. Added sloshing motion also means that the additional wave energy transmitted into the chamber is converted into kinetic energy in the form of sloshing. This superposed type of sloshing behavior on to the already generated motion in the chamber by the particular incident wave properties, reduces the average free surface fluctuations in the chamber. Because the mathematical vibration model does not involve such motion, all energy transmission after the α value of 0.67 is represented as an increasing pressure under the water column. Therefore, mathematical model results slightly deviate from the experimental values such that the deviation is only 3.2% and 6.3% for α values of 0.75 and 0.83, respectively. After all, at the design stage this critical opening height values should be avoided because the sloshing motion is an undesired effect for the converter's efficiency.

For wave series W2, based on Figure 3.13, mathematical model results tend to follow a similar trend with experimental values in the validation phase for all different α values. A combination of piston and sloshing type motions where piston type motion is dominant, is generated in the chamber due to the wave characteristics of wave series W2. It is also measured that the magnitude of the sloshing motion increases with the opening height. From the experimental model results, it has been found that, sloshing motion of the water column arises from two facts. First one is because of the relatively short wavelength of the incident wave with respect to chamber length and second is due to the excessive harmful energy defined by Çelik and Altunkaynak, (2018). Thus, due to the characteristics of W2, an inherent sloshing motion forms in addition to the piston type behavior of the water column. Also, the authors found that the ratio of the combination of these two type behaviors in the overall motion is a function of the value of the ratio of wavelength to chamber length. Therefore, for W2, part of the transmitted wave energy into the chamber is converted to kinetic energy in the form of asymmetrical vertical velocities of water particles with respect to the center of the water column. The other important conclusion from the experimental measurements and observations is, generated sloshing motion due to wave excitation increases with the opening height of the chamber. Bigger immersion depths act as a low pass filter which depresses the high frequency content of the incident wave where, after the α value of 0.67, smaller immersion depths behave like a high pass filter by enhancing the sloshing motion via stopping low frequency content transmitting into the chamber. For example, for the smallest α value, inherent (due to the wave characteristics) sloshing motion is so highly suppressed that, even for the wave series W4 which is expected to generate an almost fully sloshing motion in the chamber due to its very short wavelength, behavior of the motion approaches to piston type. Sloshing of the water column may be thought as dissipated energy because the trapped air above the water column cannot be forced to exit the orifice since the air volume in the chamber remains mostly unchanged. Therefore, estimated average water column fluctuations by the mathematical model deviate from the experimental results as opening heights get bigger. Excessive harmful energy concept is independent of wave parameters, but its effect becomes more dramatic as the wavelength decreases. Therefore, the gap between the mathematical model results and the experimental values even more increases after the α value of 0.67. As can be seen from Figure 3.14, the relationship of the results of the mathematical model with the experimental values under wave series W3, has a similar trend with the results under wave series W2. Also, there is a bigger deviation from the experimental values compared to wave series W2 as opening height increases. It is because water column motion is transformed into a combination of piston and sloshing motion types where sloshing motion is dominant. Thus, the mathematical model overestimates the experimental values under wave series W3 more than it was for the case of wave series W2. It is obvious that W3 forces the water column surface act in a sloshing dominant behavior where rigid body motion assumption becomes far from reality.

Nevertheless, for the smallest α values of 0.33 and 0.42, the mathematical model results have good agreement with the experimental values with overestimations of 3%

to 10% for W2 and W3 (even 7% for W4 and α, 0.33), respectively. This is because, relatively small opening heights depress the sloshing motion to a great extent and compel the water column act as a flat rigid body. This fact can be important in the design stage of the OWC geometry where inevitable sloshing motions occur in the OWC chamber. Under the assumption of the rigid body motion, these results additionally indicate the success of the developed mathematical model and also the accuracy of the determined damping coefficient values which constitute the most important component of the estimation model.

As regards W4, an almost fully sloshing motion was formed in the chamber. Figure 3.17 shows the fluctuation magnitudes of the water column at the center right, middle, and left of the chamber for α value of 0.42. Obviously, right and left fluctuations are almost 180^0 out of phase and middle fluctuations are negligibly small.

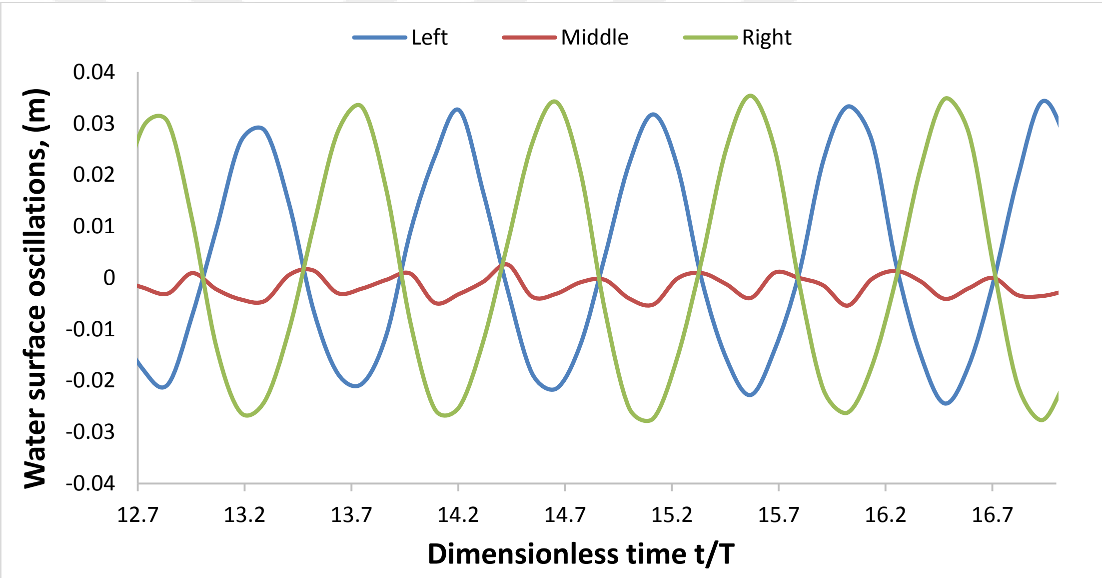

Figure 3.17 : Center right, middle and left displacements (W4 and α, 0.42).

Even though the mathematical model results seem to be in very good agreement with the experimental values for only wave series W1, developed mathematical model is very valuable in terms of feasible energy extraction. Because, most of the wave energy applications involve planar surface fluctuations (Wang et al, 2002) and this fact coincides with the assumptions of the developed mathematical model. Besides, sloshing motion behavior of the water column is literally an enemy for feasible wave energy extraction. Thus, design features of OWC energy converter systems are established to avoid this kind of motion in the chamber. Therefore, what will be important ultimately, is to be able to determine the damping coefficients, so that the equation of the dynamics of the water column can be solved which is achieved very well by the developed mathematical vibration model in this study.

Phase angle response

Figs. 3.18-3.20 show the mathematical model phase angle results and the experimental model phase angle values with respect to relative opening heights for wave series W1, W2 and W3, respectively.

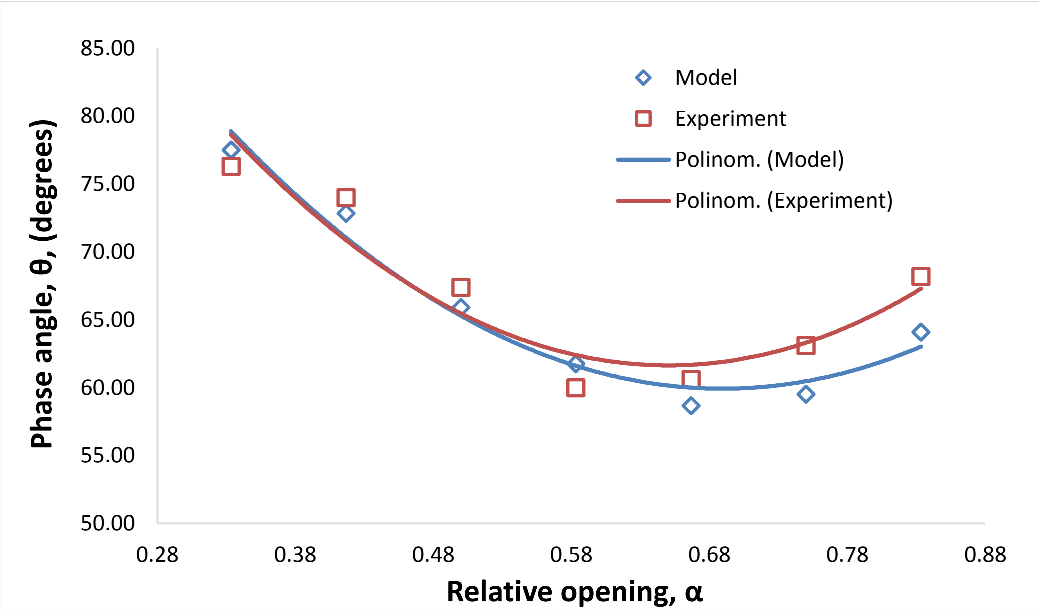

Figure 3.18 : Mathematical model versus experiment (W1).

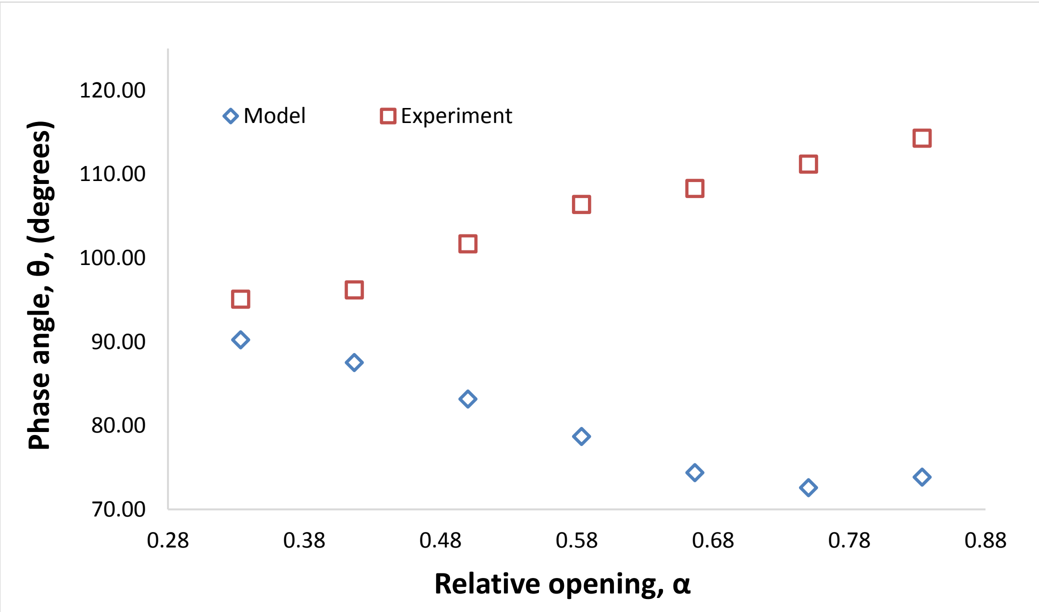

Figure 3.19 : Mathematical model versus experiment (W2).

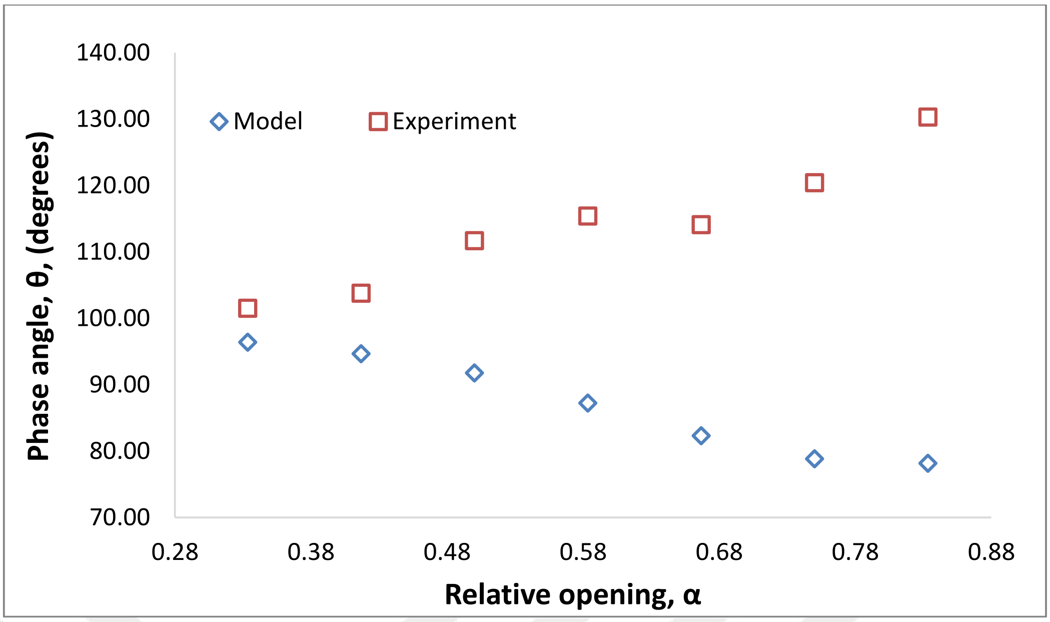

Figure 3.20 : Mathematical model versus experiment (W3).

Not surprisingly, the phase estimations of the mathematical model for W1 have very good agreement with the experimental model values. Due to the sloshing mode initiated after the critical α value, the mathematical model slightly overestimates the experimental phase values. For the remaining wave series, calculated average phase angles are always above the experimental model values with an increasing magnitude as the incident waves become shorter. Apparent effect of diverging from the assumption of a planar surface rigid body motion results in underestimating the phase angle response of the oscillating water column.

Phase angle approximations are important because large water level differences can cause high hydrodynamic forces on the structure. Again, phase angle response of the OWC system can be estimated by using the developed model with a good accuracy for relatively long waves, therefore, inner-outer water elevation differences may easily be calculated.

One thing to note here is, during the experiments it was observed that when the water column sloshes with respect to center of the chamber, phase angle difference of the water level fluctuations on the left and right-hand side of the front wall (inner and outer surfaces, respectively) were almost always under 60°. This phenomenon kept the water elevation difference at moderate levels, even though average phase angle response was more than 120°. This is especially important where the hydrodynamic forces on the front wall are important.

3.2 Underdamped Case

Freely decaying oscillation of the water column took place for all the orifice ratio values but for the smallest orifice ratio in the free decay tests. Therefore, except the orifice ratio 0.20, underdamped system dynamics govern the motion of the water column which enables utilizing free decay tests to obtain the hydrodynamic parameters of the OWC.

3.2.1 Determination of hydrodynamic parameters

3.2.1.1 Validation of the numerical model results

In the present study, free decay tests are performed with developed experimental and 3D numerical models for determination of hydrodynamic parameters of a fixed OWC under all opening heights and orifice sizes. Remarkable agreement is found between numerical model results and corresponding experimental model values of oscillation water column time series data. A comparison of typical experimental and numerical free decay time-series is depicted in Fig 3.21. Oscillation amplitude of the water column is normalized by the still water depth. As can be seen from this figure, the results of numerical free decay time-series tend to follow the corresponding experimental free decay time-series of oscillation water column data very closely. It is immediately realized that peak values, frequency information and trend of the response are very well captured by the numerical model.

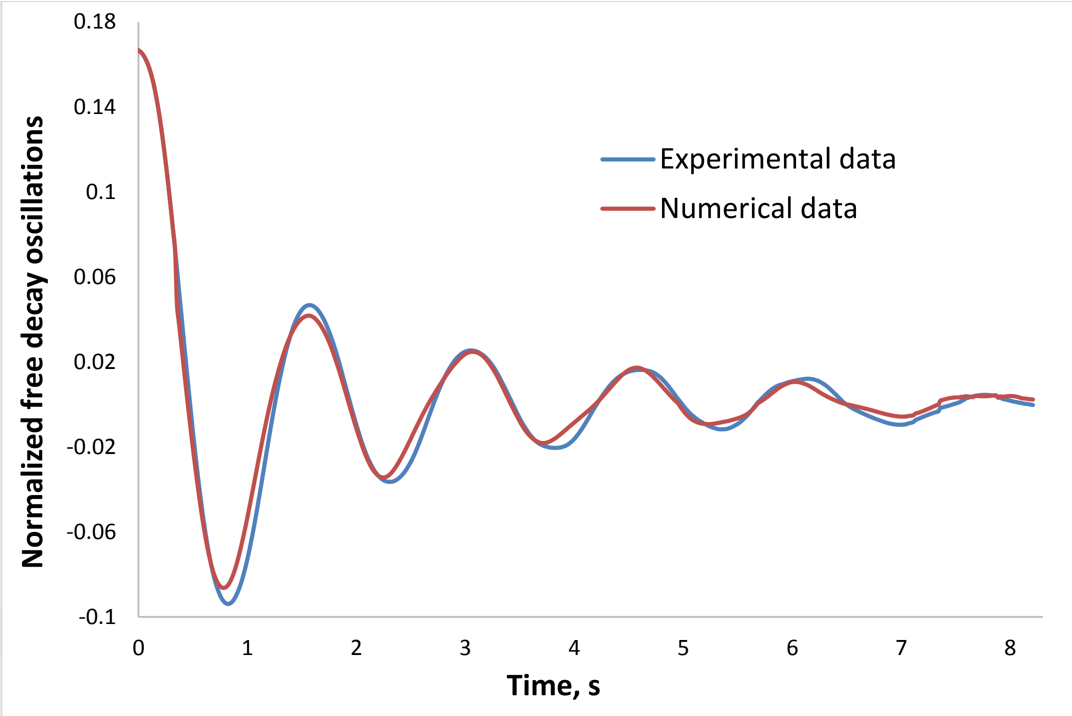

Figure 3.21 : A typical experimental and numerical free decay time-series.

Calculated RMSE values of experimental and numerical models for damping ratio, ζ and damped natural period, T_d are found to be 0.016 and 0.052s, respectively, while CE values are 0.928 and 0.879, respectively.

Calculated experimental and numerical damping ratios and damped periods for all different relative openings and orifice ratios are presented in Table 3.1, respectively.

From the preceding discussion, it can safely be concluded that, for all chamber and damping configurations, numerical model results closely mimic the experimental model data, therefore, the numerical models can be utilized for free decay simulation of OWCs.

Table 3.1 : Damping ratio and damped period values.

Relative opening (α)	Orifice ratio (τ)	Damping Ratio		Damped Period	
		Exp.	Num.	Exp.	Num.
0.33	0.060	0.409	0.435	2.090	2.169
	0.080	0.320	0.331	2.010	2.056
	0.010	0.261	0.250	2.040	2.003
	0.130	0.221	0.232	1.980	2.022
0.42	0.060	0.366	0.348	1.990	2.074
	0.080	0.289	0.269	1.950	1.899
	0.010	0.248	0.257	1.930	1.974
	0.130	.206	0.199	1.920	1.956
0.5	0.060	0.358	0.334	1.930	1.862
	0.080	0.278	0.291	1.900	1.946
	0.010	0.245	0.256	1.850	1.883
	0.130	0.196	0.183	1.890	1.907
0.58	0.060	0.328	0.307	1.870	1.949
	0.080	0.250	0.262	1.860	1.925
	0.010	0.242	0.255	1.880	1.833
	0.130	0.199	0.184	1.810	1.843
0.67	0.060	0.320	0.302	1.840	1.930
	0.080	0.255	0.267	1.760	1.711
	0.010	0.229	0.215	1.800	1.838
	0.130	0.191	0.188	1.800	1.771
0.75	0.060	0.290	0.322	1.690	1.756
	0.080	0.230	0.211	1.690	1.731
	0.010	0.215	0.198	1.660	1.627
	0.130	0.188	0.196	1.620	1.638
0.83	0.060	0.259	0.239	1.668	1.730
	0.080	0.209	0.229	1.600	1.554
	0.010	0.189	0.201	1.570	1.605
	0.130	0.171	0.161	1.550	1.521
RMSE		0.016		0.052	
CE		0.928		0.879	

3.2.1.2 Evaluation and surface motion behaviour investigations

To extract the ocean energy in an efficient manner system's heave resonant frequency has to be tuned to the prevailing incident wave. In this case the water column approximately acts as a rigid body with high amplitude. In the vicinity of resonant frequency, motion of the water column mostly depends on system's total equivalent linear damping including viscous, radiation and PTO dampings because restoring and inertial forces cancel each other. For this reason, according to Chakrabarti and Cotter, 1992, determination of the system's overall damping is crucial for design considerations.

Figure 3.22 shows the calculated overall damping ratios (according to the method described in 2.2.3) versus different orifice ratios for the opening heights used in this study. For a clear vision and better understanding damping ratios for only some of the relative openings are depicted and quadratic fitting lines are included in the figure. As it can be seen damping decreases with the increase of orifice ratio as expected but in a quadratic manner which adequately describes the relationship between the damping and orifice ratios. Note that as the relative opening increases quadratic relationship weakens.

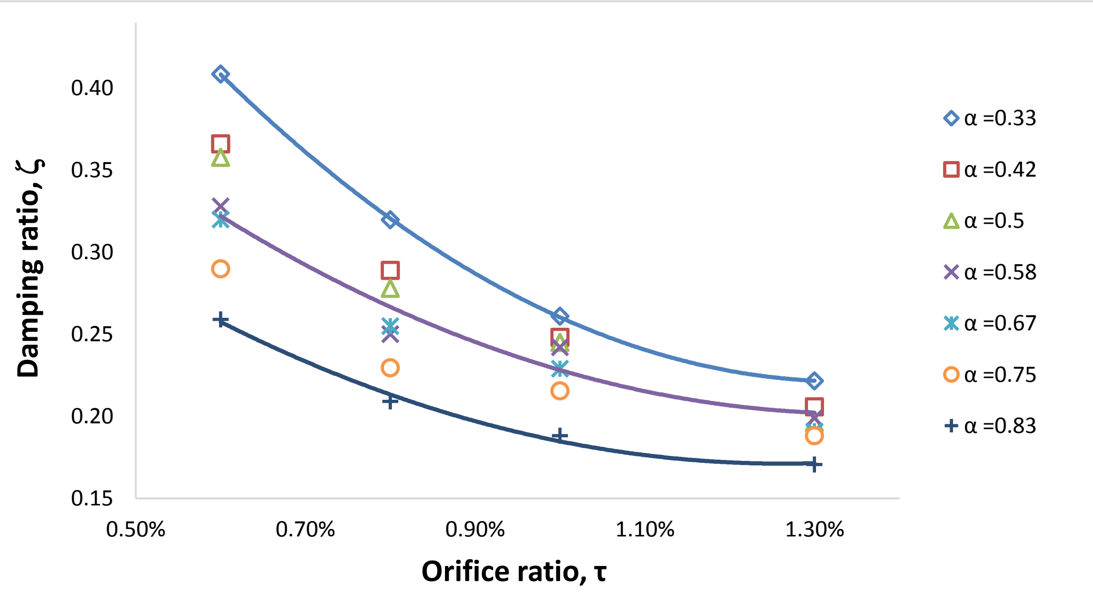

Figure 3.22 : Damping ratio versus orifice ratio.

Inversely, the relationship between the damping and the relative opening for different orifice ratios is shown in Figure 3.23. Clearly, relative opening has also a significant effect on the overall damping of the system. It is readily observed that the damping ratio decays with the relative opening with an almost linear fashion for all orifice ratios. Linear regression lines are also inserted for better interpretation. Water column within the chamber communicates with the exterior water mass through the lower opening of the chamber. If the opening is relatively bigger, alternating water mass between the chamber and the outside region moves more easily causing the system damping to decrease. It is to note that, as the orifice ratio increases slope of the linear decaying behavior of the damping ratio with respect to relative opening diminishes implying that the damping ratio of systems with low PTO damping are more insensitive to the opening height of the chamber. Examination of the Figure 3.23 further illustrates that the differences in the damping value with respect to varying orifice ratio decrease as the relative opening increases. For example, for the biggest relative opening, damping ratios become very close even though the orifice ratios vary in a broad range. However, for the smallest relative opening damping values are quite apart from each other for different orifice ratios. This separation is responsible for the varying strength of the quadratic relationship presented in Figure 3.22. As stated in the previous discussion, it demonstrates that the smaller the orifice ratio, the higher the sensitivity of damping ratio to the opening height of the chamber. It can be concluded that for a constant geometry, damping ratio is a function of orifice ratio and relative opening in a quadratic and linear fashion, respectively. From the obtained empirical regression lines overall damping ratio can be determined for a broad range of orifice and opening sizes.

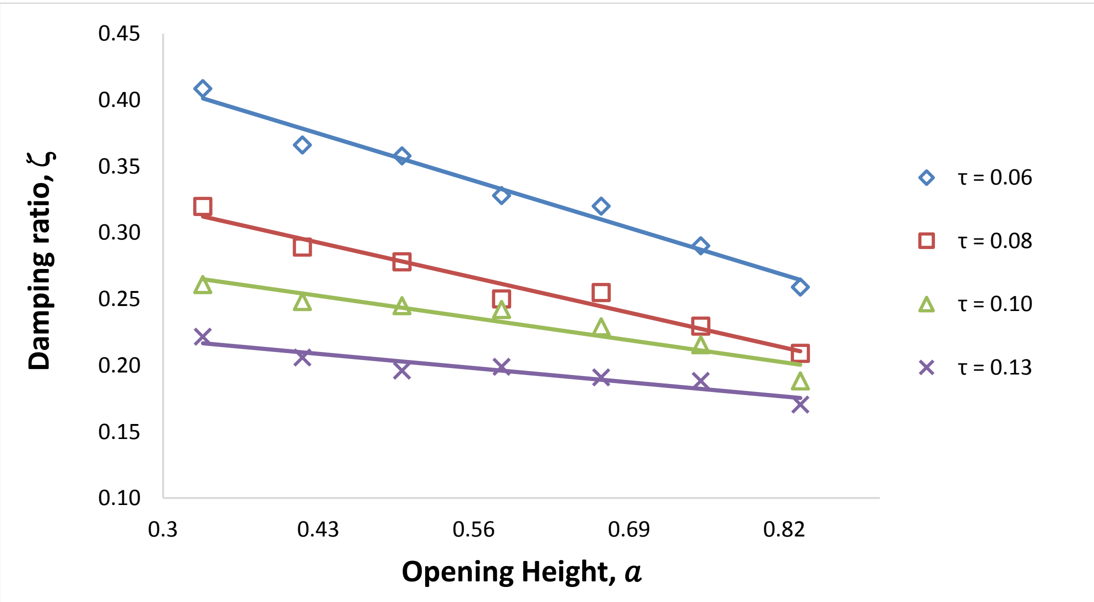

Figure 3.23 : Damping ratio versus relative opening.

Calculated natural frequencies according to 2.31 versus orifice ratios for relative openings used in this study are plotted in Figure 3.24. Expectedly, plotted natural frequencies for different orifice ratios (damping values) have very similar values since by definition they represent the resonant condition for undamped systems. However, frequency values heavily depend on the relative opening.

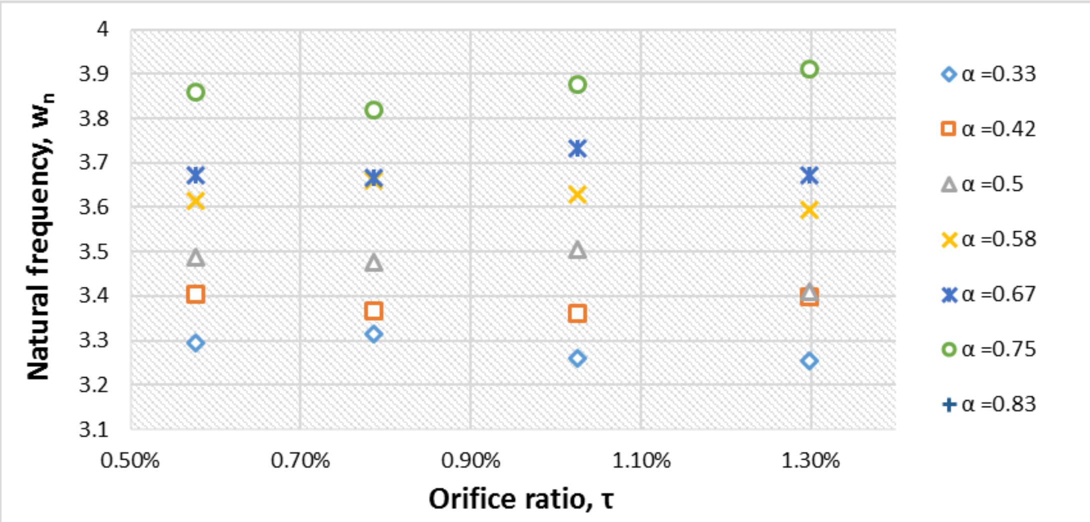

Figure 3.24 : Natural frequency versus orifice ratio.

Figure 3.25 shows the natural frequencies versus relative openings. Each value corresponding to a distinct relative opening is the average of the natural frequencies calculated for different orifice ratios. Frequently in the literature, natural frequency is calculated by the following formula as a first approximation.

$$w_n = \sqrt{\frac{g}{y}} \tag{3.18}$$

where, g is the gravitaitonal constant (m/s^2) and y is the immersion depth of the chamber's front wall (Evans and Porter, 1995). A more general formula is given by McCormick, (1981).

$$w_n = \sqrt{\frac{g}{(y+y')}} \tag{3.19}$$

where, y' is the so called "effective length" representing the added mass set in motion by the oscillation of the water column. In an experimental study, y' is empirically obtained by Fukuda, (1977):

$$y' = 0.41\sqrt{A_w} \tag{3.20}$$

where, A_w is the water column surface area (m^2).

There is also another formula for determination of the natural frequency of an oscillating water column which is derived by the potential flow assumptions within the framework of linear water wave theory (Molin, 2001). To the best of the author's knowledge Molin's formula has not been used for calculation of any wave energy converter tool, nevertheless, it has been included for completeness. This formula describes the effective length as follows.

$$y' = \frac{b}{\pi}\left[\sinh^{-1}\left(\frac{l}{b}\right) + \frac{l}{b}\sinh^{-1}\left(\frac{b}{l}\right) + \frac{1}{3}\left(\frac{b}{l} + \frac{l^2}{b^2}\right) - \frac{1}{3}\left(\frac{b}{l} + \frac{l^2}{b^2}\right)\sqrt{\frac{b^2}{l^2} + 1}\right] \quad (3.21)$$

where, l and b are the length and width of the water column, respectively.

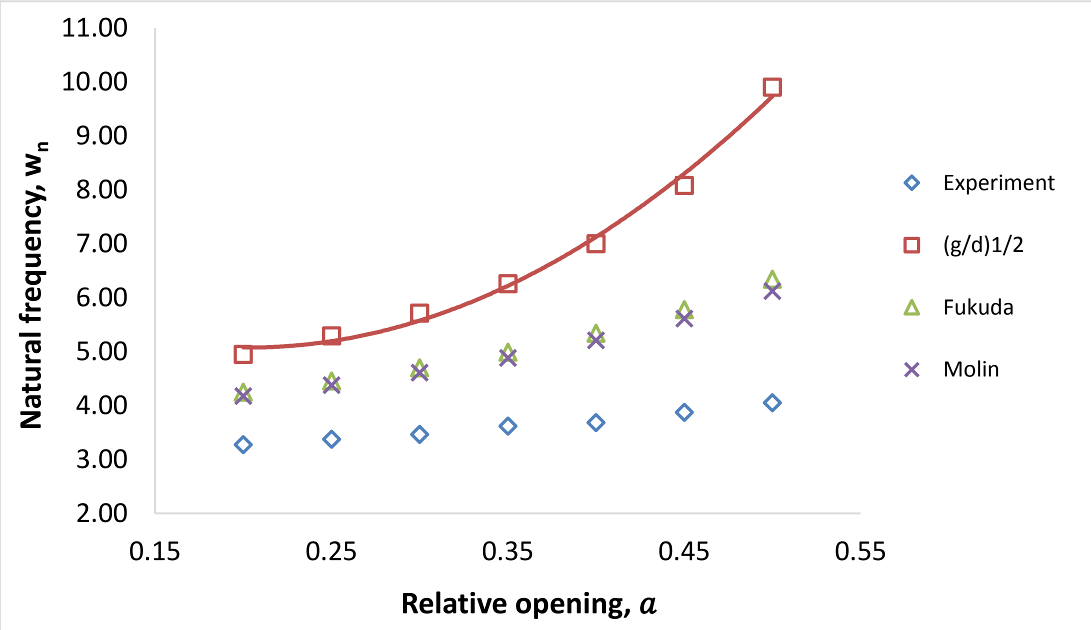

Figure 3.25 : Natural frequency versus relative opening (different formulas).

Computed natural frequencies by the above equations found in the literature are also inserted in Figure 3.25 for comparison. It is clearly observed that natural frequencies obtained via 3.18 are higher than those that were calculated by equations 3.20 and 3.21 greatly overestimates the experimental values. It is not surprising because in 3.15 added mass is ignored. For relatively bigger openings obtained values further diverges from the rest of the calculations as quadratic fitting well represents the natural frequencies calculated by 3.15. This formula is actually a limiting case for very narrow water columns where added mass is infinitesimal small. Despite the crude approximation obtained, it is often used for practical purposes to gain physical insights, because of the challenging nature of determination of the added mass. But, according to the results of this present study, natural frequencies calculated by 3.18 are unrealistic especially for relatively bigger openings. In addition, Morris-Thomas et al. (2007) reported a caveat that, calculated natural frequencies according to 3.18 should always be considered as an upper bound for the actual value. Fukuda (1977) and Molin (2001) determined the natural frequency by means of experiments and potential theory, respectively. As reported by Veer and Tholen (2008), Molin's (2001) formula, which is somewhat unwieldy, always yields slightly smaller natural frequencies. Indeed, this is the case as Figure 3.25 illustrates. However, both of them provided higher values than those of determined in this study. One reason for this should be, Fukuda (1977) used both rectangular and circular cross-sections in the experiments and empirical formula was derived to represent both cross-sections. Another reason could be lying on the underwater geometry of the tested chamber. In the present study right, left and back plate of the OWC extends all the way down to the bottom of the wave flume, where Fukuda and Molin used structures that pierce the free surface evenly for all sides without reaching the bottom of the tank. Besides, they model the water columns in moonpools which are located in ships or offshore structures. In some sense, they resemble floating rather than fixed OWCs where hydrodynamics would be different due to the coupling of the water column and floating structure. According to Ning et al. (2016), Fukuda's formula may not yield accurate values for OWCs. Therefore, Fukuda's expression is modified based on the physical experimental model data gathered in the present study. The modified formula for calculation of effective length is defined as:

$$y' = 1.44\sqrt{A_w} \qquad (3.22)$$

Calculated natural frequencies by using the empirically obtained effective length very closely follow those that obtained based on physical experimental model data of this present study.

Figure 3.26 shows the natural frequency values computed by utilizing the results of the experimental data developed in the present study and the empirical formula in x and y axes, respectively. 45^{o} diagonal (1:1) line is also plotted to provide better visual understanding for model performance. Figure 3.26 clearly reveals that modified formula values are found to be remarkably in accord with experimental data.

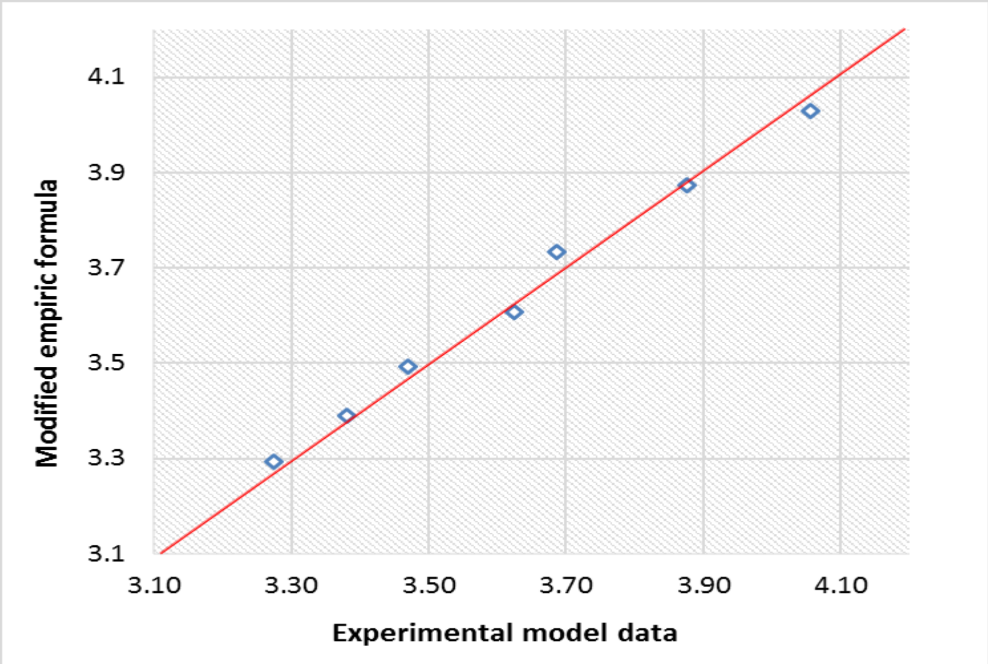

Figure 3.26 : Empirical versus experimental natural frequeny.

According to McCormick et al. (2018), empirical representations are very valuable as they enhance prediction accuracy and decreases the analytical complexity.

OWC wave energy converters are dynamical systems which diversely respond to the various excitation frequencies. In a real-sea condition incident wave forces exciting the water column possess different frequencies. Analysis of the wave climate of a specific region, where an OWC is planned to be deployed, reveals the dominant wave frequency present in that region. Most of the available incident wave energy can only be extracted if the OWC structure is tuned for this frequency. Therefore, determination of the resonant frequency for a variety of geometric parameters and applied PTO dampings is of great importance. For $0 < \zeta < {}^{1}/_{\sqrt{2}}$, where the damping ratios found in the present study lies in, resonant frequency is given by the following expression (Rao, 2011):

$$w_r = w_n\sqrt{1 - 2\zeta^2} \tag{3.23}$$

Figure 3.27 illustrates the calculated resonant frequencies for different relative openings and orifice ratios. It is readily observed that resonant frequency increases with the relative opening for all orifice ratios. Reported values are also compatible with a recent experimental study carried out by Çelik and Altunkaynak (2018) where the same OWC tool, geometric and damping parameters are used under the excitation of various monochromatic waves. Relevant frequencies used in the mentioned study are 3.49rad/s and 4.99rad/s. For all openings and orifice ratios, interior water column oscillations of the OWC were found to be maximum under the excitation with an angular frequency value of 3.49rad/s. It is noted that all calculated resonant frequencies are much closer to 3.49rad/s rather than 4.99rad/s.

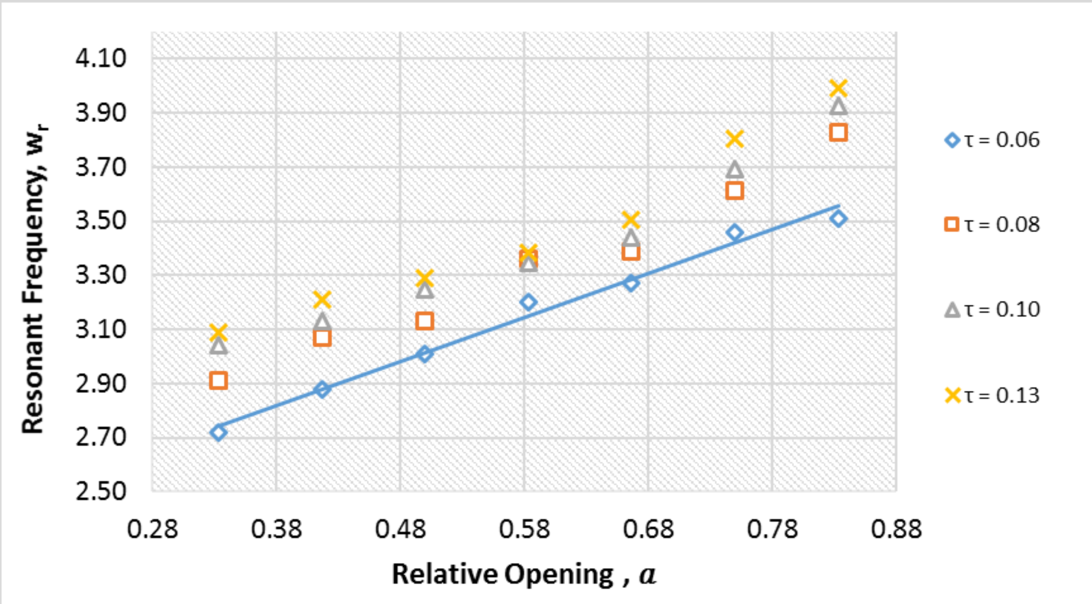

Figure 3.27 : Resonant frequency vs relative opening.

In addition, resonant frequency versus orifice ratio relations for different relative openings are shown in Figure 3.28. For a clear and better understanding the results are shown for only some of the relative openings. However, remaining results exhibit similar behavior.

A rectilinear relationship is evidently realized from the data depicted in Figure 3.28. Therefore, for the rectangular OWC geometry used in this present study, resonant frequency can be adequately approximated with a linear function of chamber opening and PTO damping which can be used for accurate determination of resonant frequency under different system parameters.

Within the scope of this present study added mass is also calculated by using 2.32. Figure 3.29 demonstrates the relationship between the added mass and the opening ratio for different orifice ratios. Similarly, for a clearer vision results for only some of the cases are shown, however, they resemble each other.

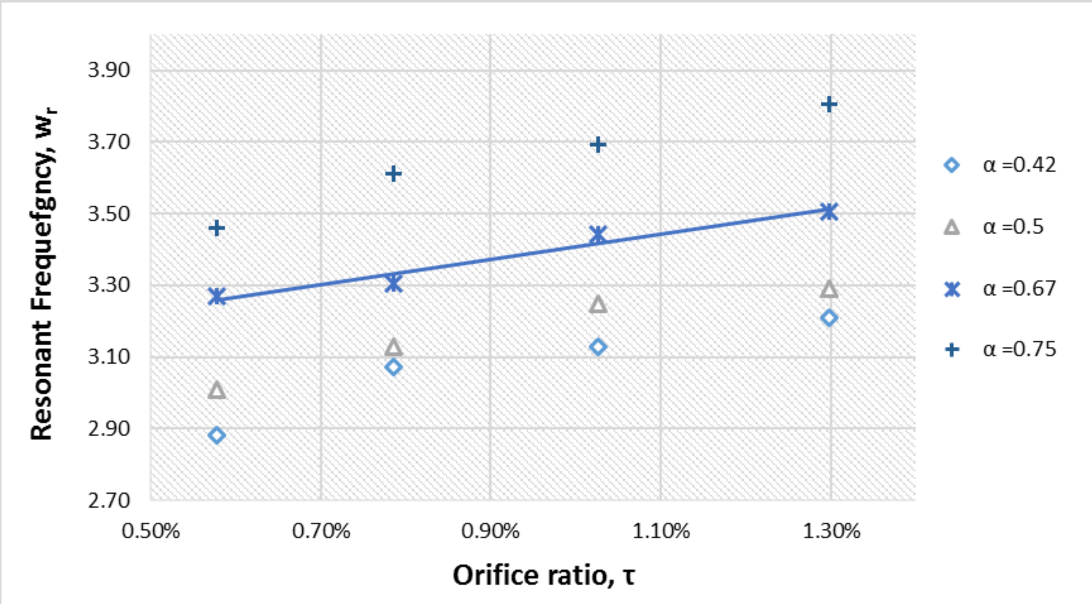

Figure 3.28 : Resonant frequency vs orifice ratio.

According to Figure 3.29 there is no evident variation pattern for the added mass values as the relative opening and orifice ratio varies. However, depicted values are very close to each other and scattered in a narrow band. Essentially, this should be the case. Expression of natural frequency is originally derived from undamped equation of motion (McCormick, 1981).

$$\omega_n = \sqrt{\frac{\rho g A_w}{m+m_a}} \tag{3.24}$$

However, if the horizontal cross section of the OWC is constant above formula reduces to 3.19. This implies that effective length (y') represents the added mass term in 3.19 and evidently, empirically obtained natural frequency expression in this study has a constant effective length. This was also the case for the empirical expressions (3.17 and 3.18) represented by Fukuda (1977) and Molin (2001), respectively. Furthermore, in an experimental study conducted by Chakrabarti and Cotter (1992), free decay tests were used to determine the hydrodynamic coefficients of a semisubmersible and very closed values of added mass for different natural frequencies are reported.

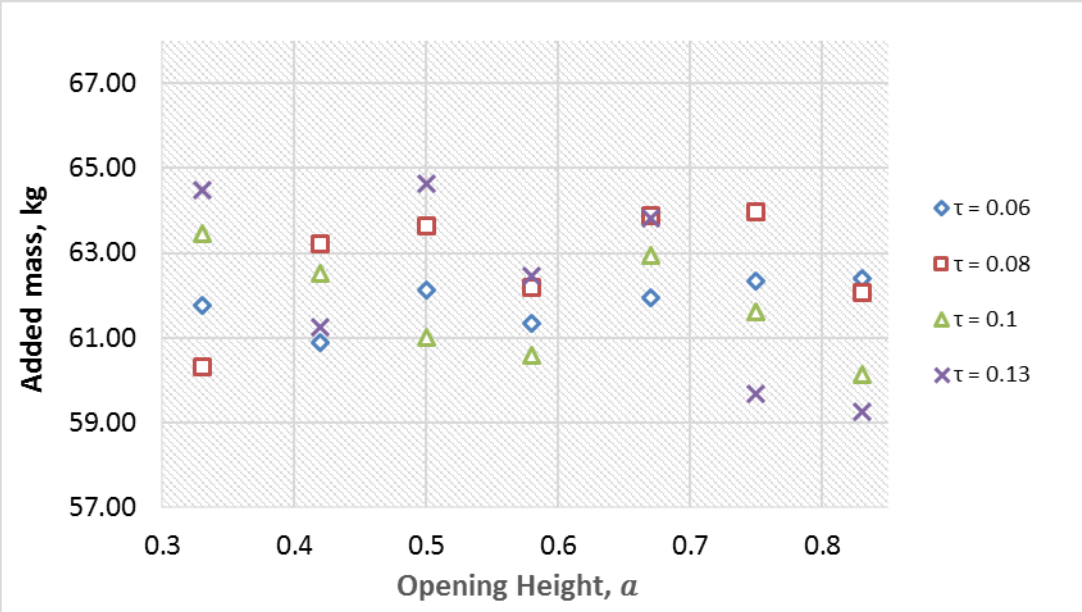

Figure 3.29 : Added mass versus relative opening.

3.2.2 Validation and simple mechanical model results

Determined damping and added mass values are used in the analytical model and the water column surface displacements with respect to still water level are calculated. Subsequently, analytical model results are evaluated with corresponding measured water column displacements which obtained from physical model experiments performed in this study. All analytical calculations and experimental measurements are carried out for all relative openings and orifice ratios under the generated incident waves.

Figure 3.30 compares the experimentally measured and analytically computed time histories of the water column surface displacement time series for $\alpha = 0.67$ and $\tau = 0.13$ under the excitation of W1, W2 and W3. Surface displacements are non-dimensionalised by the still water depth. This representative case ($\alpha = 0.67$ and $\tau = 0.13$) is similar to most of the results obtained by different relative openings and orifice ratios. Small amount of divergent cases will be discussed later. As it is obviously seen that harmonic behavior of the motion and the frequency content is very well matched by the analytical model. It is to note that well matching frequency content is valid for all orifice and chamber opening values used in this study.

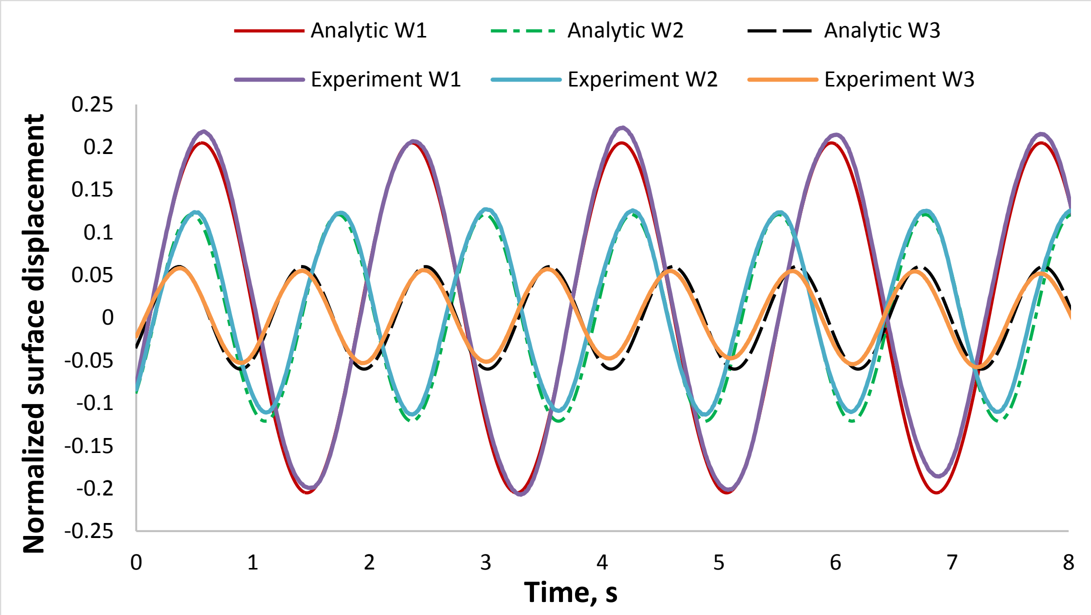

Figure 3.30 : Comparison displacements for $\alpha = 0.67$ and $\tau = 0.13$.

To be able to represent all comparisons between the experimental data and analytical model results, experimentally obtained steady-state harmonic amplitudes are averaged and for each opening height and orifice ratio, a representative amplitude is determined. Figure 3.31 indicates the analytically and experimentally obtained water column harmonic amplitudes with respect to relative openings (constant orifice ratio) under the excitation of incident wave, W1. Due to the closeness of the values to be presented, to represent a clearer vision, Figure 3.31 only shows the comparisons for the orifice ratios, 0.06 and 0.1. However, the comparison plots for the remaining orifice ratios are very similar. As it can be seen, there exists a remarkable agreement between the analytical model results and corresponding experimental model values for all relative openings and orifice ratios under the excitation of incident wave, W1.

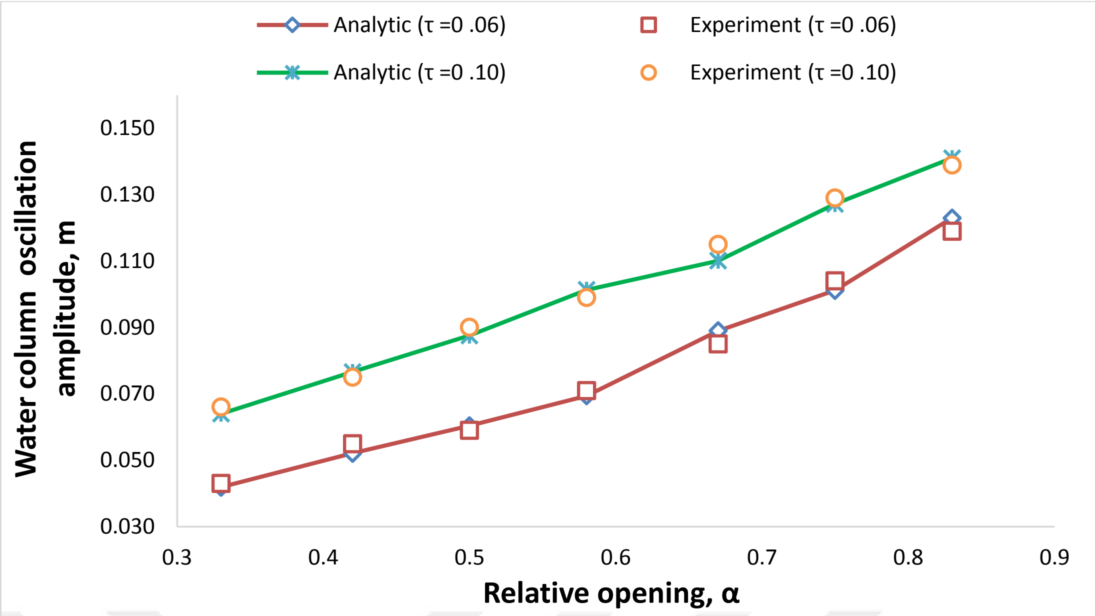

Figure 3.31 : Comparison of amplitudes for $\tau = 0.06$ and $\tau = 0.10$ under W1.

For the excitation of incident wave, W2, Figs. 3.32 and 3.33 demonstrate the analytical and experimental amplitude comparisons for all relative openings with respect to constant orifice ratios 0.06 and 0.13, respectively. In the same fashion, Figs. 3.34 and 3.35 illustrate the results for the excitation of incident wave, W3. However, unlike the W1 case, the comparisons for different constant orifice ratios had to be given in separate figures to be able to present readable and thus understandable figures because the obtained values are very close to each other and thus overlap. Not to represent overwhelmingly large number of figures and since the undemonstrated comparisons are similar to the given ones, only results for two distinctive orifice ratios are depicted. These particular orifice ratios are chosen because they are the edge values of the orifice ratio interval used in this study and accordingly, represent the extreme cases where the results and existing trends for the intermediate orifice sizes are always between those of orifice ratios 0.06 and 0.13 and hence can easily be envisaged.

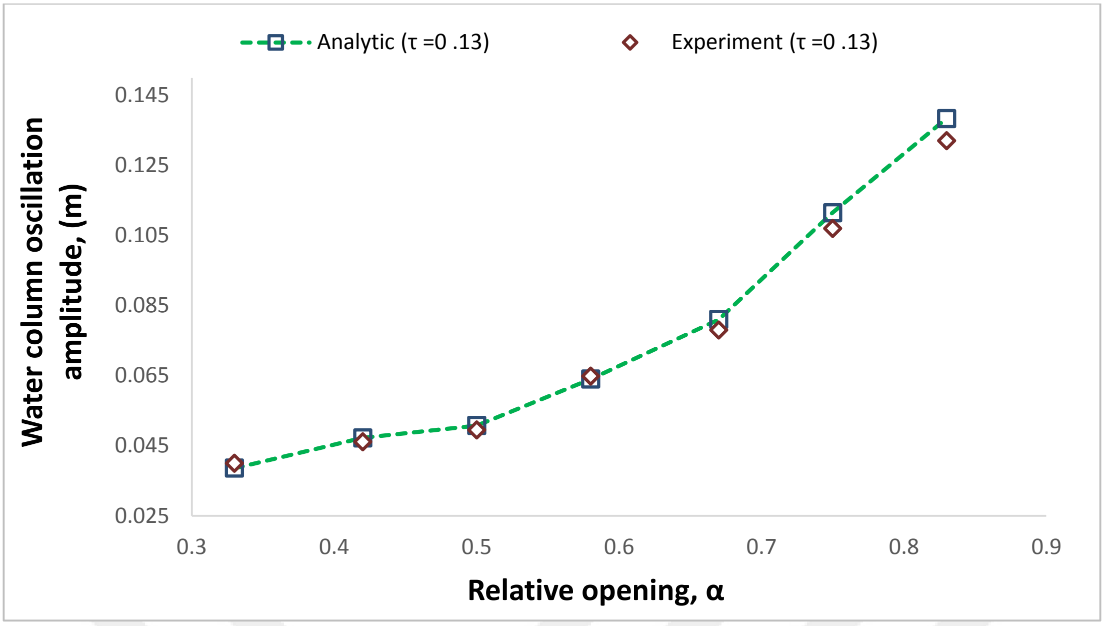

Figure 3.32 : Comparison of amplitudes for $\tau = 0.13$ under W2.

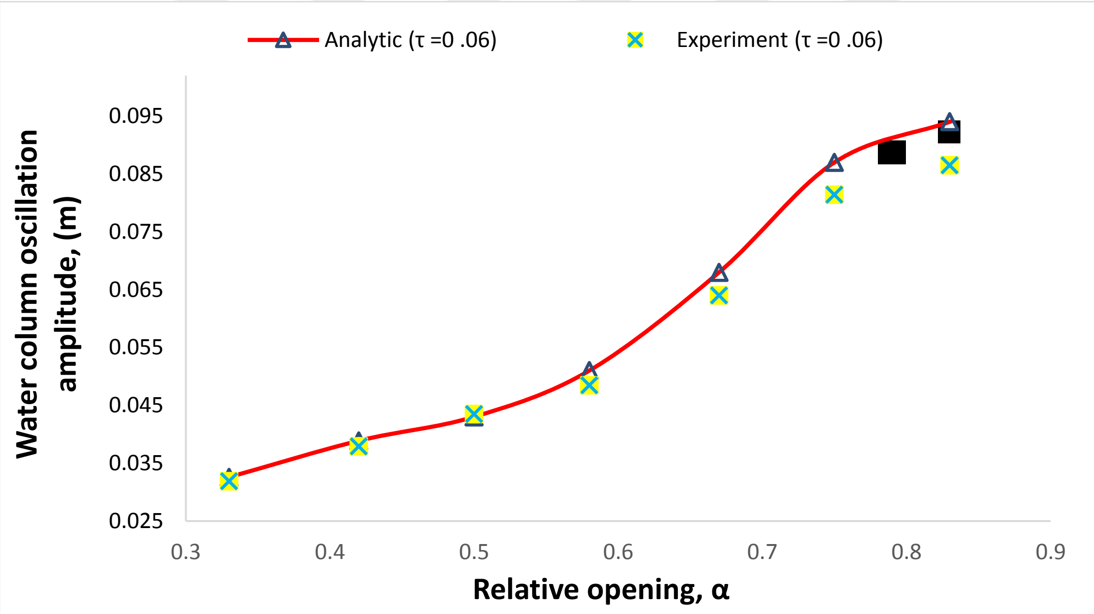

Figure 3.33 : Comparison of amplitudes for $\tau = 0.06$ under W2.

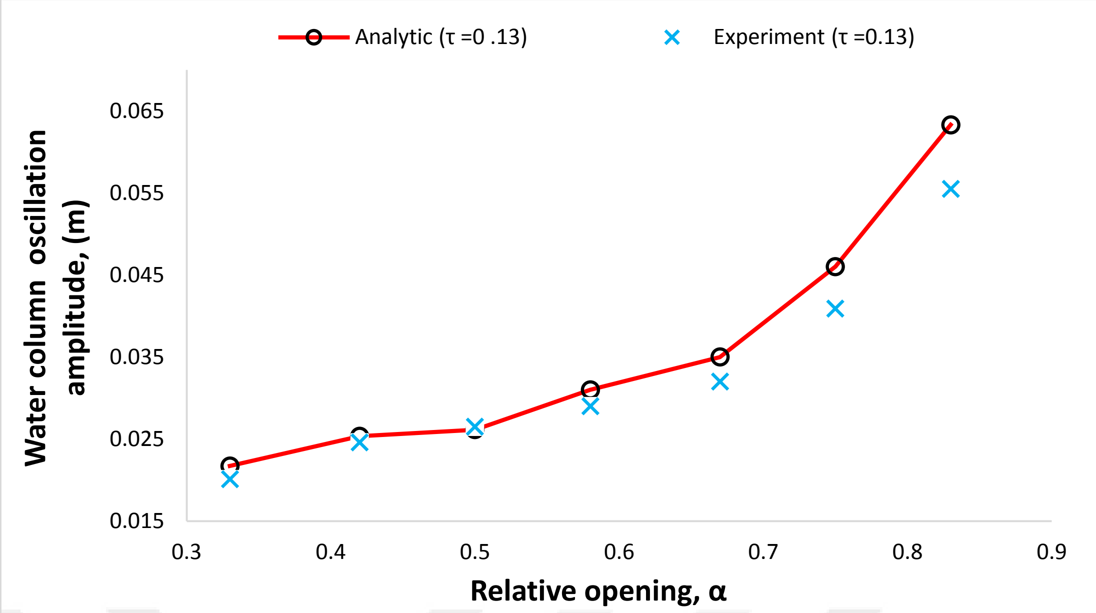

Figure 3.34 : Comparison of amplitudes for $\tau = 0.13$ under W3.

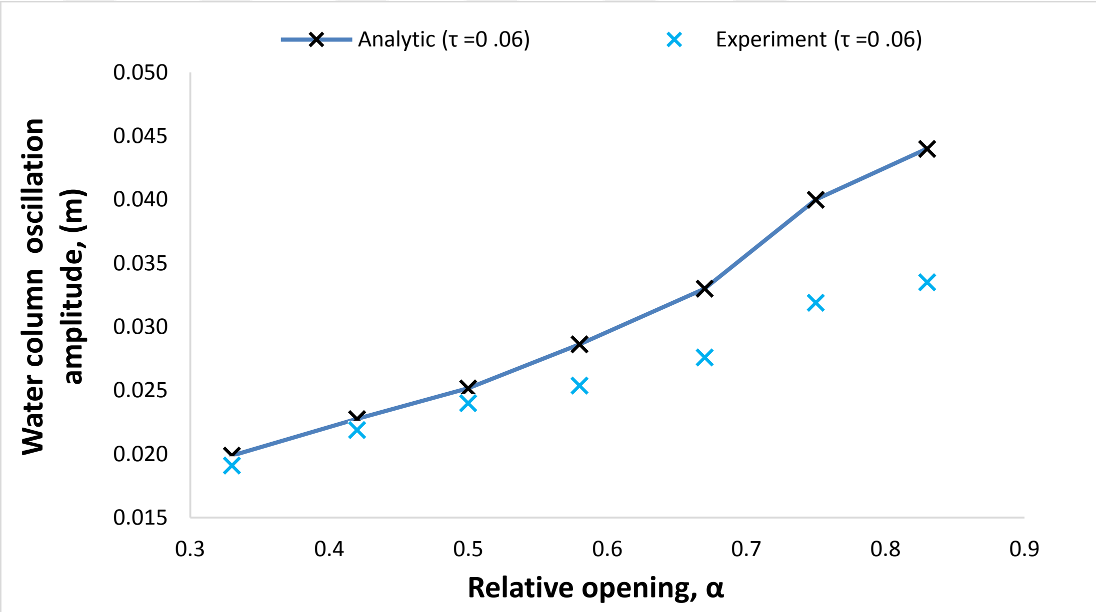

Figure 3.35 : Comparison of amplitudes $\tau = 0.06$ under W2.

For incident wave W2, Figs. 3.32 and 3.33 show that the analytical model results very closely follow the experimental model values for all relative openings except for α = 0.75 and α = 0.83 and, τ = 0.06 where small deviations from experimental values occurred. Associated relative errors are only 0.064 and 0.08 for α=0.75 and α=0.83, respectively. However, in the case of W3, a visual inspection of Figs. 3.33a and 3.33b reveals that higher deviations are present for relatively higher openings. When τ=0.13 relative errors are 0.069, 0.094, 0.125 and 0.14 where for τ=0.06 they are 0.130, 0.196, 0.254 and 0.313 for α=0.58, α=0.67, α=0.75 and α=0.83, respectively. As a result of the represented comparisons, it can be concluded that for the incident wave, W1 and W2 (most cases) remarkable accuracy is found between the analytical model results and experimental model values. For W3 however, especially for the relatively smaller orifice ratios and higher relative openings analytical model results highly diverged from the experimental model values. The reason for the divergence should be due to the introduced sloshing mode into the surface motion behavior of the water column. For the smaller divergent cases under W2, a slight sloshing motion is observed in addition to the piston motion of the water column. As regards the incident wave W3, a significant amount of sloshing penetrates into the chamber especially for relatively smaller and bigger orifice ratios and relative openings, respectively. Analytical model assumes SDOF motion in the piston mode for the water column, therefore, it cannot accurately estimate the water column oscillation amplitude if a sloshing motion is also present. Some of the transmitted wave energy into the chamber is transformed into kinetic energy in the form of axisymmetric motion of the water column and thus sloshing forms. Since the measured values of the right, middle and left water column motion amplitudes are averaged to obtain a representative value, analytical model results mostly overestimated the experimental model values. Another justification for this reasoning is, for incident wave W1, where analytical model results very well matched with the corresponding experimental model values, horizontal surface of the water column stayed planar during the water column oscillations and moved as a rigid body. Even though the excitation of incident wave, W3 triggers the sloshing motion in the chamber, underwater opening size of the chamber and the applied PTO damping also modulates the amplitude of the sloshing in such a way that relatively smaller relative openings and PTO dampings restrict the sloshing amplitude. Furthermore, sloshing motion is even negligibly suppressed if the underwater chamber opening and PTO damping is small enough. For example, under the incident wave, W2, slightly sloshing motion is introduced on top of the water column surface piston like motion. But, it only becomes noteworthy when the orifice ratio is 0.06 and the relative opening is 0.75 and 0.83. This should be why the relative error increases and only deserves attention for the mentioned cases. But, incident wave W3 causes water column act in such a way that sloshing motion is dominant over the piston mode. Even in this case, for the biggest orifice size (smallest PTO damping) and five lowest relative openings 0.33, 0.42, 0.5, 0.58 and 0.67 the biggest relative error is 0.094. However, as the orifice ratio decreases analytical model amplitude estimation results further diverges from the experimental amplitude values. Eventually, for the smallest orifice ratio and the highest relative opening relative error attains the value 0.313. Preceding discussion exposes the importance of the water column surface motion behavior in terms of the success of the analytical model as well as determined damping and added mass values. Sloshing motion is the key factor that affects the accuracy of the analytical model results. In effect, it is also a well-known fact that sloshing motion of the water column surface is strictly undesired for efficient wave energy conversion rates. Inherently, sloshing motion generated in the OWC chamber depends on the incident wave characteristics. Incident wave W1, which has a frequency that is close to the resonant frequency of the OWC for all geometric and damping values (will further be discussed later in the section), caused the water column act purely in piston mode for all different relative openings and orifice ratios. Also, during the free decay tests water column surface stayed almost horizontal. On the other hand, a minor and a relatively larger sloshing motions are generated inside the chamber under the incident waves W2 and W3, respectively. However, introduced sloshing motion amplitude is further found to be dependent on the underwater opening size and PTO damping of the OWC.

Effect of the relative opening and orifice ratio on the sloshing motion amplitude, which is considered as the main reason of the analytical model's overestimation of the oscillation amplitudes, is obviously seen from Figure 3.34 and 3.35. In these figures, analytical model results diverge with higher acceleration from the experimental values as the relative opening increases and orifice ratio decreases. Energy density of an incident wave mostly exists at near surface depths. As the opening of the chamber through the exterior water mass decreases, relatively smaller portion and density of the wave energy, which corresponds to relatively lower fluid particle velocities under the front wall opening, is transmitted into the chamber. This phenomenon is thought to be the reason of the decaying sloshing motion as the opening decreases. Also it is found that as the orifice ratio increases (PTO damping decreases), amplitude of the sloshing motion also diminishes. To further examine this phenomenon, comparison of experimental and analytical model amplitude results for W3 and varying orifice ratios are given for constant relative openings 0.67, 0.75 and 0.83 in Figure 3.36. As it can be inferred from Figure 3.34, for all given constant relative openings, as the orifice ratio increases analytical model yields more accurate amplitude estimations and provide better matching with the experimental model values. Since the sloshing motion violates the rigid body assumption of the analytical model, this should imply that sloshing phenomenon retreats as the orifice ratio increases.

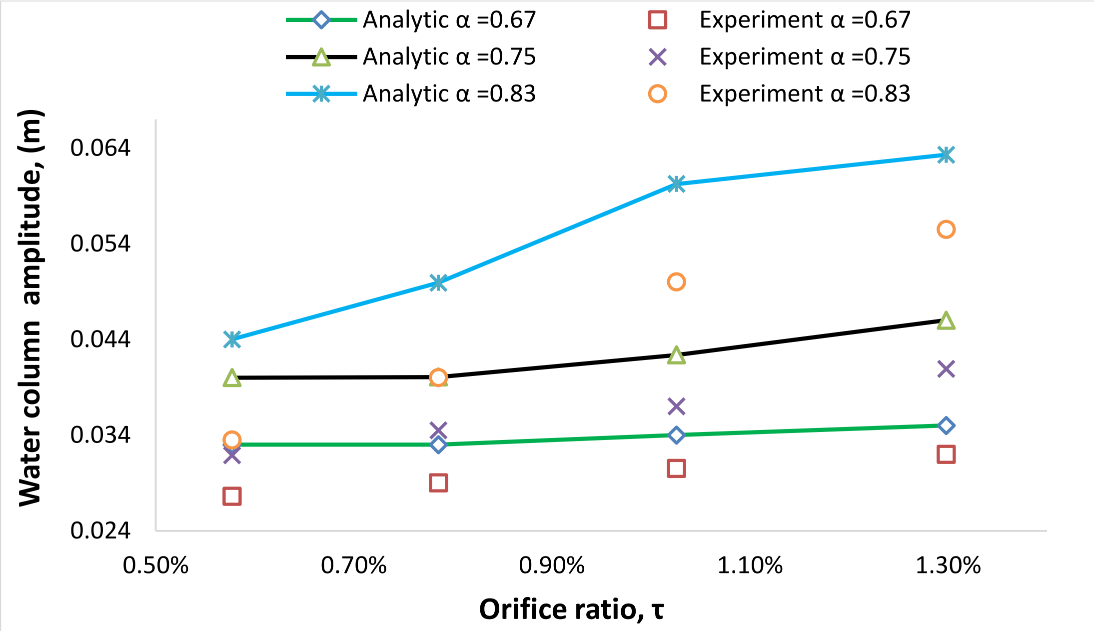

Figure 3.36 : Amplitude versus orifice ratio for W3.

From the above overall results and discussions, it is readily realized that the developed mathematical model very accurately estimates the water column surface motion behavior especially when the water column moves approximately as a rigid body. During the experiments, rigid body motion is observed when the water column is excited by the generated monochromatic incident wave, W1 independent of the value of the front wall opening and applied PTO damping. As regards the incident wave, W2, even though a minor sloshing motion is introduced onto the motion of the water column, for most of the cases, this small amount of sloshing motion is filtered out by the opening and orifice sizes used in this study except for the two biggest and the smallest relative openings and orifice size, respectively. Under the excitation of incident wave, W3 a large sloshing motion amplitude is generated in the chamber in addition to the piston motion behavior of the water column yet relatively smaller opening and bigger orifice sizes diminished the sloshing motion amplitude to a great extent. If it is recognized that very accurately obtained analytical results mostly corresponds to the cases where the water column is rather excited in piston mode, for this cases, it can safely be concluded that the equation of motion of the water column yields remarkably accurate results if the overall linear damping and the added mass of the system is correctly approximated. It is understood that two reasons underlie the high accuracy of the determined hydrodynamic parameters of the system and success of the analytical model under piston dominant motion of the water column. First one is, during the free decay tests water column acted as a rigid body and thus obtained parameters are mostly associated with the piston-type motion of the water column. Secondly, to some degree, obtained damping values via free decay tests include viscous losses that possibly occur under the front wall of the chamber. Identification of this type of viscous losses is very problematic and formidable since it requires to solve full nonlinear N-S equations with complicated boundary conditions or using PIV type methods, which are expensive and can cause permanent blindness without appropriate precautions, to visualize the motion of the fluid particles in order to determine the kinetic energy of the rotating viscous fluid particles. The studies in the past that modeled the water column motion as a simple mechanical system could not include this type of quantitatively unobtainable (mostly) damping in their model. On the other hand, analytical solutions obtained by potential flow theory inherently neglects this type of damping because the theory assumes irrotational flow and ideal fluid, thereby omits viscous forces. Success of the model implies that viscous losses are adequately included into the approximated value of the damping of which its importance has to be highly taken into consideration. Moreover, if it is appreciated that for most practical purposes water column surface can be considered planar (corresponding to the piston-like motion) in real sea states (Wang, 2002), with accurate determination of hydrodynamic parameters, developed SDOF model can be applied for most practical purposes.

3.2.3 Hydrodynamic efficiency (performance) of the OWC device

Aim of this section is to quantify the hydrodynamic efficiency of a bottom-fixed OWC with different combinations of chamber opening heights and PTO dampings under the excitation of different monochromatic wave conditions for optimization purposes in order to achieve the highest possible efficiency. In this manner, PTO damping value that yields the maximum efficiency is determined, interrelations between PTO damping and opening height of the chamber under various wave conditions and how the hydrodynamic characteristics of an OWC are influenced by these factors are also investigated.

3.2.3.1 Hydrodynamic efficiency evaluation

Orifice size effect

For the extreme cases of applied turbine damping i.e. the zero orifice diameter (very high damping) and very large orifice diameter (zero damping), velocity and pressure terms in 2.46 will be zero, respectively. Accordingly, absorbed pneumatic power from the incident waves will also be zero. For the orifice diameters between, absorbed power will be a varying non-zero value and effects of different turbine induced damping values on the hydrodynamics of the OWC tool can be evaluated.

Hydrodynamic efficiency of the OWC tool versus orifice ratio for different relative openings, are illustrated in Figs. 3.37, 3.38, 3.39 and 3.40 under wave steepness values, 0.02, 0.045, 0.072 and 0.096, respectively. For better interpretation curve fitting polynomials and correlation coefficient (R^2) values are also indicated on the figures (for some relative openings to obtain graphical clarity).

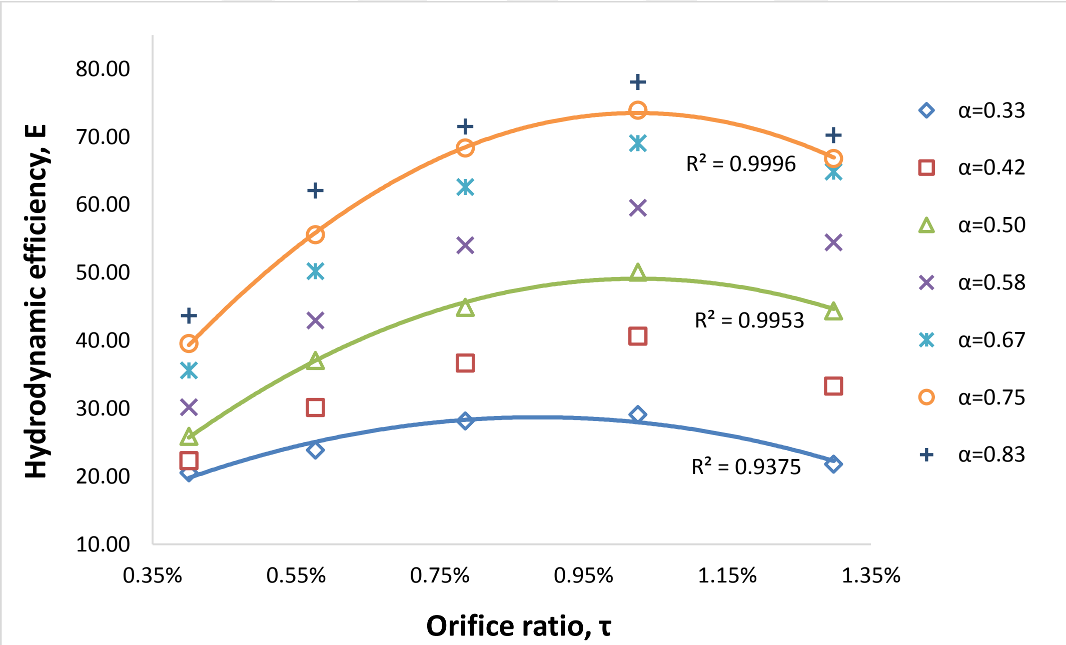

Figure 3.37 : Efficiency versu orifice ratio for wave steepness 0.02.

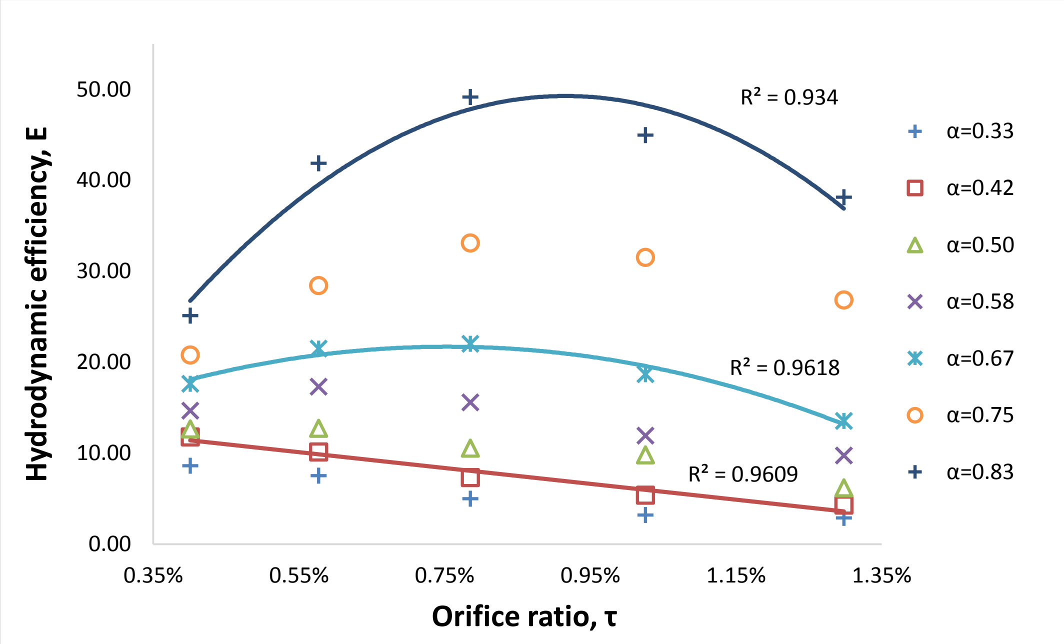

Figure 3.38 : Efficiency versus orifice ratio for wave steepness 0.045.

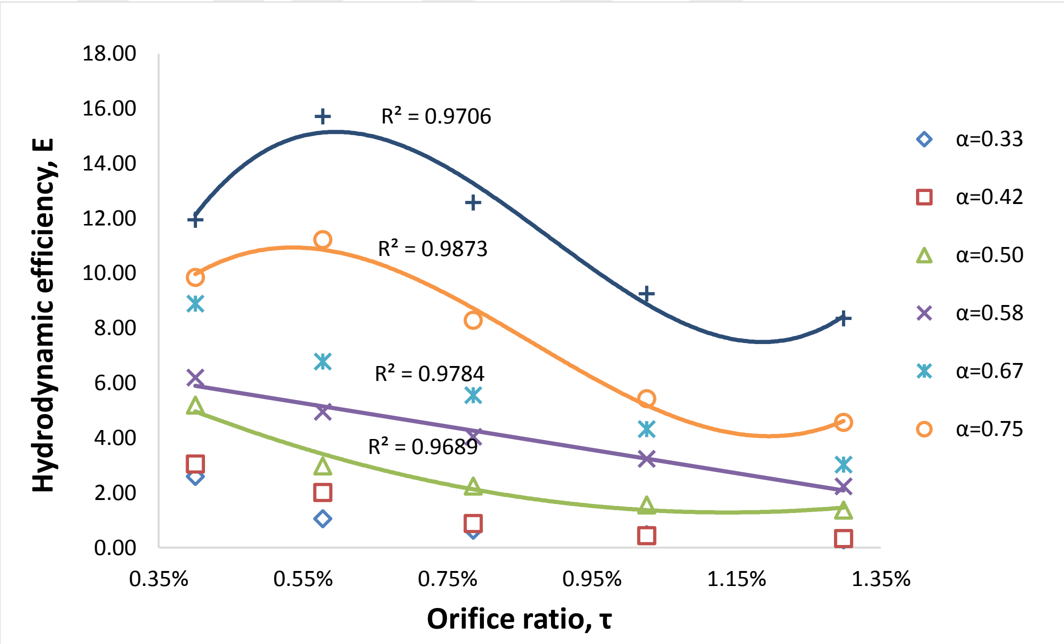

Figure 3.39 : Efficiency versus orifice ratio for wave steepness 0.073.

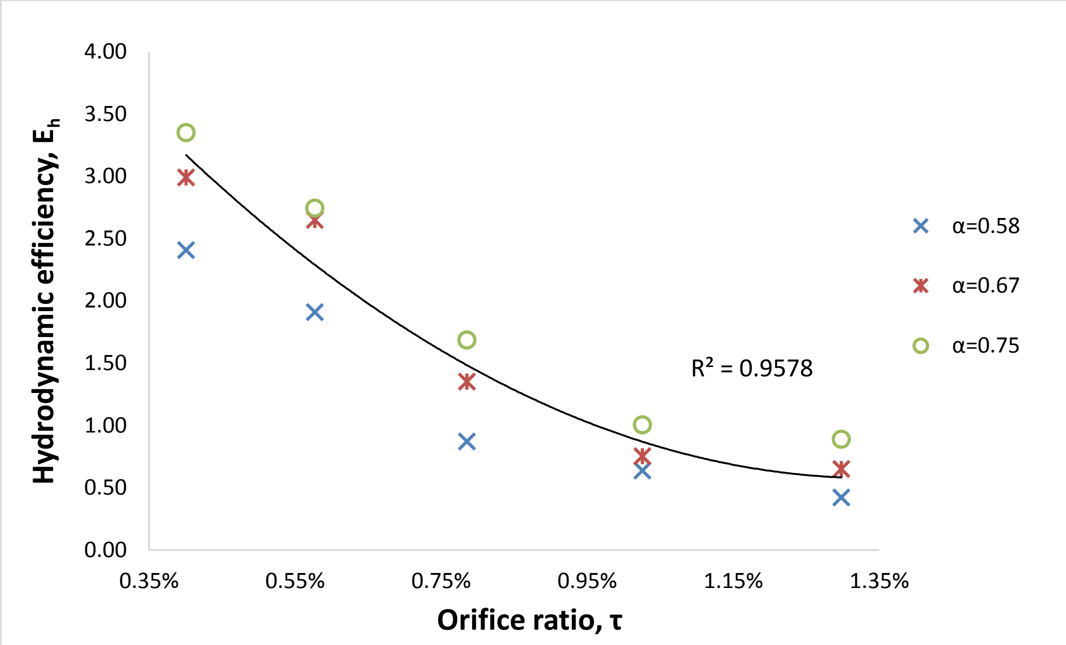

Figure 3.40 : Efficiency versus orifice ratio for wave steepness 0.096.

As can clearly be observed from Figure 3.37 which corresponds to excitation of the least steep wave generated in this study, the smallest orifice ratio yielded the smallest efficiency for all relative openings. When the orifice diameter is widened, hydrodynamic efficiency increased with a growing rate as the relative opening became bigger. This uptrend reached a peak for the orifice ratio value of 1.03% and initiated to decline afterwards. Note that this phenomenon is valid for all relative openings utilized in this study. This fact implies that for this particular wave steepness, optimal damping that has to be imposed on the system to obtain the highest efficiency is independent from the relative opening of the OWC chamber. As a result, the optimal orifice ratio (damping value) is found to be 1.03% for wave steepness 0.02. As regards the wave steepness value of 0.045, optimal PTO damping for the system was found to be different. Furthermore, unlike the previous case there was not a unique optimal PTO damping value but more than one depending on the relative opening of the chamber.

For the first two smallest relative openings, $\alpha_1$and α_2, maximum efficiency was obtained for the smallest orifice ratio 0.40% and efficiency decreased in a close to linear fashion when orifice ratio increased as depicted in Figure 3.38. For α_3 and α_4, hydrodynamic efficiency of the OWC became maximum for the orifice ratio 0.58%, however for the highest relative openings, α_5, α_6 and α_7, orifice ratio 0.79% provided the highest efficiencies. Quadratic curve fittings satisfactorily define the behavior of efficiency with respect to varying orifice ratios for relative openings $\alpha_4, \alpha_5, \alpha_6$ and α_7, where a linear relationship exists for the smallest relative openings α_1, α_2 and α_3. Interestingly enough, a coupling between the inlet (relative opening) and outlet (orifice ratio) of the chamber was formed in terms of the required PTO damping to reach the highest possible efficiency when wave steepness increased from 0.02 to 0.045. For wave steepness 0.073, similar to the previous case, performance of the converter is maximum for the smallest orifice ratio 0.40% for $\alpha_1, \alpha_2, \alpha_3$ and additionally for α_4 and α_5 values (Figure 3.39). However, for the biggest α values, α_6 *and* α_7, the optimal orifice ratio shifts up to 0.58%. Further increase of orifice ratio reduces the efficiency of the converter. The relationship between the hydrodynamic efficiency and orifice ratio can be estimated by a convex quadratic curve for α_1, α_2 and α_3, where third order polynamial with a concave shape which corresponds to the same convex parts of the quadratic curve, can be fitted for $\alpha_{5,}$ α_6 *and* α_7. In between, namely the α_4 case, where a linear relationship exists between hydrodynamic efficiency and orifice ratios, is like a transition between two distinct behaviors.

For the steepest wave generated in this study, for all α values, the smallest opening ratio 0.40% yielded the highest hydrodynamic efficiency. Figure 3.38 shows the calculated efficiencies for only $\alpha_{5,}$ α_6 *and* α_7, since for the remaining relative openings calculated efficiencies were almost zero. Surprisingly, like for the least steep incident wave optimal damping does not depend on the relative opening of the chamber at least for the relative opening range used in this study. As a result, relatively steeper incident waves require relatively higher PTO dampings to obtain the highest hydrodynamic performance where its numeric value depends on the relative opening of the OWC tool. To investigate this phenomenon optimal orifice ratios corresponding to the incident wave steepness values are plotted in Figure 3.41. For cases that have more than one optimal damping for a given wave steepness, corresponding relative opening value is also inserted. For relative openings α_6 and α_7, a remarkable inverse linear relationship exists between the optimal orifice ratio and incident wave steepness as depicted in Figure 3.41. But, as the incident wave steepness increased from 0.02 to 0.045, optimal orifice ratio decreased to 0.58% for α_3 α_4 and to 0.40% for α_1 and α_2. For relatively smaller relative openings optimal orifice ratio becomes more sensitive to wave steepness change, i.e. further increase of the orifice ratio for the wave steepness (0.0723) yielded the best performance when orifice ratio was 0.40% for $\alpha_1, \alpha_2, \alpha_{3,}$ α_4 and α_5. For the steepest incident wave, effect of the wave steepness on the required PTO damping on the system becomes so pronounced that, inevitably, for all relative opening values optimal optimal orifice ratio was the smallest (0.40%).

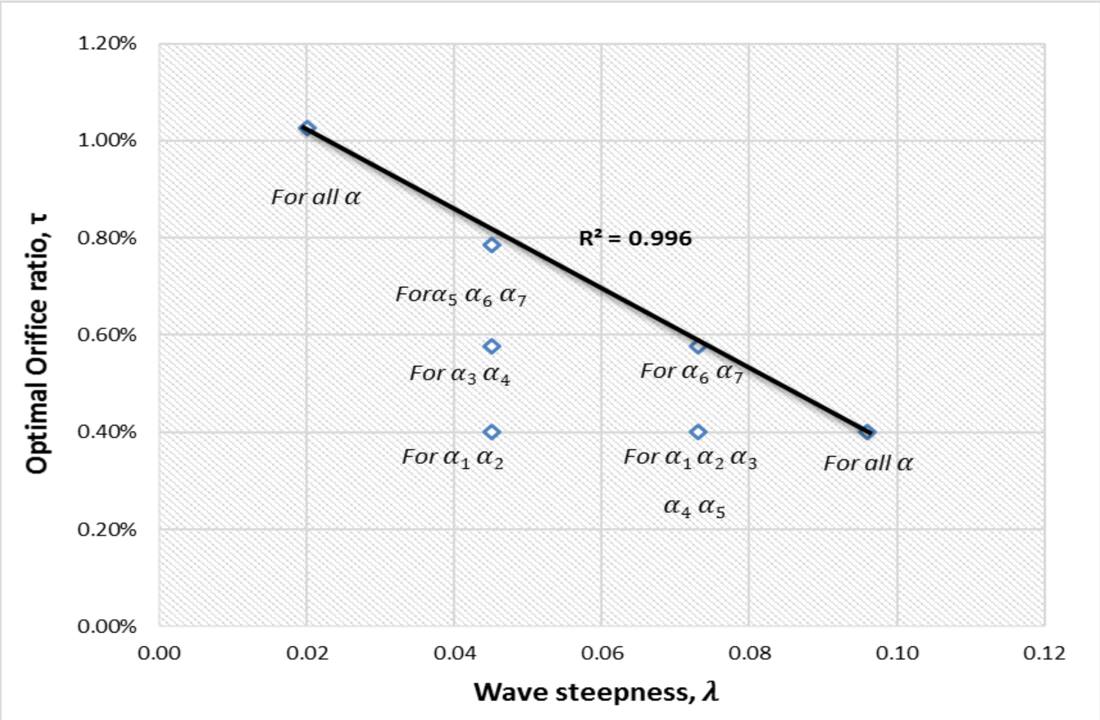

Figure 3.41 : Optimal orifice ratio versus wave steepness.

Turbine induced damping is what makes wave energy extraction possible via generating a pressure differential in the air chamber by constraining the air column motion. According to 2.46, maximum pneumatic power can be generated by an appropriate combination of both instantaneous average free surface velocity and air pressure differential in the chamber. Experimental investigation results indicated that, relatively large dampings imposed on the system generated high pressure differential but confined the free surface motion and accordingly, reduced the velocities. Conversely, relatively low damping values allowed high velocities of the water column but in parallel substantially decreased the air pressure.

To further analyze this phenomenon, Figs. 3.42 and 3.43 illustrate the differential pressure and 1000 times the average vertical velocity of the free surface versus dimensionless time, t/T (time (t) divided by period of the incident wave (T)) relationship in the same graph with respect to particular values of $\lambda_2, \alpha_7, \tau_1$ and τ_3, which are 0.045, 0.83, 0.40% and 0.79%, respectively. Differences in the two figures reveal the effects of different orifice ratios on the differential pressures and average free surface vertical velocities. The relatively smaller orifice generated higher air pressure in the chamber, which in turn, tightened the water column motion so that, relatively lower velocities could only form. The relatively bigger orifice allowed higher velocity formation while lower pressures occurred in the chamber.

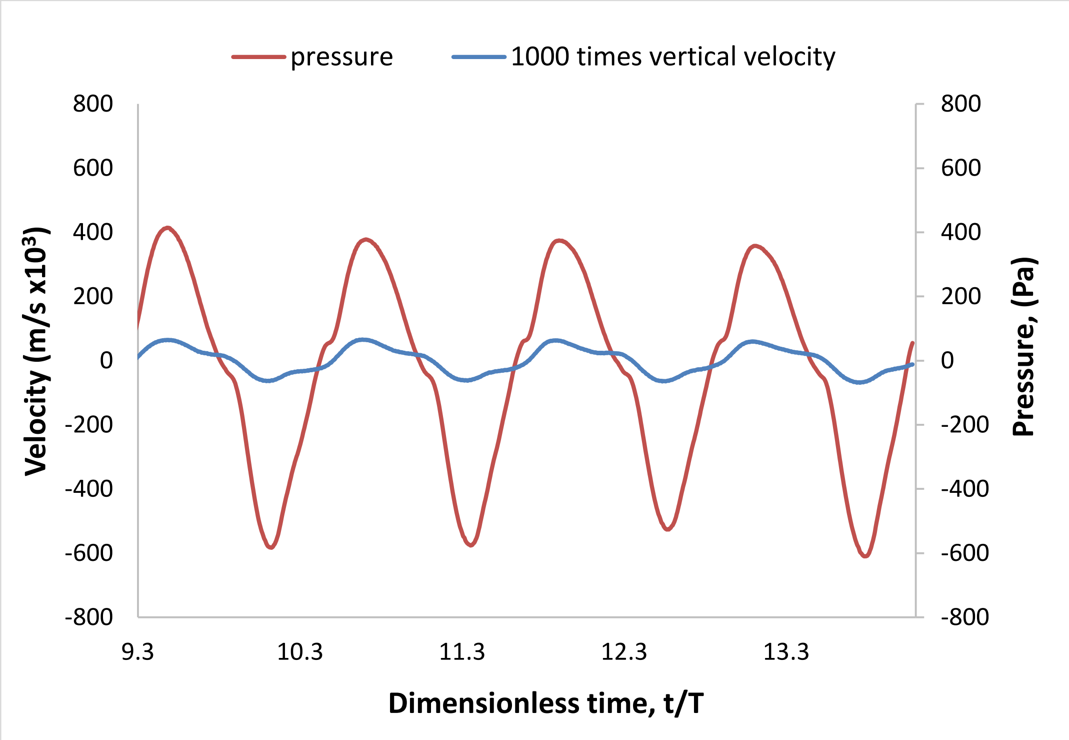

Figure 3.42 : Differential pressure and velocity time series for λ_2 , α_7 , τ_1.

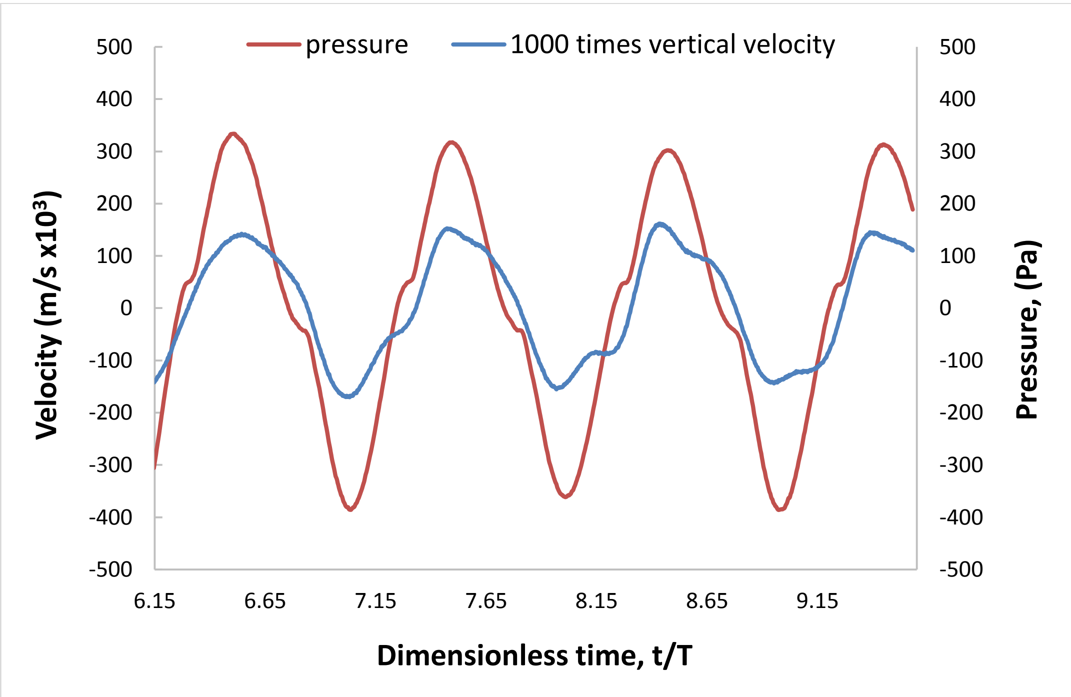

Figure 3.43 : Differential pressure and velocity time series for λ_2 , α_7 , τ_3.

Figs. 3.42 and 3.43 reveal the inverse relationship between the measured air pressure and the vertical velocity of the water column. However, to extract the most of the incident wave energy from the particular incident wave, orifice size has to be optimized so that summation of the product of these two physical quantities becomes maximum.

As a result, under the excitation of the incident waves with a steepness of 0.02, orifice ratio of 1.03% generates the optimal damping for all relative openings. But, as the wave steepness increases, optimal damping value reduces in an interesting manner as follows: This reduction becomes more pronounced for smaller relative openings. Namely, for wave steepness 0.045 and relative openings α_5, α_6 and α_7, orifice ratio needed to generate optimal damping is shifted down from 1.03% to 0.79% whereas for α_3 and α_4 , to 0.58% and for $\alpha_1$and α_2 , to 0.40. Also, when incident wave steepness increased from 0.02 to 0.072, for α_5, α_6 and α_7, optimal orifice ratio is shifted down from 1.03% to 0.58% whereas, for α_1, α_2, α_3, α_4 and α_5, to 0.40%. Moreover, the most dramatic down-shift occurred for the steepest wave where for all relative openings, optimal orifice ratio was found to be 0.40%. Finally, following outcome reveals itself that, optimal damping value not only depends significantly on the wave conditions but further influenced by the opening height of the chamber in such a way that higher damping is required to absorb the maximum pneumatic power out of the incident wave as the wave steepness increases and the relative opening decreases.

One thing to note here is, a close look to peak air pressure values formed in the chamber exposed a surprising fact that, magnitudes of the negative peak values were mostly greater than the positive peak pressure values for all cases (i.e. Figs. 3.42 and 3.43). One reason for this phenomenon may be as follows: As soon as the water column in the chamber raises due to the incident wave forces, exhalation process begins almost instantly. While vertical upwards motion of the water column strives to increase the air pressure in the chamber, on the contrary, air mass exiting the orifice reduces the air pressure. When the water column initiates to retreat, inhalation process could not react to this sudden change immediately. Therefore, while positive displacement of the water column and exiting air exhibited synchronized flow of motion, a hysteresis phase lag formed for the inhalation process. So, air in the chamber stays rarefied due to the delayed inhalation of air which causes a greater absolute peak value of negative pressure than positive pressure value.

Effects of opening height

In the present study, hydrodynamic parameters are investigated for seven different opening height values. For each orifice ratio, Figs. 3.44, 3.45 and 3.46 show the hydrodynamic efficiency versus relative opening plots under wave steepness values, 0.02, 0.045 and 0.072, respectively. Results obtained for the steepest incident wave are excluded since the performance of the OWC converter came out to be negligibly small. Figures apparently signify that the hydrodynamic efficiency tends to increase with the increasing relative opening of the OWC chamber for all steepness values consequently, highest relative openings yielded the maximum hydrodynamic efficiency values. This result is somewhat intuitive as relatively bigger openings enable greater portion of the incident wave energy to penetrate into the chamber, hence, more energy becomes available for pneumatic energy conversion.

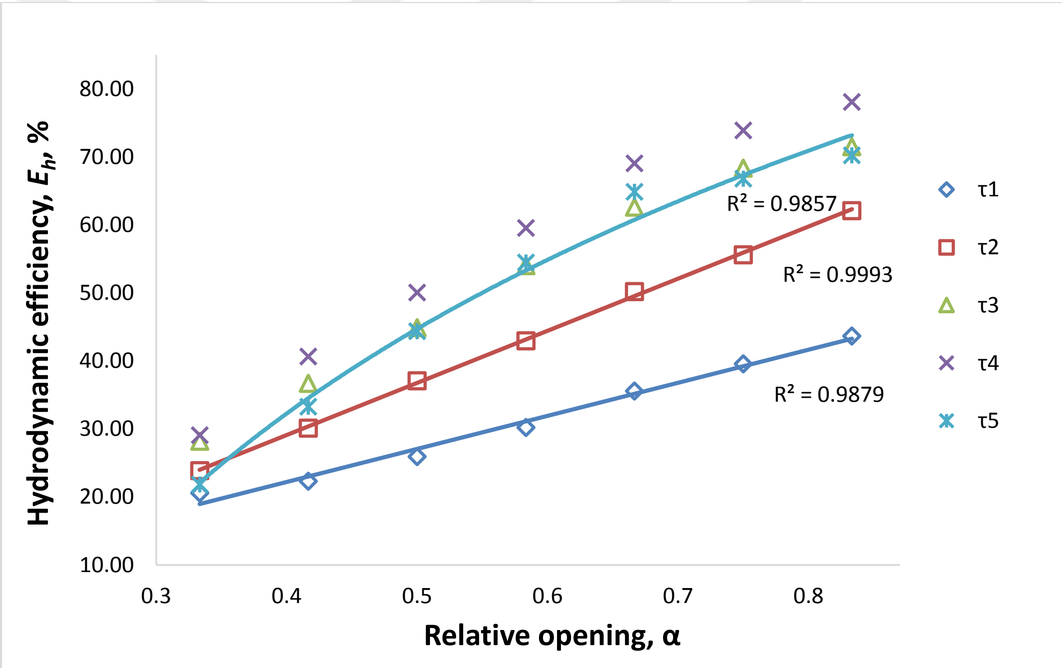

Figure 3.44 : Efficiency versus relative opening for wave steepness 0.02.

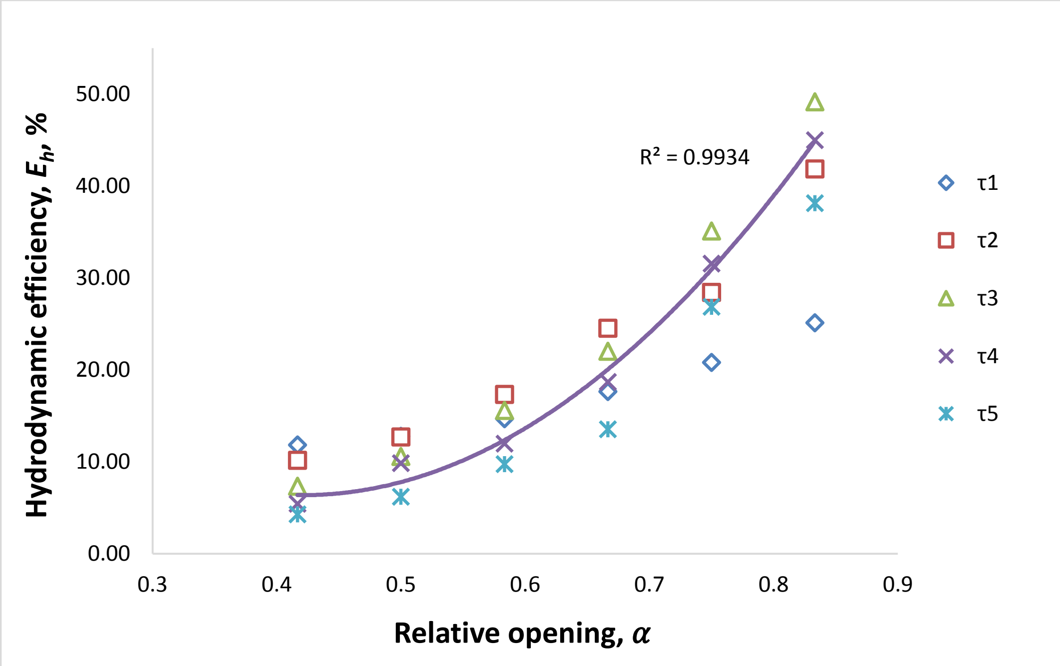

Figure 3.45 : Efficiency versus relative opening for wave steepness 0.045.

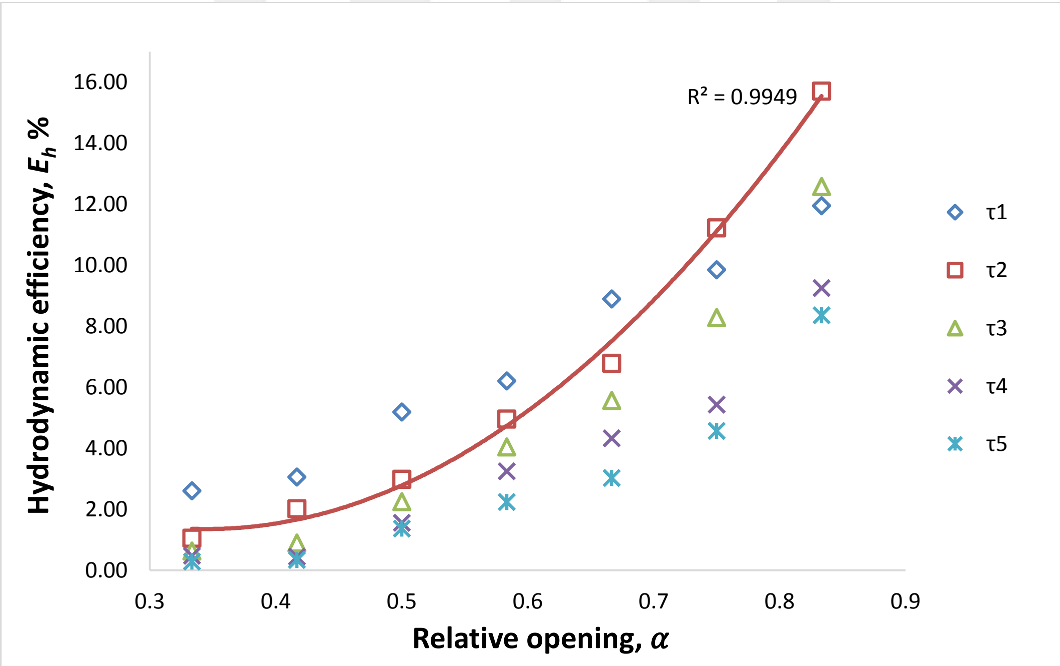

Figure 3.46 : Efficiency versus relative opening for wave steepness 0.073.

For wave steepness 0.02 and orifice ratios 0.40 and 0.58, hydrodynamic efficiency increased almost linearly with respect to relative openings, where for the remaining orifice ratios, logarithmic variation represented the relationship. However, for wave steepness values, 0.045 and 0.072 efficiency increased exponentially as relative opening increased for all orifice ratios.

In the frame of linear wave theory, dynamic pressure amplitude under an incident wave is expressed as (Dean and Dalrymple, 1984):

$$p(z) = \rho g \frac{H}{2} \frac{\cosh k(h+z)}{\cosh kh}, \tag{3.25}$$

where, z is the water depth that has to be taken negative beneath the water surface.

Figure 3.47 may help to explain this phenomenon via showing the calculated dynamic pressure distribution according to 3.25 under the incident waves for wave steepness 0.02 and 0.045. To obtain a real physical insight, ordinate and abscissa of the plot indicate the water depth to obtain a real physical insight and the corresponding dynamic pressure, respectively. It is evaluated at the depth corresponding to bottom lip of the front wall. Therefore, relative openings are placed into the plot so that their y coordinate represents bottom lip of the front wall and their x coordinate shows the corresponding pressure value. Wave energy is not distributed evenly beneath the surface in such a manner that, near surface depths contain relatively more energy. Figure 3.47 indicates the exponential growth of dynamic pressure under the incident waves towards the free surface but obviously, increase rate is much bigger for the steeper incident wave. This means that, as relative opening increases, more pressure is available to be transferred to the air column compared to the relatively less steep wave and this phenomenon causes the exponential efficiency growth observed in Figs. 3.45 and 3.46.

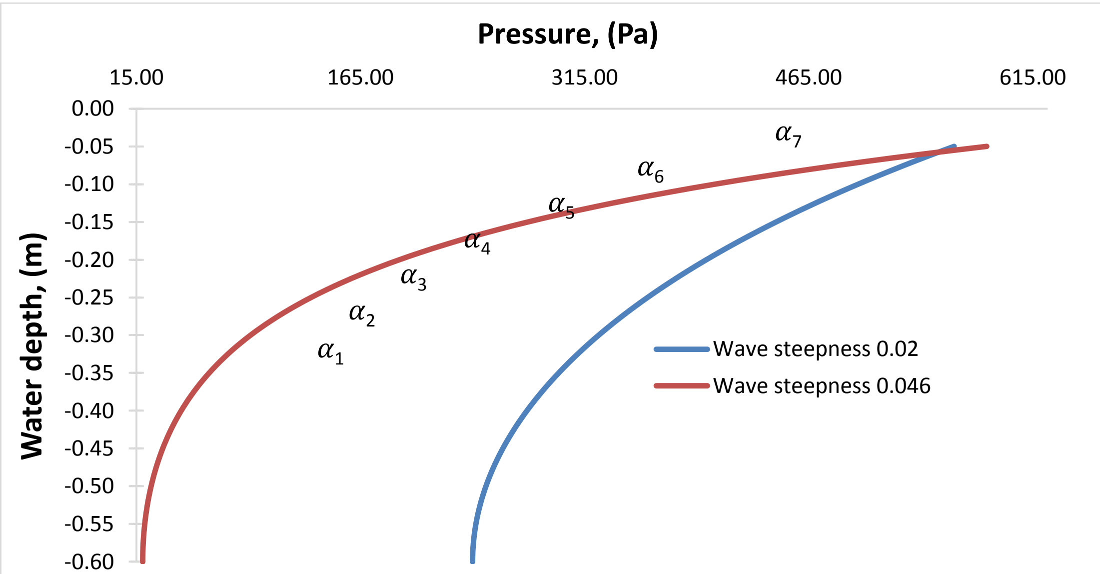

Figure 3.47 : Underwater pressure distribution (steepness 0.02 and 0.046).

Furthermore, it is to note that, even though the pressure values in deeper regions under the wave steepness 0.046 are much smaller than the corresponding pressure values under wave steepness 0.02, due to the relatively bigger increase rate (especially at near surface depths), pressure values become equal and for further decrease in depth, pressures under the steeper incident wave exceeds the pressures generated by the less steeper wave.

Effects of wave parameters

Wave characteristics are very important in terms of feasible energy extraction (Mahnamfar and Altunkaynak, 2015; Dizadji and Sajadian, 2011). The effect of the dimensionless parameter wave steepness on the hydrodynamic efficiency is investigated in this present study. It is clearly observed from the Figs. 3.37, 3.38, 3.39 and 3.40 that an inverse relationship exists between the wave steepness and obtained efficiencies for a given relative opening and orifice ratio. 0.78 was the highest calculated efficiency, which was obtained under the wave steepness 0.02 when the orifice ratio was 1.03%. On the other hand, the steepest wave generated the minimum efficiencies where the highest calculated value was 0.04. The experimental model results indicated that the energy of relatively less steep waves is better transmitted into the chamber in a smoother manner resulting relatively higher fluctuations and vertical water column velocities. Moreover, for a given relative opening and orifice ratio, calculated efficiencies for a relatively steeper wave were always smaller than the efficiencies generated by the relatively less steep waves. One reason for this phenomenon should be that the horizontal water particle velocities under relatively steeper waves are greater and beneath the front lip of the chamber higher flow separation occurs and accordingly bigger vortices are formed. Vortices are kind of energy dissipation mechanisms, which are not available to PTO mechanism of the wave energy converter (Fleming et al., 2012).

Another factor that affects the absorbed incident power is the motion behavior of the water column free surface. The results of the present study revealed that incident wave steepness 0.02 generated an almost rigid-piston type of free surface motion inside the chamber. But as the wave steepness increased piston type motion behavior breaks down and so called 'sloshing' mode is introduced. For an arbitrary orifice ratio and relative opening value, Figs. 3.48(a-d) illustrate the representative fluctuation behaviors at the center right, middle, and left of the chamber with respect to wave steepness 0.02, 0.046, 0.073 and 0.096, respectively. A synchronized free surface fluctuation is evidently seen from Figure 3.48 for steepness value 0.02. But for steepness 0.046, sloshing motion with respect to water level at the middle of the chamber penetrates into the rigid body motion behavior and magnitude of the sloshing increases as the incident waves become steeper (Figure 3.48). For the steepest wave series, water column free surface experiences an almost fully sloshing mode where the fluctuations of the right side of the water column are approximately 180^{o} out of phase with the left side fluctuations. Sloshing motion of the free surface traps some of the transmitted wave energy as kinetic energy in the form of asymmetrical right and left vertical velocities with respect to center of the water column. This phenomenon reduces the average vertical fluctuations of the water column and thus the efficiency. Most pronounced efficiency reduction due to the sloshing mode is for the steepest wave series and average fluctuations are so small that appreciable amount of differential pressure cannot be generated in the chamber. Therefore, design aspects of an OWC tool should be configured to avoid this type of motion.

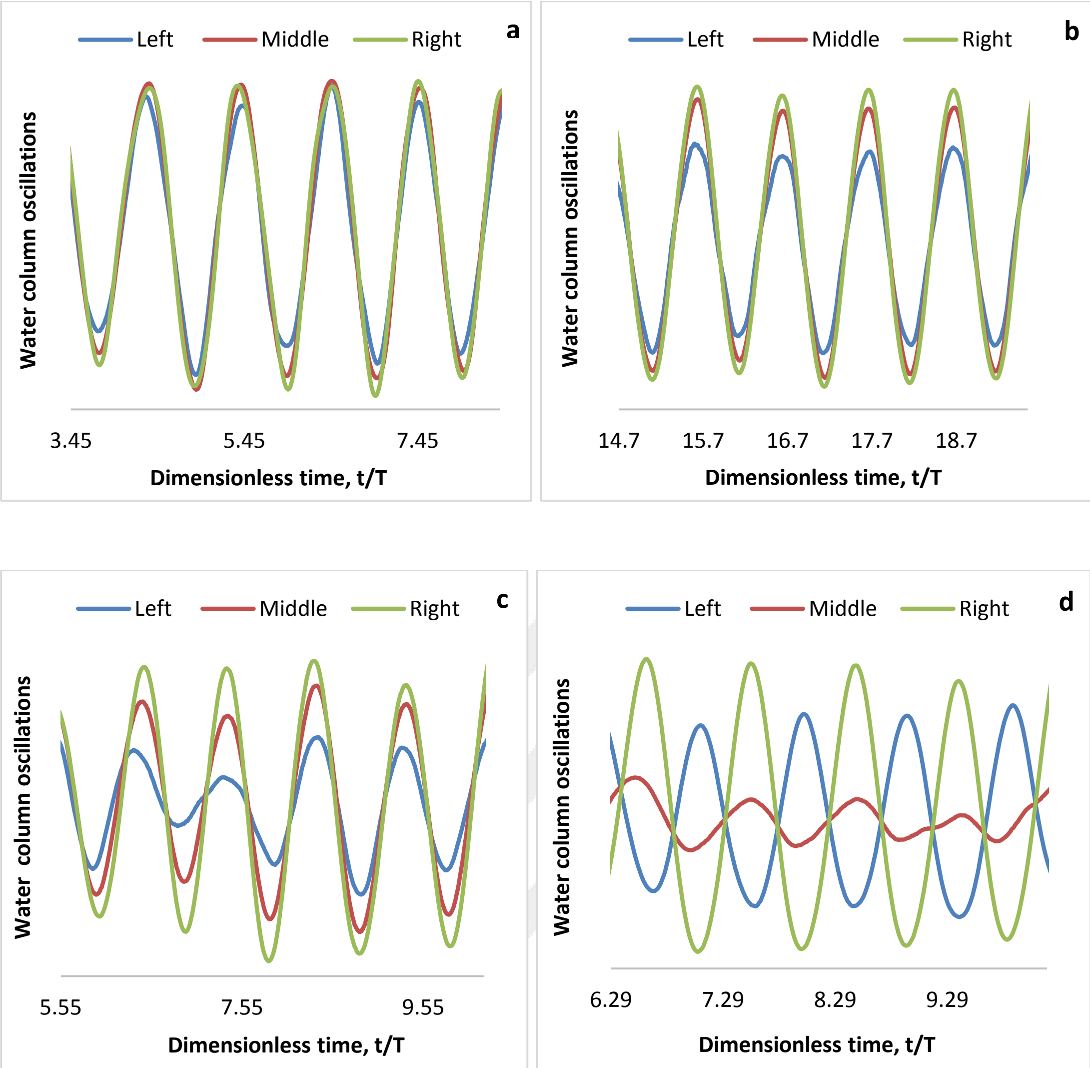

Figure 3.48 : Displacement for steepness a) 0.02 b) 0.046 c) 0.073 d) 0.096.

4. CONCLUSION AND RECOMENDATIONS

Even though OWC type wave energy converters have reached full-scale prototype stage, streaming data from the field indicates that performance of the converters are well-below the estimated values. This is the main reason why the conversion of wave energy is not cost-effective compared to well-developed solar and wind energy technology. Therefore, a better physical and operational understanding of OWC power plants in the fundamental level is required. With this spirit, this thesis has been initiated to contribute to the corebody of knowledge and state of the art OWC technology. Water column surface oscillations and motion behaviors, applied PTO (power take-off) damping and underwater chamber geometry as well as their interactions with different incident waves are reported as the most influential factors on the device performance.

Depending on the amount of the PTO damping, water column motion could be overdamped or underdamped. Both cases are investigated in detail. It is found that among the range of orifice ratios used in this thesis, OWC system was overdamped for the smallest orifice ratio value, 0.02% whereas larger orifice sizes yielded underdamped systems.

Four different regular wave series and nine opening height values are experimentally studied under a constant water depth in a wave flume. However, the two largest opening heights caused air leakage from chamber when the incident wave trough reached the front-wall, which, in turn, depressurized the air column preventing any consistent measurement to take place.

Overdamped case experiments showed that as frequency of incident wave gets smaller a greater portion of wave height (transmitted wave height) penetrates into the chamber regardless of the opening ratio (In effect, this result is also valid for underdamped cases). An attempt has been made to estimate the average chamber surface oscillation amplitudes and phase angles of a fixed OWC device by developing a simple mechanical model based on a rigid body motion assumption of the water column with a planar surface.

Average chamber water column surface fluctuation, d can be approximated accurately by the exponential fittings that follow the data closely for all relative opening heights. A linear relationship is found between captured wave length ratio δ and transmitted wave height μ. A critical relative opening is found. Relative opening height close to this value generates the highest average fluctuations in the chamber regardless of wave parameters. Furthermore, if this ratio is exceeded average fluctuations start to decrease which should be taken into consideration in OWC plant frontwall design. Using the experimental data, relative average water column oscillating amplitudes are mathematically modelled in terms of relative opening height and wave parameters. For all cases there exists a remarkable fit between mathematical model and experimental data. Developed mathematical expressions may serve as a simple analytical tool to determine the average fluctuations in the chamber with respect to immersion depth and wave parameters in a practical way. Since optimization of front wall underwater geometry with respect to different wave climates alter the water coumn oscillations that generate the pressure oscillations within the trapped air, derived mathematical model may be exploited by engineers and investigators for future studies. Sloshing motion of the surface profile should strictly be avoided in terms of energy harvesting. Waves with relatively high frequency generate sloshing motion in the chamber. In addition to that, from the observations of the study, an additional cause for this phenomenon is found. It is the excessive energy transmitted into the chamber due to the additional height above the critical relative opening. This amount of energy is defined as excessive harmful energy for obvious reasons.

For all the wave series, the highest average oscillation amplitude of the water column occurs at relative opening height α is equal to 0.67 which is a unique value. The amount of energy transmitted into the chamber after this ratio generates an additional sloshing to the water column motion. This phenomenon is another reason for sloshing regardless of wave parameters. Opening ratios around critical ratio 0.67 should be avoided in the geometric design. Average oscillation amplitudes are normalized and mathematically modeled with respect to the variables (relative) opening height and (relative) immersion depth. For constant relative opening, a similar mathematical model with respect to wave parameters is constructed. Physical experimental model results agree with mathematical model values remarkably. After approximating (or experimentally measuring) an average water column oscillation amplitude, constant of the mathematical relationship can be found and oscillation amplitudes for different incident wave parameters and opening heights can be calculated.

In this thesis, chamber water column is further modeled as a SDOF (single degree of freedom) system with a rigid body assumption via simple mechanical model. For the first time, overall damping coefficient of the system with respect to different opening heights has been estimated experimentally by a novel method and reason of existing a critical relative opening value has been clarified; determined damping value is minimum for the critical relative opening where maximum oscillations are observed for all incident waves.

The mathematical model results are compared with experimental model values under different incident wave for all opening heights. For the longest incident wave, a very good model performance has been found. This is significant because for most practical purposes, OWCs are designed so that dominant incident wavelength is large compared to OWC length. A slight difference between the mathematical model results and experimental values occurred due to the added sloshing motion when the relative opening height value of 0.67 is exceeded. While W1 generated almost a piston type oscillatory motion in the chamber, W3 and at a lesser extent W2, forced the water column act in a gradually increasing sloshing mode as relative opening height of the chamber increased. The developed mathematical model overestimated water column oscillation amplitudes and underestimated phase angle responses for W2 and W3 except relative openings 0.33 and 0.42, but more importantly followed the trend. It is because while relative openings are smaller than 0.67, the chamber acts as a low pass filter but for relatively bigger values behaves as a high pass filter. Because of that, the water column is repressed to heave as a rigid body. This design aspect may be taken into account where sloshing motions are inevitably generated in the OWC chamber. Therefore, under W2 and W3 for relatively lower opening heights, the model estimation values may be used at least as a first approximation.

Underdamped systems enable utilizing physical and numerical free decay experiments and LDM (Logarithmic Decrement) method so that, hydrodynamic parameters of an OWC for various chamber openings and PTO dampings can be estimated and physical insights can be obtained.

Free decay tests are performed and oscillation time series of the water column free surface is recorded. Two initial displacements are used to deliver the required energy to the system to enable free decaying oscillations. It is found that obtained results are very close to each other regardless of the applied initial displacement value. 3D free decay tests are also simulated by a commercial 3D Navier-Stokes solver for the exact same settings of the physical experiments. Numerical model results are validated by experimental model data and applicability of the numerical model is proved. To obtain the hydrodynamic parameters for different structure geometries and settings, numerical model can safely be applied in relatively shorter computation time whereas experimental studies require more effort, labor force, money and time and, analytical studies are only available for simple geometries. Overall linear equivalent damping ratio of the OWC device, which represents all kind of dampings that the water column experiences are calculated for all configurations. Besides, the obtained quantitative values reveal that the damping ratio diminishes quadratically and linearly with increasing orifice ratio and decreasing relative opening, respectively. Illustrated regression lines express an approximate analytical relationship for determination of damping ratio in a broader range. Natural frequency of the system is very important in estimating the response of the system to the incident wave excitation. Natural frequencies of the OWC are calculated according to the experimental model data gathered in this present study, for all relative openings and orifice ratios. Determined natural frequencies by experimental means are compared and found to be lower than those that were calculated by different formulas (empirically derived for systems other than WECs yet are used for OWCs) existing in the literature. However, in this study for the first time, an empirical formula is developed to compute the natural frequency of a fixed OWC. Empirical formulas can be widely used to estimate the response of an OWC in an accurate, simple enough way reducing the analytical complexity. Resonant frequencies of the OWC device were also determined. Found values increase almost linearly with both increasing relative opening and the orifice ratio. Inserted regression lines into the plots imply that for a generic rectangular-shaped OWC structure, resonant frequency is a linear function of both opening size and PTO damping. Added mass of the system is calculated for different orifice sizes and chamber openings. Results showed that for all configurations added mass is very close to each other implying the insensitivity of the added mass to PTO damping and chamber opening height variations for this very tested structure.

Experimental findings and empirical formula obtained in this present study are readily available for a wide range of opening sizes and PTO dampings especially when it is realized that all recommended opening and PTO damping values in the literature to extract feasible amount of wave energy lie in this range.

In addition, by accommodating the determined damping and added mass values, developed simple mechanical model is solved and water column oscillation time series is calculated. To test the validity of the analytical model results as well as the damping and added mass values, water column oscillations are measured by performing physical experiments under the excitation of the same previously generated incident waves during the closed orifice tests. Waves with different characteristics gave rise to different type of water column surface motion behaviors. While W1 excited the water column in a piston mode, W2 introduced a minor sloshing and W3 caused a hybrid water column motion involving both sloshing and piston modes where sloshing behavior was dominant. All experimental tests are carried out for various chamber openings and PTO dampings (orifice sizes). It is found that relatively higher chamber openings and lower dampings filter out the sloshing phenomenon to a great extent for all incident waves. Analytically and experimentally obtained water column oscillation amplitudes are compared and a remarkable agreement is found for all chamber openings and PTO dampings under W1 for all configurations and also W2 except for the highest PTO damping and two biggest chamber openings. Even so, the biggest calculated relative error was 0.08. However, for W3 discrepancies developed between the analytical model results and experimental values up to relative error value of 0.313. It is considered that errors are due to the sloshing mode occurred in the OWC chamber because, for the cases where sloshing motion is highly suppressed by relatively smaller chamber opening and damping values, solutions well approximated the experimental values. It can clearly be reported that analytical model is performed very good if a major sloshing mode does not exist in the chamber. Two reasons are considered for accurate determination of the hydrodynamic parameters and success of the developed mathematical model. First one is, during the free decay experiments, water column acted in unison like a rigid-body hence obtained parameters are mostly related to piston type behavior of the water column and secondly, found representative damping of the system also includes viscous losses that possibly occur under the chamber front wall opening. Quantifying this kind of viscous damping is very challenging and startling. It requires the solution of non-linear N-S equations or a detailed and carefully performed PIV type experiment to determine the rotational kinetic energy of the fluid particles which dissipate some of the transmitted wave energy reducing the available wave power to be extracted. Moreover, to obtain the hydrodynamic parameters of an OWC device, analytical and numerical techniques widely make use of the potential theory which assumes irrotational flow and ideal fluid where viscous effects inherently neglected. This further shows the importance of the findings of this study, since it is the first time that viscous losses under the front wall are considered in an experimentally determined damping value. Relatively larger sloshing amplitudes decreases the accuracy of the simple mechanical model. However, as many previous studies indicate, for most practical purposes, water column surface may be considered planar in real sea states. Besides, it is well-known that sloshing mode is literally an enemy for efficient wave extraction, therefore, in the first place, natural frequencies of all OWCs have to be tuned to dominant wave frequency present in the installation region to ensure the piston motion in the chamber. In other words, for most of the time, geometric design considerations and the determination of applied PTO damping for an OWC device are already in the direction of generating piston motion in the chamber to exploit most of the incident wave energy. Hence, findings of this study is applicable for most general and practical purposes. For all chamber front wall openings and applied PTO dampings, resonant frequency of the OWC is also calculated by free decay tests. For all opening and applied damping configurations, the largest oscillation amplitudes are attained under the excitation of W1 which has a frequency very close to the calculated resonant frequencies of the OWCand the results obtained are further verified. The simple mechanical modelling approach that is utilized to simulate the water column surface motion in this present study, is very simple and practical yet embracing the essence of the physics of the complex wave-structure and wave-water column interactions; when the required parameters to solve the mechanical model is determined accurately. Therefore, it is believed that techniques and models implemented and results inferred in this present study may be very beneficial and widely used by the wave energy community.

In the last step of this thesis, a comprehensive experimental campaign was carried out to determine the effects of different underwater chamber openings and turbine-induced dampings on the efficiency of an OWC tool under different wave conditions. To achieve this task, a broad range of opening height and orifice diameter values were implemented and performance of the OWC tool is quantified by the ratio of absorbed pneumatic power to incident wave power for all different configurations under regular incident waves. Motion behaviors of the water column free surface are also examined.

A novel result of the particular study is, to obtain the highest wave energy conversion efficiency, there is not a unique optimal damping value that the system should possess but it depends on the incident wave characteristics, however, for a range of wave steepness values, optimal damping further varies with the seaward opening height of the chamber. For wave steepness values 0.02 and 0.096, optimal orifice ratio is found to be 1.03% and 0.40%, respectively. Therefore, optimal damping is a function of only incident wave characteristics for these steepness values where it becomes a function of both relative opening of the chamber and incident wave characteristics for incident wave steepnesses 0.046 and 0.073. For steepness 0.046 and relative openings 0.67, 0.75 and 0.83, optimal orifice ratio is determined as 0.78%, for relative openings 0.50 and 0.58, 0.58% and for relative openings 0.33 and 0.42, 0.40%. For steepness 0.072 and relative openings 0.50, 0.58, 0.67, 0.75 and 0.83, 0.58% was the optimal orifice ratio, where, for relative openings 0.33 and 0.42, optimal orifice ratio was found to be 0.40%. An inverse relationship is determined between the incident wave steepness and OWC efficiency. While the highest efficiency was obtained under the least steep incident wave, the steepest wave yielded negligibly small efficiencies. For all cases, hydrodynamic efficiency is increased with the relative opening of the chamber. In addition, it is revealed that the free surface motion behavior of the water column significantly influences the efficiency of the OWC tool, that is, rigid-piston type motion of the free surface enhances the performance where sloshing motion behavior of the water column reduces the efficiency. It is observed that sloshing motion introduced into the increases with the incident wave steepness.

Interestingly, absolute negative peak pressures generated in the chamber were mostly greater than positive peak pressures regardless of orifice ratio, relative opening and wave characteristics used in the present contribution.

The presented results that emerged from both quantitative and qualitative exploration of the OWC device performance under different parameters and circumstances, it is understood that, wave climate of the OWC deployment region significantly influences the selection of optimal PTO damping value but, since for some wave steepness values, an interaction with seaward opening and turbine induced damping exists, for a relatively more feasible energy harnessing, damping values have to be chosen not only in terms of wave characteristics but also the relative opening height of the chamber.

4.1 Recommendations

Scientific query is and endless and joyful journey, however, human life is limited and full of necessary constraints. There are numerous investigation subjects to fulfill to further improve the understanding of the wave energy conversion phenomenon. First of all, for the porposes of this study only regular waves were utilized. Findings of this study have to be assessed under more realistic sea states via further research that would be conducted under irregular waves.

To achieve high capacity electricity generation, wave energy converter farms including many OWCs (or any type of WEC for that matter) are constructed. In this case, incident wave field is affected from reflected and diffracted incident waves due to the presence of many OWC structures. Inevitably, hydrodyna

mics of OWC devices would be altered and overall efficiency would be influenced. Therefore, spacings between individual OWCs should be properly aligned. Experimental investigations have to performed in a wave basin with more than one (the more, the better) OWC to understand their interactions with each other.

It is well known that compressibility effects become important in full-scale prototypes. However, this subject is not fully studied, and thus, not comprehended in a satisfactory fashion. How performance of an OWC is influenced by compressibility effects should be quantitatively and qualitatively investigated. In order to fulfill these investigations, OWC device that have very large air column (compared to the water column) as the experimental facilities and economic aspects would permit have to be constructe

REFERENCES

Asmuth, H., Schmitt, P., Elsaesser, B., Henry, A. (2015). Determination of non-linear damping coefficients of bottom-hinged oscillating wave surge converters using numerical free decay tests. *1st International Conference on Renewable Energies Offshore,* Lisbon, Portugal, November 24 - 26.

Bouali, B., Larbi, S. (2013). Contribution to the Geometry Optimization of an Oscillating Water Column Wave Energy Converter. *Energy Procedia* **36**, 565-573.

Brendmo, A., Falnes, J., Lillebekken, PM. (1996). Linear modelling of oscillating water columns including viscous loss. *Appl Ocean Res* **18**:65e75.

Brusca, S., Galvagno, A., Lanzafame, R., Garrano, A. M. C., Mauro, S., Messina, M. (2017). On the turbine-induced damping in Oscillating Water Column wave energy converter. *Energy Procedia* **126**: 581-588.

Carbon Trust Marine Energy Challenge (2005). *Oscillating Water Column Wave Energy Converter Evaluation Report*. Retrieved from https://www.carbontrust.com/media/173555/owc-report.pdf

Chang, C., Chou, F. N., Chen, Y., Hsieh Y., Chia-Tzu C. (2016). Analytical and experimental investigation of hydrodynamic performance and chamber optimization of oscillating water column system. *Energy* **113** 597-614.

Chakrabarti, S. K., Cotter, D. C. (1992). Hydrodynamic Coefficients of a Moored Semisubmersible in Waves. *J Offshore Mec Arc Eng* **114**/9.

Çelik, A., Altunkaynak, A. (2018). Experimental investigation on chamber water surface fluctuations and motion behaviors of water column type wave energy converter. *Ocean Engineering* **150**: 209-220.

Dean, R. G., Dalrymple, R. A. (1984). *Water wave mechanics for engineers and scientists.* Singapore: World Scientific Publishing.

Drew, B., Plummer, R. A., Sahinkaya, M. N. (2009). A review of wave energy converter technology *J. Power and Energy* **223** Part A.

Elhanafi, A., Fleming, A., Macfarlane, G., Leong, Z. (2017). Underwater geometrical impact on the hydrodynamic performance of an offshore oscillating water column wave energy converter. *Renewable Energy* **105**: 209-231.

Elhanafi, A., Fleming, A., Macfarlane, G., Leong, Z. (2017). Numerical hydrodynamic analysis of an offshore stationary–floating oscillating water column–wave energy converter using CFD. *Int J Nav Ar Ocean Eng* **9** 77-99.

Evans, D. (1978). The oscillating water column wave-energy device. *IMA J Appl. Math* **22**:423e33.

Evans, D. (1982). Wave-power absorption by systems of oscillating surface pressure distributions. *J. Fluid. Mech.* **114**:481e99.

Evans, D. V., Porter, R. (1995). Hydrodynamic characteristics of an oscillating water column device. *Appl. Ocean Res* **17**: 155e164.

Fairhurst, J., Van Niekerk, J. L. (2016). Modelling, simulation and testing of a submerged water column. *Int J Marine Energy* **16** 181-195.

Falcao, F. O. A., Henriques, J. C. C. (2016). Oscillating Water Column Wave Energy Convertors and air turbines: A review. *Renewable Energy* **85** 1391-1424.

Falcao, A. F. O., Henriques, J. C. C. (2014) Model-Prototype similarity of oscillating-water-column wave energy converters. *Int. J. Marine Energy* **6** 18-34.

Falcao, A. F. O., Sarmento, A. (1980). Wave generation by a periodic surface pressure and its application in wave-energy extraction. *15th International Congress of Theoretical and Applied Mechanics,* Toronto, Canada, August 17-23.

Falnes, J, McIver, P. (1985). Surface wave interactions with systems of oscillating bodies and pressure distributions. *Appl Ocean Res* **7**:225e34.

Fang M.C., Luo, J. (2005). The nonlinear hydrodynamic model for simulating a ship steering in waves with autopilot system. *Ocean Engineering* **32** Issues 11–12 1486-1502.

Ferguson, T. M., Fleming, A., Penesis, I., Macfarlane, G. (2015). Improving OWC performance prediction using polychromatic waves. *Energy* **93** 1943-1952.

Fleming, A., Penesis, I., Macfarlane G., Bose N., Dennis T. (2012). Energy balance analysis for an oscillating water column wave energy converter. *Ocean Engineering* **54** 26-33.

Flow science Inc. (2012). *Flow-3D User's Manuals*. Retrieved from https://www.flow3d.com/wp-content/uploads/2019/03/FLOW-3D-v12-0-Install-Instructions.pdf

Freeman, K., Dai, M., Sutton, R. (2013). Control strategies for oscillating water column wave energy converters. *Underwater Technology* **32** No 1 3-13.

Fukuda, K. (1977). Behavior of Water in Vertical Well with Bottom Opening of Ship, and its Effects on Ship-Motion. *J Soc Naval Architects of Japan* **141** 107-122.

Handschel, S., Feder, D-F., Abdel-Maksoud, M. (2015). Estimation of Ship Roll Damping - a Comparison of the Decay and the Harmonic Excited Roll Motion Technique for a Post Panamax Container Ship. *Proceedings of the 12th Int Con Stability of Shps and Ocean Vhc* Glasgow, UK, June 14-19.

He, F., Hung, Z. (2014). Hydrodynamic performance of pile-supported OWC-type structures as breakwaters: an experimental study. *Ocean Engineering* **88** 618-626.

He, F., Huang, Z., Law, A. W. (2013). An experimental study of a floating breakwater with asymmetric pneumatic chambers for wave energy extraction. *Applied Energy* **106** 222–231.

Heath, T. V. (2012). A review of oscillating water columns. *Phil Trans R Soc A* **370** 235-245.

Hirt, C. W., Nichols, B. D. (1981). Volume of fluid (VOF) method for the dynamics of free boundaries. *J Computational Physics* **39** 201–25.

Hsieh, M., Lin, I., Dorrell, D. G., Hsieh, M.-J., Lin, C. (2012). Development of a Wave Energy Converter Using a Two Chamber Oscillating Water Column. *IEEE transactions on sustainable energy* **3** no 3.

Hughes, S. A. (1993). *Physical models and laboratory techniques in coastal engineering*. New Jersey: World Scientific.

Ibn al-Haytham, H. (1021). *Vikipedi*. Retrieved May 25 2019, https://tr.wikipedia.org/wiki/İbn-i_Heysem

Kamath, A., Bihs, S., Arnsten, A. (2015). Numerical modeling of power take-off damping in an Oscillating Water Column device. *International Journal of Marine Energy* **10**(0): 1-16.

Kamath, A., Bihs, H., Arntsen, Ø. A. (2015). Numerical investigations of the hydrodynamics of an oscillating water column device. *Ocean Engineering* **102** 40-50.

Karami, V., Ketabdari, M. J., Akhtari, A. K. (2012). Numerical modelling of Oscillating Water Column Wave Energy Convertor. *Int Jrn of Advanced Renewable Energy Research* **1-4** 196-206.

Kelly, T., Dooley, T., Ringwood, J. V. (2017). Experimental determination of the hydrodynamic parameters of an OWC. *12th European Wave and Tidal Energy Conference*, Cork, Ireland, Aug 27 – Sept 1.

Kuo, Y., Chung, C., Hsiao, S., Wang, Y. (2017). Hydrodynamic characteristics of Oscillating Water Column caisson breakwaters. *Renewable Energy* **103** 439-447.

Liu, L., Incecik, A., Zhang, Y., Tang, Y. (2014) Analysis of heave motions of a truss spar platform with semi-closed moon pool. *Ocean Engineering* **92** 162–174.

Lopez, I., Pereiras, B., Castro, F., Iglesias, G. (2014). Optimisation of turbine-induced damping for an OWC wave energy converter using a RANS–VOF numerical model. *Applied Energy* **127**: 105–114.

Lopez, I., Castro, A., Iglesias, G., (2015). Hydrodynamic performance of an oscillating water column wave energy converter by means of particle imaging velocimetry. *Energy* **83**: 89-103.

Lopez, I., Pereiras, B., Castro, F., Iglesias, G. (2015). Performance of OWC wave energy converters: influence of turbine damping and tidal variability. *Int J Energy Res* **39**:472–483.

Luo, Y., Nader, J.-R., Cooper, P., Zhu, S.-P. (2014). Nonlinear 2D analysis of the efficiency of fixed Oscillating Water Column wave energy converters. *Renewable energy* **64** 255-265

Mahnamfar, F., Altunkaynak, A. (2015). OWC-Type Wave Chamber Optimization Under Series of Regular Waves. *Arab J Sci Eng* **41**:1543-15.

Mahnamfar, F., Altunkaynak, A. (2017). Comparison of numerical and experimental analyses for optimizing the geometry of OWC systems. *Ocean Engineering* **130**: 10-24.

Mark, G., Barstow, S., Pontes, M. T., Kabuth, A. (2010). Assessing the global wave energy potential. *Proceeding of the OMAE2010 (ASME), 29th International Conference on Ocean, Offshore Mechanics and Arctic Engineering,* Shanghai, China, June 6-11.

McCormick, M. E. (1974). Analysis of a wave energy conversion buoy. *J Hydronautics* **8** (3) 77e82.

McCormick, M. E. (1976). A modified linear analysis of a wave-energy conversion buoy. *Ocean Engineering* **3**:133–44.

McCormick, M. E. (1981). *Ocean Wave Energy Conversion* New York: Wiley-Interscience.

McCormick, M. E. (2009). *Ocean Engineering Mechanics with Applications*. New York: Cambridge University Press.

McCormick, M. E., Murtha, R. C., McCormick, M. E. II (2018). Empirical deep-water heave added-mass and radiation-damping expressions for 2-D rectangular sectioned floating bodies. *Ocean Engineering* **164** 529-535.

Molin, B. (2001). On the piston and sloshing modes in moonpools. *J Fluid Mech* **430** 27-50.

Morris-Thomas, M. T., Irvin, R. J., Thiagarajan K. P. (2007). An investigation into the hydrodynamic efficiency of an oscillating water column. *Journal of Offshore Mechanics and Arctic Engineering* **129**:273–8.

Ning, D., Wang R., Zou, Q., Bin, T. (2016). An experimental investigation of a fixed OWC Wave Energy Converter. *Applied Energy* **168**: 636-648.

Ning, D.-Z., Wang, R.-Q., Zou, Q.-P., Teng, B. (2016). Numerical and experimental investigation of wave dynamics on a land-fixed OWC device. *Energy* **115** 326-337.

Oh, J-S., Jang, J-H. (2015). OWC design to increase wave energy absorption efficiency in wave conversion systems. *Journal of Mechanical Science and Technology* **29**-7 2987-2993.

Payne, G. (2008). *Guidance for the experimental tank testing of wave energy converters*. Retrieved April 25 2018 https://www.supergen-marine.org.uk/sites/supergen-marine.org.uk /files/publications/WEC_tank_testing.pdf

Penalba, M., Giuseppe, G., Ringwood, J. V. (2017). Mathematical modelling of wave energy converters: A review of non-linear approaches. *Renewable and sustainable energy reviews* **78** 1188-1207**.**

Rao, S. S. (2011). *Mechanical Vibrations*. Singapore: Pearson Education.

Renewables (2018). *Analysis and Forecasts to 2023.* Retrieved August 13 2018 https://www.iea.org/renewables2018/

Rodi, W. (1980). *Turbulence Models and Their Application in Hydraulics. A State of the Art Review*. Rotterdam, Netherlands: A.A. Balkema.

Rezanejad, K., Soares, C. G., Lopez, I., Carballo, R. (2017). Experimental and numerical investigation of the hydrodynamic performance of an oscillating water column wave energy converter. *Renewable Energy* **106** 1-16.

Rezanejad, K., Soares, C. G. (2018). Enhancing the primary efficiency of an oscillating water column wave energy converter based on a dual-mass system analogy. *Renewable Energy* **123** 730-747.

Sheng, W., Alcorn, R., Lewis, T. (2014). Physical modelling of wave energy converters. *Ocean Engineering* **84** 29-36.

Sheng, W., Lewis, A. (2016). Wave energy conversion of oscillating water column devices including air compressibility. *Jr of Rnw Sustainable Energy* **8** 054501-1.

Sarmento, A. J. N. A., Falcao F. O. A. (1985). Wave generation by an oscillating surface-pressure and its application in wave-energy extraction. *J Fluid Mech* **150**: 467e485.

Sheng, W., Thiebaut, F., Babuchon, M., Brooks, J., Lewis, A., Alcorn, R. (2013). Investigation to air compressibility of oscillating water column wave energy converters. *32nd Inter Conf on Ocean Offshore and Arctic Eng,* Nantes, France, June 9-14.

Simonetti, I., Cappietti, L., Elsafti, H., Oumeraci, H. (2015). Numerical Modelling of Fixed Oscillating Water Column Wave Energy Conversion Devices: Toward Geometry Hydraulic Optimization *34th Int Con Ocean Offshore Eng.,* St. John's, NL, Canada, May 31 - June 32.

Simonetti, I., Cappietti, L., Elsafti, H., Oumeraci, H. (2017). Optimization of the geometry and the turbine induced damping for fixed detached and asymmetric OWC devices: A numerical study. *Energy* **139**: 1197-1209.

Szumko, S. (1989). Mechanical model for oscillating water column with compressibility. *J Eng Mech*, **115**(9): 1851-1866.

Stewart, T. P. (1993). *The influence of harbor geometry on the performance of oscillating water column wave power converters* (Doctoral Dissertation), Retrieved from http://encore.qub.ac.uk/

Sundar, V (2016). Ocean Wave Mechanics Applications in Marine Structures John Wiley & Sons Ltd., United Kingdom.

Thiruvenkatasanny, K., Neelamani, S. (1997). On the efficiency of wave energy caissons in array. *App Ocean Res* **19** 61-72.

Url-1 <*https://ocw.mit.edu/courses/mechanical-engineering/2-016-hydrodynamics-13-012-fall-2005/readings/2005reading8.pdf*>, date retrieved 20.01.2019.

Url-2 <*https://www.worldenergy.org/wp-content/uploads/2016/10/World-Energy-Resources_ExecutiveSummary_2016.pdf*>, date retrieved 15.06.2017.

Url-2 <*http://www.conserve-energy-future.com*>, date retrieved 15.06.2017.

Viviano, A., Naty, S., Foti, E., Bruce, T., Allsop, W., Vicinanza, D. (2016). Large-scale experiments on the behaviour of a generalised Oscillating Water Column under random waves. *Renewable Energy* **99** 885-887.

Viviano, A., Naty, S., Foti, E. (2018). Scale effects in physical modelling of a generalized OWC. *Ocean Engineering* **162** 248-258

Veer, V. R., Tholen, J. H. (2008). Added resistance of moonpools in calm water. *27th International Conference on Offshore Mechanics and Arctic Engineering*, Estoril, Portugal, June 15-20.

Vyzikas, T. Deshoulières, S., Giroux, O., Barton, M., Giroux, O., Greaves, D., Simmonds, D., (2017). Experimental investigation of different geometries of fixed oscillating water column devices. *Renewable Energy* **104** 248-258

Wang, D.J., Katory, M., Li, Y.S. (2002). Analytical and experimental investigation on the hydrodynamic performance of onshore wave power devices. *Ocean Engineering* **29**: 871-885.

Weber, J. (2007). Representation of non-linear aero-thermodynamic effects during small scale physical modelling of OWC WECs. *Proceedings of the 7th European Wave and Tidal Energy Conference*, Porto, Portugal, September, 11-13.

Zhang, Y., Zou, Q.P., Greaves, D. (2012) Air–water two-phase flow modelling of hydrodynamic performance of an oscillating water column device. *Renew Energy* **41** 159–170.

CURRICULUM VITAE

Name Surname : Anıl ÇELİK

Place and Date of Birth : Ankara, 12 August 1976

E-Mail : ac@ekainsaat.com.tr

EDUCATION

- **B.Sc.** : 1998, Yıldız Technical University, Faculty of Civil Engineering Department, Departement of Civil Engineering
- **M.Sc.** : 2007, SUNY Maritime Colloge, International Transportation Management Department

PUBLICATIONS FROM THE THESIS:

- **Çelik, A.,** Altunkaynak, A., 2018. Experimental investigation on chamber water surface fluctuations and motion behaviors of water column type wave energy converter. *Ocean Engineering*, 150 209-220
- **Çelik, A.,** Altunkaynak, A., 2019. Experimental investigations on the performance of a fixed-oscillating water column type wave energy converter. *Energy*, 188 116-71
- **Çelik, A.,** Altunkaynak, A., 2020. Determination of damping coefficient experimentally and mathematical vibration modelling of OWC surface fluctuations. *Renewable Energy*, 147 1909-192
- **Çelik, A.,** Altunkaynak, A., 2020. Determination of Hydrodynamic Parameters of a Fixed OWC by Performing Experimental and Numerical Free Decay Tests. (*Ocean Engineering*)
- **Çelik, A.,** Altunkaynak, A., 2020. Estimation of water column surface displacement of a fixed OWC by a simple mechanical model with determination of hydrodynamic parameters via physical experimental model.

(*Waterway, Port, Coastal, and Ocean Engineering, ASCE*, under review second revison).